Catalytic properties of human apurinic/apyrimidinic endonuclease 1 (APE1) and development of biosensors of APE1 in living cells

Wang, Tianxiang

2021

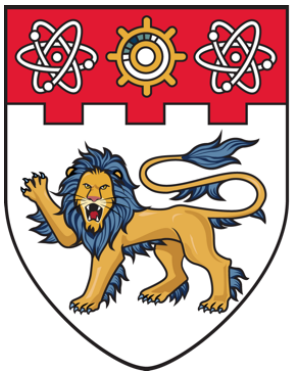

NANYANG TECHNOLOGICAL UNIVERSITY
SINGAPORE

Catalytic Properties of Human Apurinic/apyrimidinic Endonuclease 1 (APE1) and Development of Biosensors of APE1 in Living Cells

WANG TIANXIANG

SCHOOL OF PHYSICAL AND MATHEMATICAL SCIENCES

2021

Catalytic Properties of Human Apurinic/apyrimidinic Endonuclease 1 (APE1) and Development of Biosensors of APE1 in Living Cells

WANG TIANXIANG

SCHOOL OF PHYSICAL AND MATHEMATICAL SCIENCES

A thesis submitted to the Nanyang Technological University in partial fulfilment of the requirement for the degree of Doctor of Philosophy

2021

Statement of Originality

I hereby certify that the work embodied in this thesis is the result of original research done by me except where otherwise stated in this thesis. The thesis work has not been submitted for a degree or professional qualification to any other university or institution. I declare that this thesis is written by myself and is free of plagiarism and of sufficient grammatical clarity to be examined. I confirm that the investigations were conducted in accord with the ethics policies and integrity standards of Nanyang Technological University and that the research data are presented honestly and without prejudice.

2020.08.05

Wang Tianxiang

. . . . . .
Date

. . . . . .
Wang Tianxiang

Supervisor Declaration Statement

I have reviewed the content and presentation style of this thesis and declare it of sufficient grammatical clarity to be examined. To the best of my knowledge, the thesis is free of plagiarism and the research and writing are those of the candidate's except as acknowledged in the Author Attribution Statement. I confirm that the investigations were conducted in accord with the ethics policies and integrity standards of Nanyang Technological University and that the research data are presented honestly and without prejudice.

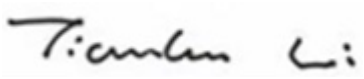

2020.08.05

. . . . . .
Date

. . . . . .
Li Tianhu

Authorship Attribution Statement

This thesis contains material from one paper published in the following peer-reviewed journal in which I am listed as an author.

Chapter 3 and 4 are published as Zhang, H.; Ba, S.; Yang, Z.; **Wang, T.**; Lee, J. Y.; Li, T.; Shao, F., Graphene Quantum Dot-Based Nanocomposites for Diagnosing Cancer Biomarker APE1 in Living Cells. *ACS Appl. Mater. Interfaces* **2020**, *12*, 13634-13643. DOI: 10.1021/acsami.9b21385.

The contributions of the co-authors are as follows:

- Assoc Prof Li Tianhu and Assoc Prof Shao Fangwei provided the initial project.
- I conducted all the experiments including construction and characterization of nanocomposites and investigations in cell-free systems and in living cells.
- Dr Zhang Hao and I prepared the manuscript drafts. And the manuscript was revised by Dr Ba Sai, Dr Yang Zhaoqi, Lee Yiqin Jasmin, Assoc Prof Li Tianhu and Assoc Prof Shao Fangwei.

2020.08.05 Wang Tianxiang

. . . .

Date Wang Tianxiang

Abstract

Apurinic/apyrimidinic endonuclease 1 (APE1) is an essential enzyme involved in the DNA base excision repair pathway and responsible for restoring mutagenic and cytotoxic abasic lesions throughout cell cycles. APE1 will cleave the 5’ end phosphodiester backbone right next to the generated apurinic/apyrimidinic site (AP site) to produce a free 5’ phosphate termini linking to the AP site and a free 3’ hydroxyl termini on the regular nucleotide. APE1 is overexpressed in various types of cancer cells, proving that APE1 is a valid biomarker for cancer diagnosis and its inhibitors show potential in monotherapy and combination therapy for fighting cancers. In spite of its potential roles in cancer diagnosis, prognosis, and chemotherapy, however, various aspects of translational research about APE1 have not yet been carried out thus far. Herein, we have successfully developed graphene quantum dot-based biosensors for APE1 diagnosis both in cell-free systems and in living cells. Besides, investigation on diversity of substrates makes a great contribution to understand the catalytic properties of APE1 and further explore sequence-specific DNA as new APE1 inhibitors.

Chapter 1introduces the background information of AP site, APE1 and nanobiosensors. Firstly, we present general pathways of the formation of AP site, biological harmfulness of accumulating AP sites and different chemical stability of three analogs of AP site. Secondly, we demonstrate detailed process and significance of base excision repair (BER) pathway, functions and mechanism of APE1 as a critical AP endonuclease and evidence for regarding APE1 as an important biomarker. Finally, unique properties of nanomaterials utilizing in biosensor, the development of DNA-based nanobiosensors and the development of fluorescence-based nanobiosensors are presented.

Chapter 2 shows studies on catalytic properties of APE1 by investigating substrate diversity. We explore the substrate scopes of APE1 relying on three categories: DNA with modifications to 5' AP site, mismatched DNA and DNA containing two AP sites as APE1 substrates. Gel electrophoresis is used for data analysis.

In **Chapter 3**, we construct graphene quantum dot-based biosensor by well-designed unimolecular DNA and prepared graphene quantum dots. Various methods are utilized in characterization of the structure of graphene quantum dot-based biosensor we designed, such as atomic force microscopy (AFM), transmission electron microscopy (TEM), infrared (IR) spectroscopy, dynamic light scattering (DLS), and fluorescence spectroscopy. In addition, we conduct a series of experiments to test the sensitivity and selectivity of quantum dot-based biosensor for detecting APE1 in cell-free systems.

Chapter 4 presents further studies on our designed graphene quantum dot-based biosensor applying in living cells environment. The results from experiments substantiate that graphene quantum dot-based biosensor is sensitive and efficiency for cellular APE1 diagnosis and can distinguish different living cells with different expression levels of APE1. Meanwhile, graphene quantum dot-based biosensor is biocompatible and efficient in cellular uptake.

Acknowledgements

First and foremost, I would like to express deep gratitude to my supervisor, associate professor Li Tianhu with my sincere respect. During past four years of my Ph. D. work, he always gives me patient guidance and kind advice. I am deeply impressed by his wide knowledge, optimistic attitude towards life and serious attitude towards work. When I have difficulty in research, he always gives me strong support and sincere encouragement. Without his great help, my Ph. D. programme can't be completed in four years.

Second, I would like to thank my former supervisor, Professor Tan Choon Hong for guidance and suggestions.

Third, I would like to thank all my current group members Dr. Zhang Hao, Dr. Ba Sai, Lee Yiqin Jasmine, Bella Rosa Liyarita and my former group members Dr. Chin Kek Foo, Dr. Teng Bo, Dr. Cao Weidi , Dr. Chen Li, Dr. Valerie Wong, Dr. Ren Jingyun, Dr. Wang Yang, Dr. Ge Yicen, Dr. Jackson Leow, Dr. Chua Zhijie, Dr. Ban Xu, Dr. Jiang Huan, Dr. Yao Zhen, Dr. Cui Xiyang, Dr. Ye Xinyi, Dr. Zhang Xin, Dr. Genevieve Lau, Mr. Song Zhijian, Ms. Esther Ang Cai Xia and Ms. Yang Ziqi for their support, collaboration and valuable advice on my research.

Fourth, great appreciations are extended to all technicians and administrative staffs in Division of Chemistry and Biological Chemistry for offering support for my research.

Fifth, I would like to thank to all dissertation examiners for their valuable guidance.

Sixth, I must take this opportunity to thank Nanyang Technological University, Division of Chemistry and Biological Chemistry for offering me this research opportunity.

Seventh, special thanks are expressed to YYF and Nvliu 66 on Douyu live-streaming. They bring me happiness during tough times of my research.

Last but not the least, I would like to thank my family members. Their love, understanding and support make me overcome difficulties and give me confident in my life.

Table of Contents

List of Figures

Figure 4.6 Cytotoxicity assays of graphene quantum dot-based Nanobiosensor 1, graphene oxide-based Nanobiosensor GO, and reduced graphene oxide-based Nanobiosensor rGO towards PANC-1 cell lines.

Figure 4.7 Confocal microscopic examinations of the cellular uptake of Nanobiosensor 1 by PANC-1 cells at varying time intervals.

Figure 4.8 Comparison of cellular uptake efficiency of nanobiosensors with the use of different nanomaterials as their carriers.

List of Table

List of Abbreviation

AFM	atomic force microscopy
AP site	apurinic/apyrimidinic site
APE1	apurinic/apyrimidinic endonuclease 1
BER	base excision repair
^{o}C	degree Celsius
DI water	deionized water
DLS	dynamic light scattering
DMEM	Dulbecco's modified eagle medium
DNA	deoxyribonucleic acid
dsDNA	double-strand DNA
DTT	dithiothreitol
EDTA	ethylenediaminetetraacetic acid
EXO1	exonuclease 1
FEN1	flap endonuclease 1
FRET	fluorescence resonance energy transfer
HR	homologous recombination
IR	infrared
LIG1	DNA ligase 1
MEBM	mammary epithelial basal medium
MMR	mismatch repair
NER	nucleotide excision repair
NHEJ	non-homologous end joining
PBS	phosphate buffered saline

POLB	DNA polymerase beta
RNA	ribonucleic acid
PARN	poly(A)-specific ribonuclease
PBS	phosphate buffered saline
SERS	surface-enhanced raman spectroscopy
ssDNA	single-strand DNA
TBE	tris, boric acid, EDTA buffer
TEM	transmission electron microscopy
TEMED	tetramethylethylenediamine
Topo I	human topoisomerase I
Topo II	human topoisomerase IIα
Tris	tris(hydroxymethyl)aminomethane

Chapter 1

Introduction

1.1 Apurinic/apyrimidinic (AP) site

1.1.1 The formation of AP site

The molecular structure of deoxyribonucleic acid (DNA), an information carrier of gene, is well studied now. There are four different common nucleobases: Adenine (A), Guanine (G), Cytosine (C) and Thymine (T) in DNA structure. A and G containing a double-ringed structure are called as purines, while C and T containing single six-member ring are named as pyrimidines. In general, bases from different complementary single-strand DNAs are well paired through hydrogen bonds according to Watson-Crick Bases Pairs[1].

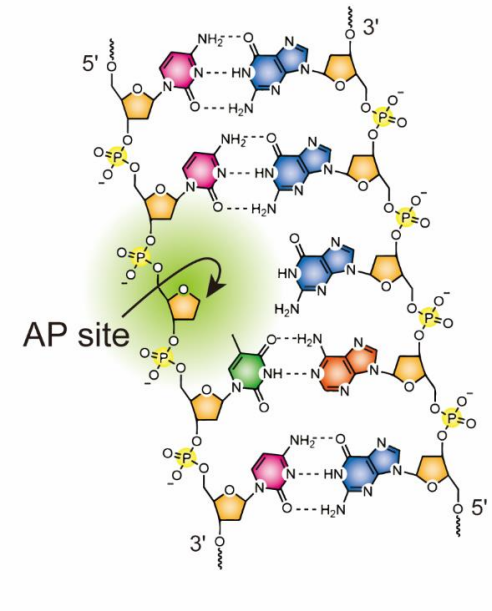

Figure 1.1 Location representation of AP site.

Apurinic/apyrimidinic (AP) site, also means an abasic site in biochemistry filed, is a location in double-strand DNA which has neither a purine nor a pyrimidine base. As illustrated in **Figure 1.1**, AP site just likes a missing blank in DNA structure, which indicates

that it is an “error” and can destroy normal functions of DNA, leading to a series of severe consequences, such as the death of cells.

AP sites are generated in human cells every day. In accordance with different sources which have an interaction with DNA by different mechanisms, generally there are four pathways to form AP sites[2]:

(i) Spontaneous formation. The glycosyl bonds are unstable in acid and high temperature conditions. Thus, the release of purine or pyrimidine bases is observed from DNA in weak acid or neutral pH with high temperature through hydrolysis[3-4].

(ii) Chemical agents. Alkylation agents induce alkylated bases with positive charge, accelerating the dissociation of the glycosyl bond and resulting in releasing bases[5]. Using strong acid such as H_2SO_4 and HNO_3 also leads to base removal from DNA. It results from the deamination of guanine to form xanthine residues, which are unstable in DNA structure and easy to be cut generating AP site[6]. Besides, depyrimidination of DNA can be generated by treating DNA with oxidants such as OsO_4, $KMnO_4$ and H_2O_2, because oxidants can low the bond energy of the glycosyl bond between deoxyribose and thymine analogs[7-8]. In addition, antitumor drugs and antibiotics such as bleomycin can easily form AP sites while mixing with DNA. By bonding to DNA, it can directly cleave thymine-deoxyribose bonds[9].

(iii) Irradiation. In aqueous solution, the hydroxyl radicals generated by irradiation directly attack the glycosyl bonds or subsequently react with the base, leading to the cleavage of the glycosyl bond[10-11]. High doses of γ-rays and ultraviolet rays cause the oxidation of deoxyribose, consequently releasing the base to generate AP site[12-13].

(iv) Specific DNA glycosylases. Certain unique bases or AP site in DNA can be recognized by specific DNA glycosylases and subsequently incised to generate an AP site and a free base. There are many discovered specific DNA glycosylases till now, such as Uracil-DNA glycosylase, Hypoxanthine-DNA glycosylase, 3-Methyladenine-DNA glycosylase I, 3-Methyladenine-DNA glycosylase II, Formamidopyrimidine-DNA glycosylase, Urea-DNA glycosylase, Thymine glycol-DNA glycosylase and Pyrimidine dimer-DNA glycosylase[14-15]. Due to the specificity and efficiency of enzymes, this method for AP sites formation is convenient and efficient.

1.1.2 Biological harmfulness effects of unrepaired AP sites

AP sites existed in living cell can lead to toxicity and lethality for cell[16]. DNA replication can be stopped while DNA polymerases encounter AP sites, leading to a single-strand or double-strand break[17]. Moreover, AP sites during DNA replication can also cause replication fork stalling and error-prone bypass synthesis[18], resulting in DNA inactivation[19] and possibly activation of cell death responses[20]. Besides, in the presence of DNA containing AP site, RNA polymerase can block the synthesis of RNA[21].

On the other hand, if left unrepaired in DNA, AP sites can lead to significant mutations during replication[17]. Loeb' review in 1985 revealed that the depurination in spontaneous way or chemical way both resulted in mutagenesis[22]. In vivo experiments, Gentil et al. (1984) discovered that AP sites existed in SV40 DNA lead to a high risk of mutagenicity in animal cells[23]. The mutagenesis was supposed to be happened even without inducting an error-prone DNA repair system. In 1985, Suet al. proved that int the presence of

UV irradiation, AP sites from alkylated single-strand DNA at parvovirus H-1 propagated in human cells show the high mutagenic potential[24].

1.1.3 AP sites analogs

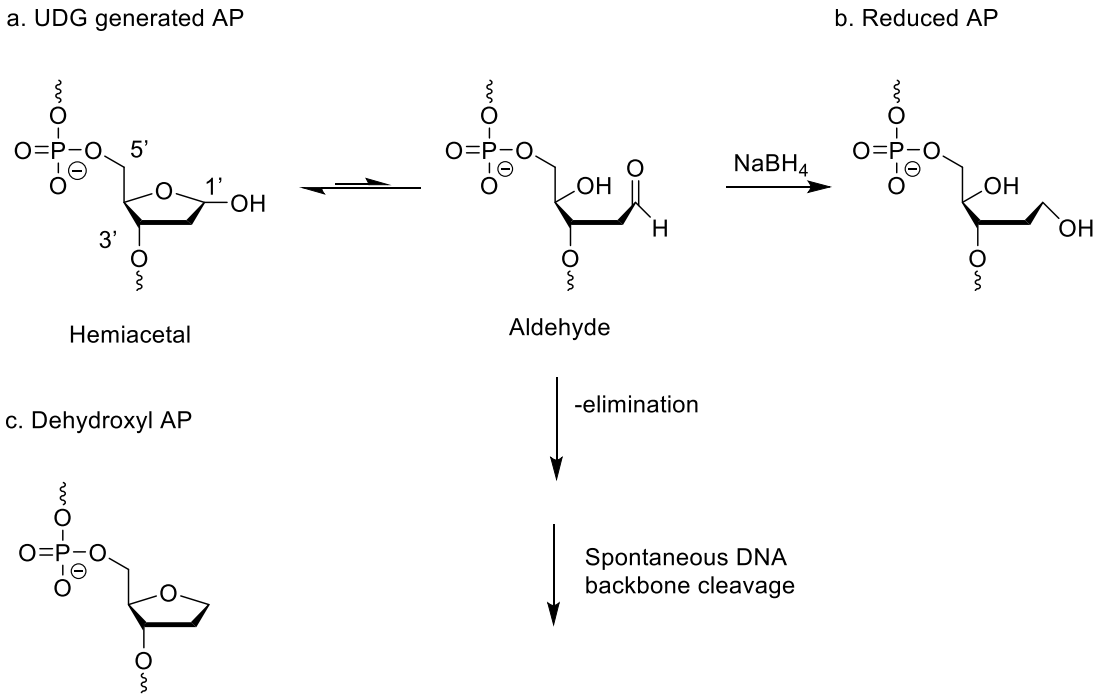

Figure 1.2 Structural comparison between different AP sites analogs. (a) Molecular structure and chemical instability of uracil-DNA glycocasylase-generated AP site. An equilibrium of hemiacetal and aldehyde followed by spontaneous DNA backbone cleavage. (b) Molecular structure of reduced with $NaBH_4$ AP site. (c) Molecular structure of chemically stable dehydroxyl AP site that is used in the current studies.

The molecular structures of AP sites generated from uracil-DNA glycosylase are shown in **Figure 1.2**(a). It's a ring closing hemiacetal and have an equilibrium to 4'-hydroxyl aldehyde form through ring opening. Undergoing β-elimination, 4'-hydroxyl aldehyde easily generates aldehyde with shorter chain and 5'-phosphate termini[25]. Therefore, the type of AP

sites leads to a spontaneous DNA backbone cleavage with a high possibility. Considering the chemical instability of AP sites generated from uracil-DNA glycosylase, there are two commonly used AP site analogs. One is shown in **Figure 1.2**(b), which is reduced with $NaBH_4$ from AP site generated from uracil–DNA glycosylase. The other one called dehydroxyl AP site, whose structure is shown in **Fugure 1.2**(c). In following chapters, we decide to use dehydroxyl AP sites located in the middle of duplex segment we designed, which are more stable in experimental systems and provide suitable recognized area for APE1 enzyme.

1.2 Apurinic/apyrimidinic endonuclease 1 (APE1)

1.2.1 Base excision repair (BER)

In human cells, due to both endogenous (such as normal metabolic activities) and exogenous (such as chemical agents and environmental effects) factors continuously lead to DNA damages, which cause 10, 000 to 1, 000, 000 molecular lesions per cell every day[26]. These unrepaired lesions further result in many human diseases and cancers. Consequently, the DNA repair process constantly help remove or tolerate these lesions to protect DNA and survive the cells from damage. Thus, investigations on different DNA repair pathways and their mechanisms can make a great contribution to discover potential toxic lesions and design related strategies to deal with factors harmful for human health. In general, there are at least five major DNA repair pathways existed in mammalian cells, base excision repair (BER), nucleotide excision repair (NER), mismatch repair (MMR), homologous recombination (HR) and non-homologous end joining (NHEJ)[27].

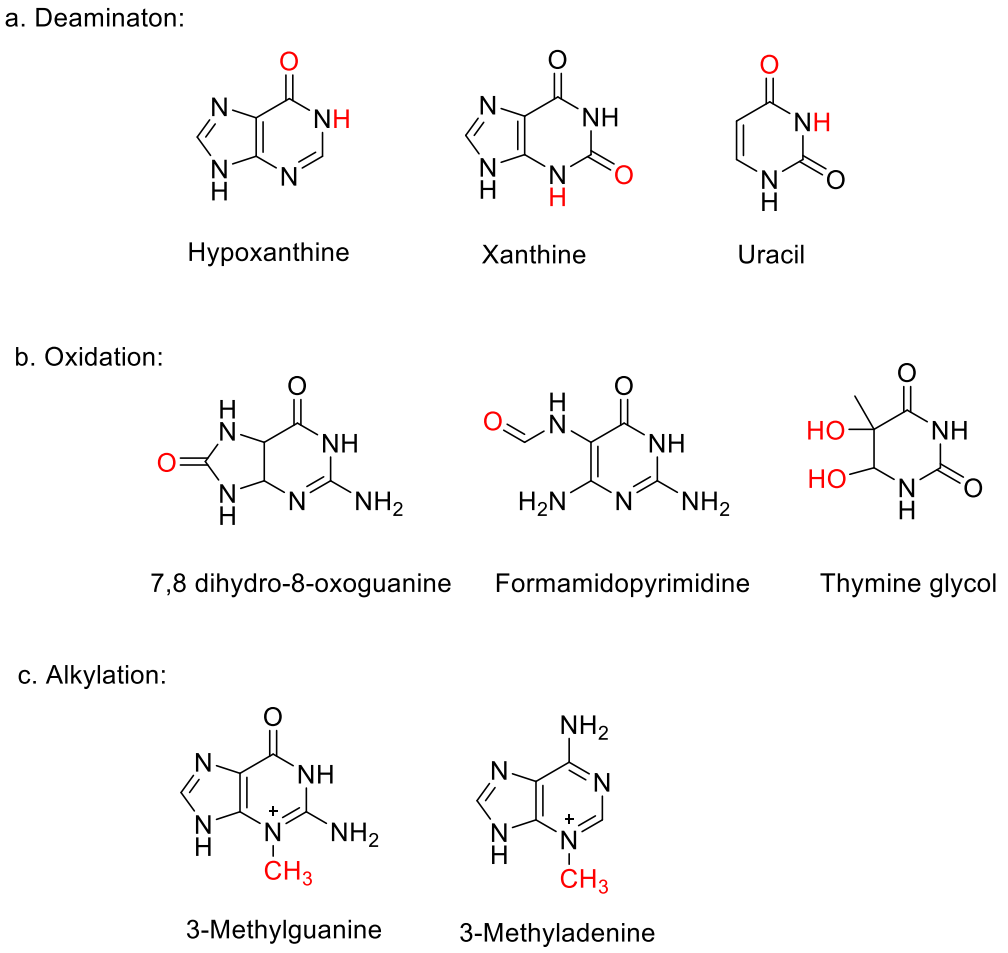

Figure 1.3 Damage bases caused by (a) deamination, (b) oxidation and (c) alkylation.

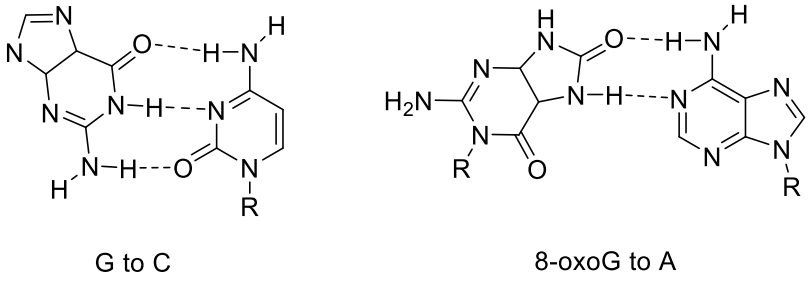

Figure 1.4 G : C Watson-Crick base pair and 8-oxoG : A Hoogsteen base pair.

BER is one of essential pathways due to repairing small and non-helix-distorting DNA lesions. The damage of single base in DNA is mainly generated from deamination,

oxidation, and methylation[28]. Examples are presented in **Figure 1.3**, resulting in huge potential threat to the living cell. In detail, these modifications can significantly change hydrogen bond formation ability of bases, leading to wrong base pairs and mutations. For example, 8-oxoguanine is one of the most common modified single bases generated from oxidation of guanine (G). Normally, guanine (G) forms a Watson-Crick base pair with cytosine (C) by forming three hydrogen bonds. While 8-oxoguanine combined with adenine (A) through two hydrogen bonds forms a Hoogsteen base pair. Followed by DNA replication, the mutation from a G : C base pair to a T : A base pair is completed (**Figure 1.4**)[29]. Thus, BER is an essential tool for removing damaged bases in case of mutations from wrong base pairs or DNA breaks during replication, and a powerful guarantee to protect living cells.

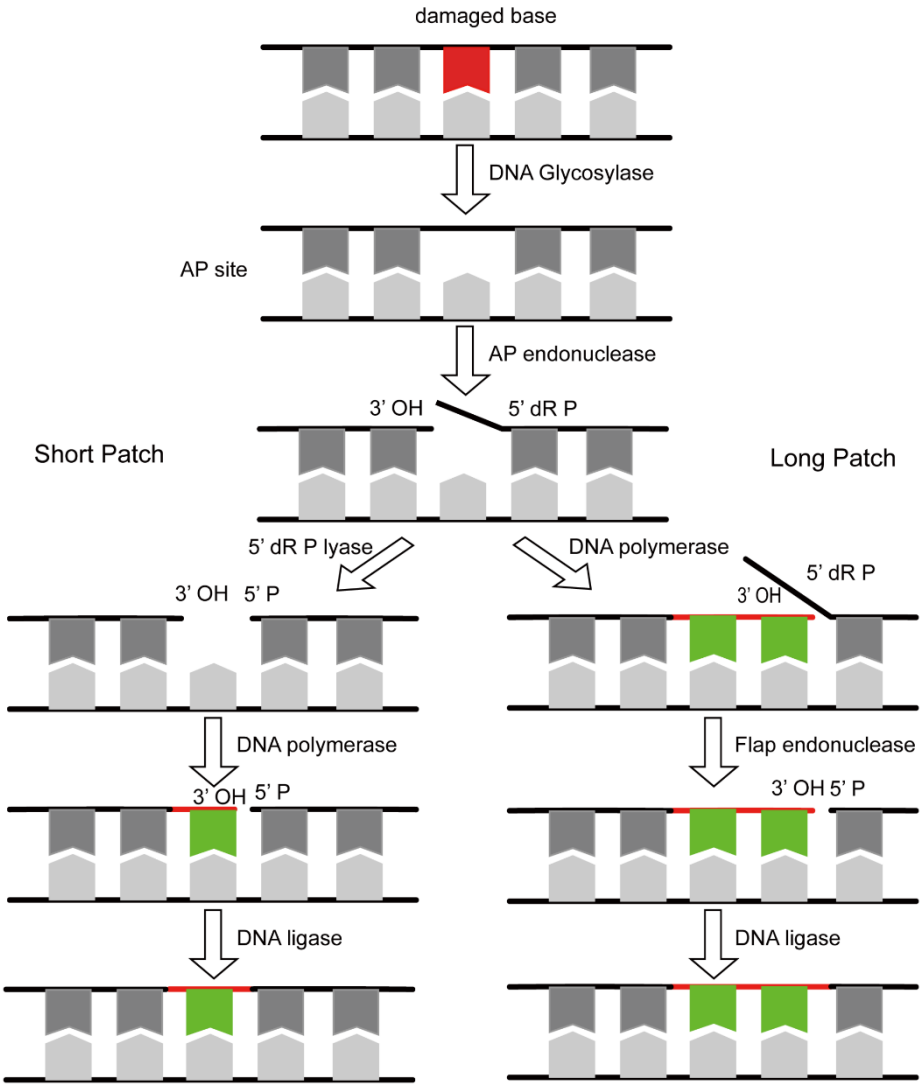

Figure 1.5 General representation of the base excision repair (BER) pathway. Reproduced with permission.[30] Copyright © 2006 Elsevier B.V.

Figure 1.5 illustrates general process of BER. The BER pathway is started with DNA glycosylases. After recognizing and cleaving specific damaged or incorrect bases, AP sites are formed. Subsequently, AP sites can be incised by a type of AP endonuclease. Followed by end processing, repair synthesis, and ligation, the resulting single-strand break can be repaired through different mechanisms, relying on the type of lesion and glycosylases,

physiological stage of the cell, and whether the cell is terminally differentiated or actively dividing[30]. One mechanism is short-patch repairing, achieving the replacement of one single nucleotide. Short-patch repair do not participate in replication and shows the same efficiency in proliferating and nonproliferating cells. The other called long-patch repairing, in which 2-10 new nucleotides are generated, mainly happening in proliferating cells and requiring a large amount of replication proteins. Meanwhile, there are many enzymes involved in BER process, DNA glycosylases, AP endonucleases, 5' dR P ylases, DNA polymerases, flap endonucleases and DNA ligase.

1.2.2 Functions and mechanism of APE1

Apurinic/apyrimidinic endonuclease 1 (APE1) is a crucial enzyme participated in BER pathway[31-32]. APE1 is considered as the most important AP endonuclease in human cells and responsible for restoring mutagenic and cytotoxic abasic lesions throughout cell cycles[33-35]. About 10,000 AP sites are estimated to occur spontaneously in every mammalian genome every day[2,17]. Thus, APE1 plays a key role in bases and DNA repairing.

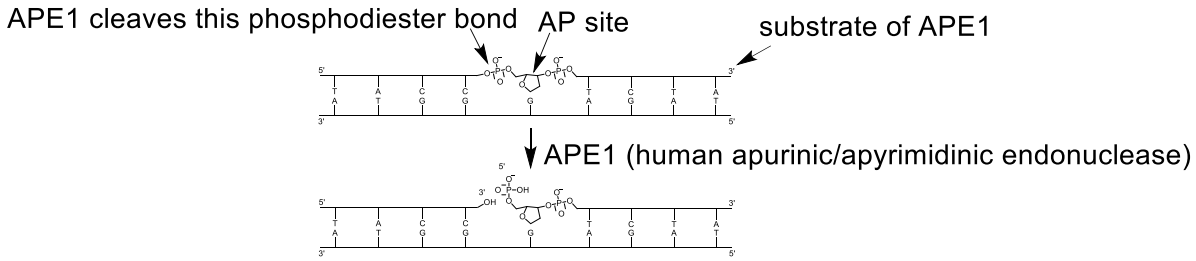

Figure 1.6 Illustration of DNA cleaving reactions of APE1 when a mono-functional glycosylase initiates a base excision repair pathway.

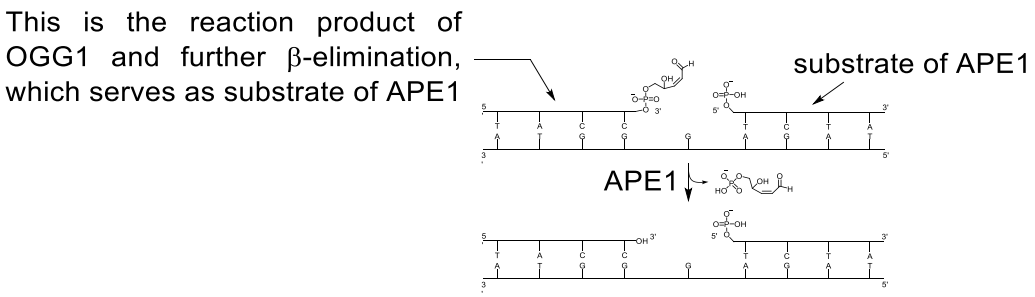

Figure 1.7 Illustration of DNA cleaving reactions of APE1 when a bifunctional glycosylase initiates a base excision repair pathway.

There are two major function of APE1, repair and redox, which are independent functions supported by the investigation that repair function and redox function can not influence each other [36-37]. If mono-functional glycosylase initiates the removal of damaged nitrogenous base in the base excision repair pathways, APE1 will cleave the 5' end phosphodiester backbone right next to the generated apurinic/apyrimidinic site (AP site) to produce a single-strand DNA break (**Figure 1.6**)[38] When a bifunctional glycosylase begins with a phosphodiester bond cleavage near an AP site, APE1 will chemically detach the resultant phospho-α, β-unsaturated aldehyde to generate free 3' hydroxyl end (**Figure 1.7**)[39]. In addition to its DNA cleaving functions (**Figure 1.6** and **Figure 1.7**), APE1 is known to serve as a redox co-activator to regulate DNA binding and activity of several transcriptional factors such as Egr-1, NF-κB, HIF1a and p53[40-42]. It has been elucidated that the APE1 redox activity presents great biological significance in eukaryotic transcriptional regulation of gene expression[43]. These above-mentioned observations illustrate that APE1 is a multifunctional protein in human cells and closely affiliated with cancer cell growth, proliferation and survival[44-50].

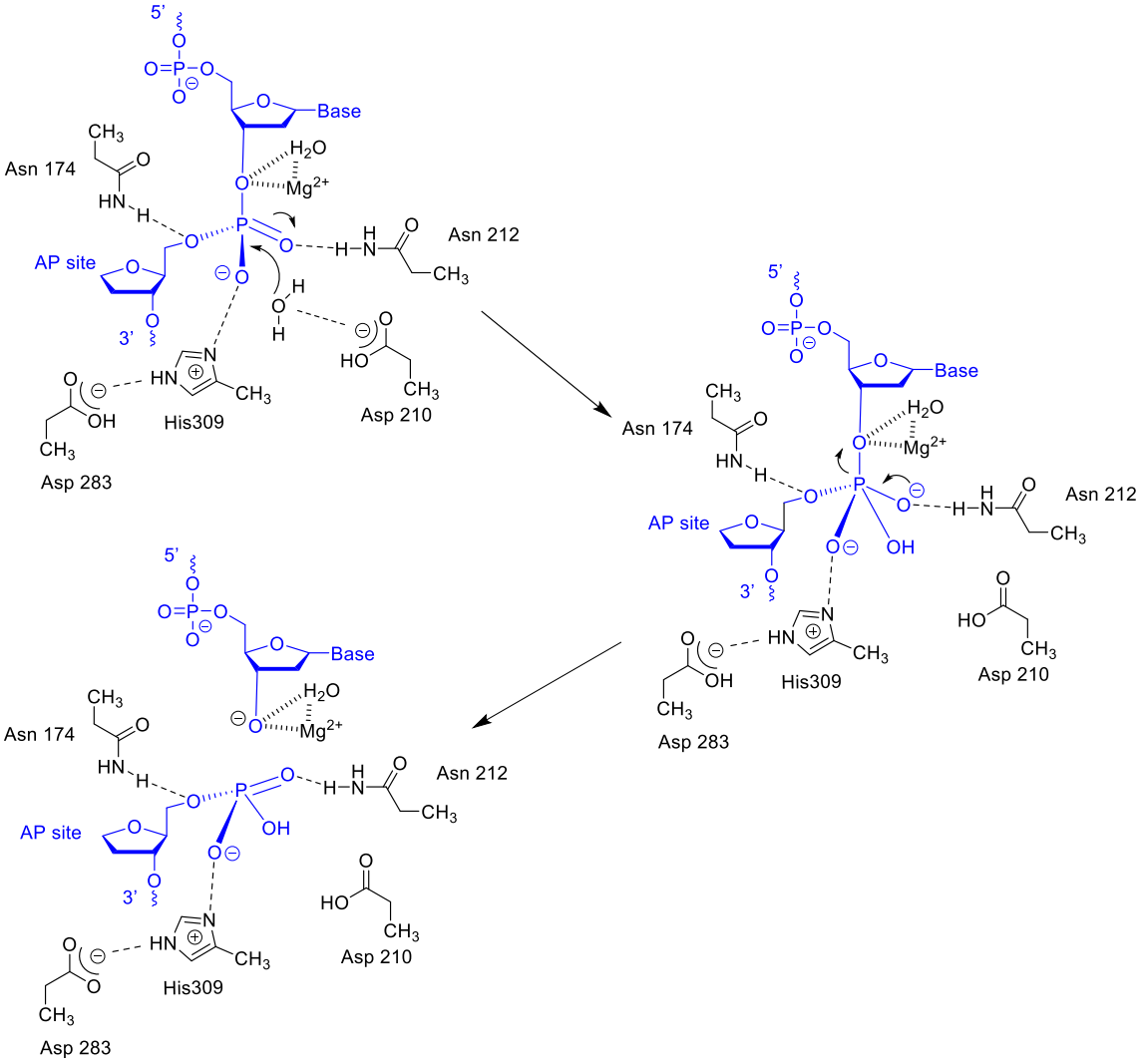

Figure 1.8 General mechanism of APE1 catalytic reaction. Reproduced with permission.[58] Copyright © 2000, Macmillan Magazines Ltd.

The mechanism of APE1 catalytic reaction has been proved since the crystal structures of APE1 with substrates were investigated[51-57]. **Figure 1.8** presents general illustration on how APE1 works. First, a water molecule is deprotonated by the Asp 210 residue in the active site, followed by a nucleophilic attack on the phosphorus atom in the phosphate group positioned 5' to the AP site. Then, a long pair from one oxygen atom hydrogen bonding to Asn 212 comes back to form phosphorus-oxygen double bond again. Finally, releasing the other one oxygen atom, a nick is generated to form a free 5' phosphate

termini linking to the AP site and a free 3’ hydroxyl termini on the regular nucleotide. These two termini structures are both stabilized by the Mg^{2+} ion[58].

1.2.3 APE1 as biomarker

APE1 is overexpressed in numerous kinds of cancer cells such as (1) breast cancer[59-60], (2) liver cancer[61-62], (3) lung cancer[60,63], (4) colorectal cancer[64-65], (5) ovarian cancer[66-67], (6) prostate cancer[68-69], (7) gastroesophageal cancer[67-68], (8) pancreatic cancer[61,70], (9) cervical cancer[71-72] (10) bladder cancer[68,73]. In addition, elevated levels of APE1 have been found in the blood serums of patients who suffer from (1) lung cancers[74] and (2) bladder cancers[75].

Radiotherapy[76] and DNA-interacting chemotherapeutic agents[77], on the other hand, are often designed to kill cancer cells by causing their genomic DNA damages. It is known nowadays, however, that many cancer cells are able to survive during radiotherapy and chemotherapy as a result of active expression of their enzymes and other functional proteins used in their DNA repair pathways[78-79]. These radioresistance and chemotherapy resistance were, for example, found in glioma[80], non-small cell lung cancer[81] and liver cancer[82], in which elevated levels of APE1 were observed simultaneously. These high expressions of APE1 exemplify that under radiation and chemotherapeutic conditions, cancer cells rely greatly on their DNA repair pathways to survive.

Since elevated expressions of APE1 are activated and associated with radiotherapy and chemotherapy in many cancer cells, it has been believed that combined use of inhibitors

of APE1 with radiotherapy or chemotherapeutic agents as a type of combination therapy[83] would be a more efficient mean for cancer treatment[84-86].

Consequently, these radiotherapy- and chemotherapy-activated expressions of APE1 along with other APE1-related observations on cancers have evidenced that APE1 is (i) a valid biomarker for cancer diagnosis and prognosis, and (ii) a potent biomolecular target of both monotherapy and combination therapy for fighting cancers.

1.3 Nanobiosensor

1.3.1 The unique properties of nanobiosensor

A biosensor is an analytical device containing a biological receptor component, used for a specific biochemical substance recognition with a physicochemical transducer[87]. The main challenge for biosensors development is achieving the rapid, accurate and convenient measurement of substances such as enzymes, antibodies, and protein biomarkers[88]. With the development of nanotechnology, the sizes of nanomaterials ranged from 1 to 100 nm such as nanoparticles, quantum dots, carbon nanotubes, graphene, graphene oxide, and graphene quantum dots have been integrated with various diagnostic biosensors[89-91].

Due to the unique optical, electronic and mechanical properties depending on special size and shape, using these nanomaterials cam improve the sensitivity and selectivity of sensors, and make biosensors convenient to use. For nanoparticles, the most significant characteristic is optical property, which show different color from the corresponding bulk structures. Though modification of nanoparticles interacted with the analyte, the

accumulation of nanoparticles can lead to the change of color[92-93]. This principle for detection has been successfully utilized in gold nanoparticles based biosensor[94]. Quantum dots are colloidal semiconductor nanocrystals and highly fluorescent. Therefore, quantum dots show great potential to use for biosensor for fluorescence detection. In 1998, Chan and Nie and reported the first example of using quantum dot-based biosensor for protein detection[95]. Carbon nanostructures such as graphene, graphene oxide, carbon nanotubes and graphene quantum dots present high surface area, great electron transport capabilities and extraordinary electrical conductivities[96-97]. Due to hexagonal networks constructed by sp^2 bond, planar structures of carbon nanostructures result in these remarkable properties[98]. Thus, carbon nanostructures have involved in many types of biosensors, for example, electrochemical, chemiluminescent, biological field effect transistors and fluorescence-based biosensors. In fluorescence-based assays, graphene and graphene oxide are widely used in the fabrication of biosensor for detection because of quenching properties[99-100].

1.3.2 DNA-based nanobiosensors

Over the past decades, DNA-based nanobiosensors have been fabricated since the development of DNA nanotechnology[101-102]. The specific recognition between a substrate and the targeted analyte and flexible DNA sequences design make biosensors cheap and sensitive for diagnosis.

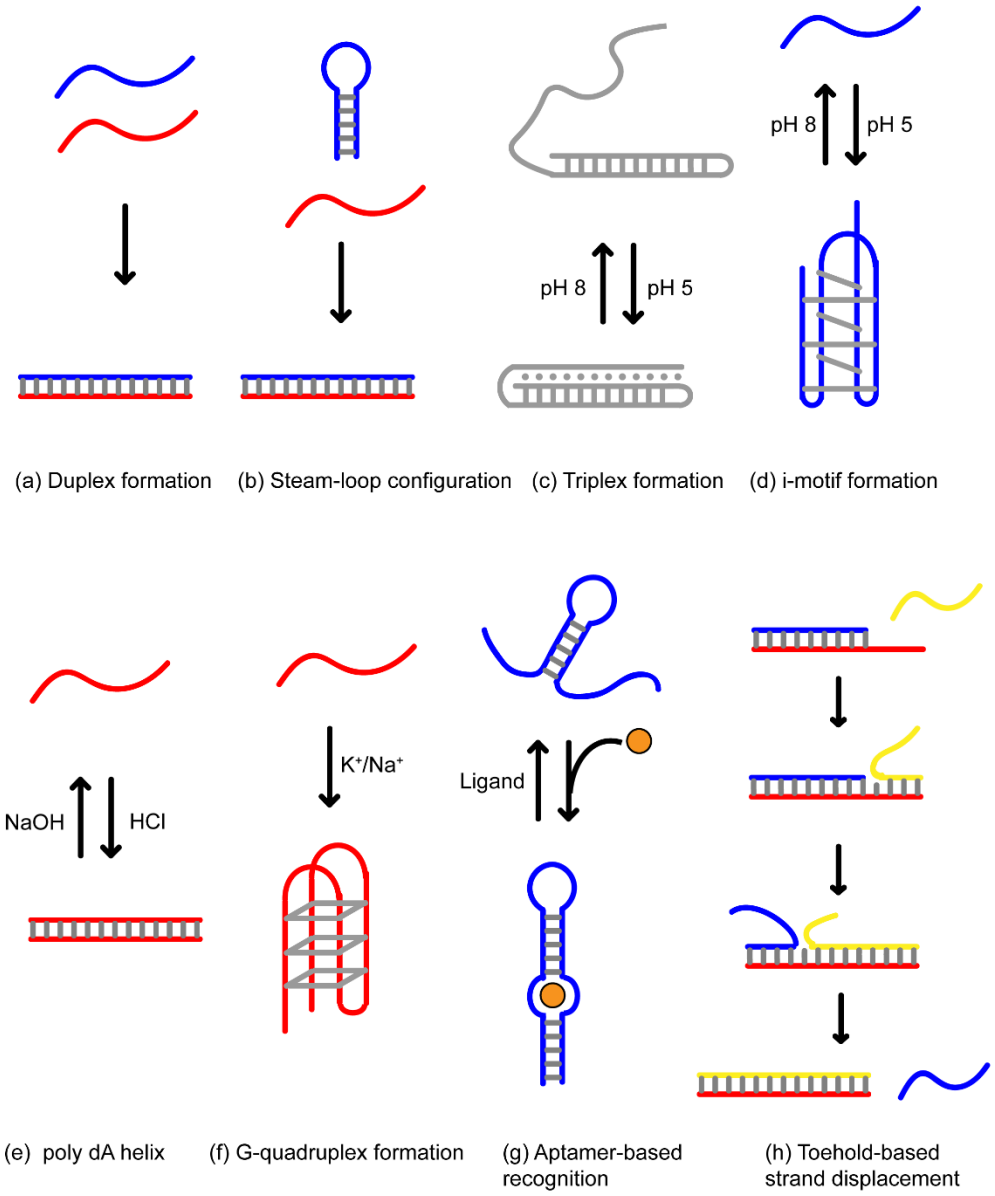

Figure 1.9 Concepts for building DNA nanobiosensors. (a) Hybridization of complementary DNA in duplex. (b) Hybridization of partly complementary DNA in stem-loop configuration. (c) Triplex formation under acidic conditions by sequence-specific oligonucleotide. (d) I-motif formation under acidic conditions by C-rich oligonucleotide. (e) Poly-dA helix formation under acidic conditions by poly deoxyadenosines oligonucleotide. (f) G-quadruplex formation in the presence of K^+ or Na^+ by G-rich oligonucleotide. (g) Aptamer recognition in the presence of specific ligands. (h) Toehold mediated strand displacement via

branch migration. Reproduced with permission.[102] Copyright © 2005 WILEY-VCH Verlag GmbH & Co. KGaA, Weinheim.

Several concepts for DNA-nanobiosensors are shown in **Figure 1.9**. Hybridization of a single-strand DNA or RNA to its complementary strand (**Figure 1.9**(a)), or a complementary segment in a stem loop (**Figure 1.9**(b)) is usually exploited in nucleic acid-based biosensors. Besides, the change of environmental factors such temperature can be monitored by this stem-loop configuration. A molecular beacon is constructed from oligonucleotide labelled a fluorophore and a quencher on the termini respectively. Triplex[103] (**Figure 1.9**(c)), i-motif formation[104] (**Figure 1.9**(d)), and poly-dA helix formation[105] (**Figure 1.9**(e)) are utilized for detecting pH changes depending on the alternation of structures under acidic conditions. The structure of G-quadruplex is formed from sequence-specific oligonucleotides in the presence of K^+ or Na^+ [106] (**Figure 1.9**(f)). Many DNA based biosensors are built according to the recognition of aptamer **(Figure 1.9**(g)). Due to high affinity binding to metal ions (such as K^+, Hg^{2+}, and Pb^{2+}), small organic molecules (such as ATP, amino acids, and vitamins), peptides, proteins (such as thrombin and growth factors), even whole cells or microorganisms (such as bacteria)[107-108], and oligonucleotides can bind with them and form a stable secondary structure. In addition, toehold mediated strand displacement[109] (TMSD, **Figure 1.9**(h)) is also a common strategy in the construction of DNA-based nanobiosensors, which is an enzyme-free pathway to swap one strand DNA with another strand.

There are many recognition methods in DNA-nanobiosensors, such as fluorescence, Fluorescence Resonance Energy Transfer (FRET), nanoparticle color change, gel electrophoresis, electrochemical signal, atomic force microscopy (AFM), and surface-

enhanced Raman spectroscopy (SERS). Fluorescence spectroscopy is one of the most common used in DNA-nanobiosensor for environmental monitoring and heavy metal ions detecting with high sensitivity and simplicity[110-111].

1.3.3 Fluorescence-based nanobiosensors

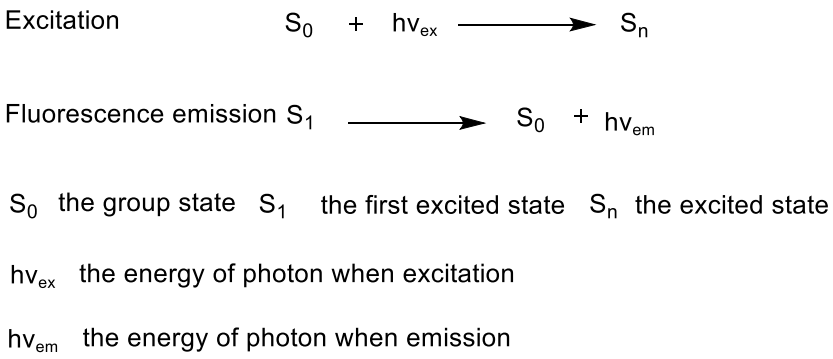

Figure 1.10 Mechanism of fluorescence generation.

Fluorescence is a phenomenon of light emission generated from a substance after absorbing light or other electromagnetic radiation. It's also a type of luminescence. Firstly, electrons in the substance are directly excited from the ground state to the excited state by absorption of a photon of energy. Subsequently, the electrons emit a photon of low energy which means light of longer wavelength and relax back to the ground state from the first excited state[112]. This process of fluorescence occurring can be described as the equations shown in **Figure 1.10**.

The average time from the excited state to relaxing to the ground state is the lifetime of fluorescence. Different fluorophores have their own lifetime based on their molecular structures. The lifetime of majority of fluorophores for common use ranges from 0.5 to 20

nanoseconds. Thus, the fluorescence lifetime is a critical property related to the application of fluorescence such as fluorescence resonance energy transfer (FRET). Besides, quantum yield is another important factor that we concern when we apply a fluorophore. The fluorescence quantum yield is used for describing the efficiency of fluorescence process, which is calculated by the number of photons emitted divided by the number of photons absorbed[108]. Fluorescence quantum yields are measured by comparison to a standard, and most common used fluorophores in our life are characterized by quantum yields within the range from 0.3 to 0.8.

Fluorescence is quite useful in many aspects, such as gemology, dyes, chemistry sensors and even energy-saving lamps. Typically, fluorescence as a labelling method plays a significant role in design of biosensor because of the sensitivity and convenience.

To induce the fluorescence signal, various fluorophores can be labelled on the nanobiosensors. Resulting from less response time and combination between a substrate and the targeted analyte with high selectivity and sensitivity, fluorescence-based nanobiosensor have further explored in disease diagnosis. For example, nanobiosensors with fluorophores are widely used for the diagnosis of cardiovascular diseases, diabetes and cancer[113]. Researchers also develop subcutaneous fat based nanobiosensors for glucose measurement in interstitial fluid[114].

Normally, fluorescent biosensor should be stable, nontoxic and nonimmunogenic to living cell. But it's not easy for fluorescent biosensor to get into to living cell. Nanostructures such as graphene quantum dots can solve this problem by serving as nanocarriers and delivering sensors into cell. Therefore, well-designed fluorescence-based nanobiosensors

show highly potential to achieve biomarkers and cancers diagnosis via biopsy extraction in living cell system[115].

References

1. Spencer, M, T *Acta Crystallographica*. **1959,** *12*, 66-71.
2. Talpaert-Borlé, M., Formation, *Mutat Res*. **1987,** *181*, 45-56.
3. Greer, S.; Zamenhof, S., *J. Mol. Biol.* **1962,** *4*, 123-41.
4. Lindahl, T.; Karlstrom, O., *Biochemistry* **1973,** *12*, 5151-4.
5. Strauss, B., Hill, T., *Biochim. Biophys. Acta* **1970,** *213*, 14-25.
6. Schuster, H., *Z. Naturforsch.* **1960,** *15b*, 298-304.
7. Iida, S.; Hayatsu, H., *Biochim. Biophys. Acta* **1971,** *240*, 370-5.
8. Demple, B.; Linn, S., *Nucleic Acids Res.* **1982,** *10*, 3781-9.
9. Müller, W. E. G.; Yamazaki, Z. I.; Breter, H. Y.; Zahn, R. K., *Eur. J. Biochem.* **1972,** *31*, 518-25.
10. Dunlap, B., Cerutti, P., *FEBS Lett.* **1975,** *51*, 188-90.
11. Troule, R.; Bert, C.; Bonicel, A., *Radiat. Res.* **1977,** *72*, 190-200.
12. Von Sonntag, C.; Hagen, U.; Schön-Bopp, A.; Schulte-Frohlinde, D., *Adv. Radiat. Biol.* **1981,** *9*, 109-42.
13. Ljungquist, S.; Lindahl, T., *J. Biol. Chem.* **1974,** *249*, 1530-5.
14. Lindahl, T., DNA glycosylases, *Progr. Nucleic Acid Res. Mol. Biol.* **1979,** *22*, 135-92.
15. Lindahl, T., DNA repair enzymes. *Annu. Rev. Biochem.* **1982,** *51*, 61-87.
16. Loeb, L. A.; Preston, B. D., *Annu Rev Genet*. **1986,** *20*, 201-30.
17. Lindahl, T., *Nature*. **1993,** *362*, 709-15.

18. Lehmann, A. R.; Niimi, A.; Ogi, T.; Brown, S.; Sabbioneda, S.; Wing, J. F.; Kannouche, P. L.; Green, C. M., *DNA Repair (Amst)* **2007,** *6*, 891-9.
19. Brakier, L.; Verly, W. G., *Biochim. Biophys. Acta*. **1970,** *213*, 296-311.
20. Boiteux, S.; Guillet, M., *DNA Repair (Amst)* **2004,** *3*, 1-12.
21. Flamée, P.-A.; Verly, W. G., *Biochem. J.* **1985,** *229*, 173-81.
22. Loeb, L. W., *Cell*. **1985,** *40*, 483-4.
23. Gentil, A.; Margot, A.; Sarasin, A., *Mutation Res.* **1984,** *129*, 141-7.
24. Su, Z. Z.; Avalosse, B.; Vos, J.-M.; Gornelis, J. J.; Rommelaere, J., *Mutation Res.* **1985,** *149*, 1-8.
25. Strauss, P. R.; Beard, W. A.; Patterson, T. A.; Wilson, S. H., *J. Biol. Chem.* **1997,** *272*, 1302-7.
26. Lodish, H.; Berk, A.; Matsudaira, P.; Kaiser, C. A.; Krieger, M.; Scott, M. P.; Zipursky, S. L.; Darnell, J., *Molecular Biology of the Cell (5th ed.)*. New York: WH Freeman. **2004,** pp 963.
27. Chatterjee, N.; Walker, G. C., *Environmental and molecular mutagenesis*. **2017,** *58*, 235-63.
28. Cheng, K. C.; Cahill, D. S.; Kasai, H.; Nishimura, S.; Loeb, L. A., *J Biol Chem*. **1992,** *267*, 166-72.
29. Krokan, H. E.; Bjørås, M., *Cold Spring Harbor perspectives in biology*. **2013**, *5*, a012583.
30. Fortini, P.; Dogliotti, E., *DNA Repair*. **2007,** *6*, 398-409.
31. Thakur, S.; Dhiman, M.; Tell, G.; Mantha, A. K., *Cell biochemistry and function.* **2015,** *33*, 101-12.
32. Li, M.; Wilson III, D. M., *Antioxidants & redox signaling.* **2014,** *20*, 678-707.

33. Antoniali, G.; Lirussi, L.; Poletto, M.; Tell, G., *Antioxidants & redox signaling.* **2014,** *20*, 621-39.
34. Esqueda, A.; Mohammed, M. Z.; Madhusudan, S.; Neamati, N., *Methods in molecular biology.* **2012,** *928*, 161-74.
35. Kelley, M. R.; Georgiadis, M. M.; Fishel, M. L., *Current molecular pharmacology.* **2012,** *5*, 36-53.
36. Luo, M.; Delaplane, S.; Jiang, A.; Reed, A.; He, Y.; Fishel, M.; Nyland II, R. L.; Borch, R. F.; Qiao, X.; Georgiadis, M. M.; Kelley, M. R., *Antioxidants & Redox Signaling.* **2008,** *10*, 1853-67.
37. McNeill, D. R.; Wilson III, D. M., *Mol. Cancer Res.* **2007,** *5*, 61-70.
38. Kazak, L.; Reyes, A.; Holt, I. J., *Nature reviews. Molecular cell biology* **2012,** *13*, 659-71.
39. Hegde, M. L.; Hazra, T. K.; Mitra, S., *Cell research* **2008,** *18*, 27-47.
40. Luo, M.; He, H.; Kelley, M. R.; Georgiadis, M. M., *Antioxidants & redox signaling.* **2010,** *12*, 1247-69.
41. Zhu, J.; Li, M.; Wang, D., *Chongqing Yixue.* **2010,** *39*, 2124-7.
42. Georgiadis, M. M., In *DNA Repair in Cancer Therapy*, Kelley, M. R., Ed. Academic Press: San Diego, **2012,** 235-55.
43. Fleming, A. M.; Ding, Y.; Burrows, C. J., *Proc. Natl. Acad. Sci.* **2017,** *114*, 2604-9.
44. Thakur, S.; Sarkar, B.; Cholia, R. P.; Gautam, N.; Dhiman, M.; Mantha, A. K., *Experimental and Molecular Medicine.* **2014,** *46*, e106.
45. Kaur, G.; Cholia, R. P.; Mantha, A. K.; Kumar, R., *J Med Chem.* **2014,** *57*, 10241-56.
46. Mantha, A. K., *J Biotechnol Biomater.* **2013,** *3*, e120.
47. Fishel, M. L.; Vascotto, C.; Kelley, M. R., In *DNA Repair and Cancer: From Bench to Clinic.*, Madhusudan, S.; Wilson III, D. M., Eds. CRC Press: FL, USA, **2013,** pp 233-87.

48. Jeon, B. H., *KSBMB News.* **2012,** *32*, 85-8.

49. Raffoul, J. J.; Heydari, A. R.; Hillman, G. G., *Journal of oncology.* **2012,** *2012*, 370481.

50. Al-Safi, R. I.; Odde, S.; Shabaik, Y.; Neamati, N., *Current molecular pharmacology.* **2012,** *5*, 14-35.

51. Beernink, P. T.; Segelke, B. W.; Hadi, M. Z.; Erzberger, J. P.; Wilson III, D. M.; Rupp, B., *J.Mol. Biol.* **2001,** *307*, 1023-34.

52. Oezguen, N.; Schein, C. H.; Peddi, S. R.; Power, T. D.; Izumi, T.; Braun, W., **2007,** *68*, 313-23.

53. Gorman, M. A.; Morera, S.; Rothwell, D. G.; de La Fortelle, E.; Mol, C. D.; Tainer, J. A.; Hickson, I. D.; Freemont, P. S., *EMBO J.* **1997,** *16*, 6548-58.

54. Mundle, S. T.; Delaney, J. C.; Essigmann, J. M.; Strauss, P. R., *Biochemistry*. **2009,** *48*, 19-26.

55. Mundle, S. T.; Fattal, M. H.; Melo, L. F.; Coriolan, J. D.; O'Regan, N. E.; Strauss, P. R., *DNA Repair (Amst).* **2004,** *3*, 1447-55.

56. Tsutakawa, S. E.; Shin, D. S.; Mol, C. D.; Izumi, T.; Arvai, A. S.; Mantha, A. K.; Szczesny, B.; Ivanov, I. N.; Hosfield, D. J.; Maiti, B.; Pique, M. E.; Frankel, K. A.; Hitomi, K.; Cunningham, R. P.; Mitra, S.; Tainer, J. A., *J. Biol. Chem*. **2013,** *288*, 8445-55.

57. Lipton, A. S.; Heck, R. W.; Primak, S.; McNeill, D. R.; Wilson III, D. M.; Ellis, P. D., *J. Am. Chem. Soc*. **2008,** *130*, 9332-41.

58. Mol, C. D.; Izumi. T.; Mitra, S.; Tainer, J. A., *Nature*. **2000,** *403*, 451-6.

59. Coskun, E.; Jaruga, P.; Reddy, P. T.; Dizdaroglu, M., *Biochemistry.* **2015,** *54*, 5787-90.

60. Woo, J.; Park, H.; Sung, S. H.; Moon, B. I.; Suh, H.; Lim, W., *PloS one.* **2014,** *9*, e99528.

61. Cesaratto, L.; Codarin, E.; Vascotto, C.; Leonardi, A.; Kelley, M. R.; Tiribelli, C.; Tell, G., *PloS one.* **2013,** *8*, e70909.
62. Di Maso, V.; Mediavilla, M. G.; Vascotto, C.; Lupo, F.; Baccarani, U.; Avellini, C.; Tell, G.; Tiribelli, C.; Croce, L. S., *PloS one.* **2015,** *10*, e0143289.
63. Wang, B.; Qiu, H., *Gouji Jianyan Yixue Zazhi.* **2013,** *34*, 3384-6.
64. Lou, D.; Zhu, L.; Ding, H.; Dai, H. Y.; Zou, G. M., *Oncology letters.* **2014,** *7*, 1078-82.
65. Canbay, E.; Cakmakoglu, B.; Zeybek, U.; Sozen, S.; Cacina, C.; Gulluoglu, M.; Balik, E.; Bulut, T.; Yamaner, S.; Bugra, D., *Current medical research and opinion.* **2011,** *27*, 1295-302.
66. Fishel, M. L.; He, Y.; Reed, A. M.; Chin-Sinex, H.; Hutchins, G. D.; Mendonca, M. S.; Kelley, M. R., *DNA repair.* **2008,** *7*, 177-86.
67. Al-Attar, A.; Gossage, L.; Fareed, K. R.; Shehata, M.; Mohammed, M.; Zaitoun, A. M.; Soomro, I.; Lobo, D. N.; Abbotts, R.; Chan, S.; Madhusudan, S., *British journal of cancer.* **2010,** *102*, 704-9.
68. Kelley, M. R.; Cheng, L.; Foster, R.; Tritt, R.; Jiang, J.; Broshears, J.; Koch, M., *Clinical cancer research : an official journal of the American Association for Cancer Research.* **2001,** *7*, 824-30.
69. Evans, A. R.; Limp-Foster, M.; Kelley, M. R., *Mutation research.* **2000,** *461*, 83-108.
70. Jiang, S.; Zhu, L.; Tang, H.; Zhang, M.; Chen, Z.; Fei, J.; Han, B.; Zou, G. M., *International journal of oncology.* **2015,** *47*, 610-20.
71. Thakur, S.; Sarkar, B.; Cholia, R. P.; Gautam, N.; Dhiman, M.; Mantha, A. K., *Experimental & molecular medicine.* **2014,** *46*, e106.
72. Qing, Y.; Yang, X. Q.; Zhong, Z. Y.; Lei, X.; Xie, J. Y.; Li, M. X.; Xiang, D. B.; Li, Z. P.; Yang, Z. Z.; Wang, G.; Wang, D., *BMC cancer.* **2010,** *10*, 71.

73. Sak, S. C.; Harnden, P.; Johnston, C. F.; Paul, A. B.; Kiltie, A. E., *Clinical cancer research : an official journal of the American Association for Cancer Research.* **2005,** *11*, 6205-11.

74. Zhang, Y.; Fan, S.; Wang, Dong.; Yang, Z.; Xiang, D.; Li, Z.; Chen, J.; Jiang, Y., *J Third Mil Med Univ.* **2007,** *29*, 776-778.

75. Shin, J. H.; Choi, S.; Lee, Y. R.; Park, M. S.; Na, Y. G.; Irani, K.; Lee, S. D.; Park, J. B.; Kim, J. M.; Lim, J. S.; Jeon, B. H., *Cancer research and treatment : official journal of Korean Cancer Association.* **2015,** *47*, 823-33.

76. Matsumoto, K., *Yakugaku zasshi : Journal of the Pharmaceutical Society of Japan.* **2015,** *135*, 719-24.

77. Baudino, T. A., *Current drug discovery technologies.* **2015,** *12*, 3-20.

78. Thoms, J.; Bristow, R. G., *Seminars in radiation oncology.* **2010,** *20*, 217-22.

79. Helleday, T.; Petermann, E.; Lundin, C.; Hodgson, B.; Sharma, R. A., *Nat Rev Cancer.* **2008,** *8*, 193-204.

80. Silber, J. R.; Bobola, M. S.; Blank, A.; Schoeler, K. D.; Haroldson, P. D.; Huynh, M. B.; Kolstoe, D. D., *Clinical Cancer Research.* **2002,** *8*, 3008-18.

81. Wang, D.; Xiang, D. B.; Yang, X. Q.; Chen, L. S.; Li, M. X.; Zhong, Z. Y.; Zhang, Y. S., *Lung Cancer.* **2009,** *66*, 298-304.

82. Cesaratto, L.; Codarin, E.; Vascotto, C.; Leonardi, A.; Kelley, M. R.; Tiribelli, C.; Tell, G., *PloS one.* **2013,** *8*, e70909.

83. Li, F.; Zhao, C.; Wang, L., *International journal of cancer. Journal international du cancer.* **2014,** *134*, 1257-69.

84. Tell, G.; Demple, B., *Oncotarget.* **2015,** *6*, 584-585.

85. Raffoul, J. J.; Heydari, A. R.; Hillman, G. G., *Journal of oncology.* **2012,** *2012*, 11.

86. Wilson, D. M., 3rd; Simeonov, A., *Cellular and molecular life sciences : CMLS.* **2010,** *67*, 3621-31.

87. Tothill, I. T., *Semin. Cell Dev. Biol.* **2009**, *20*, 55-62.

88. Haun, J. B.; Yoon, T.; Lee, H. J.; Weissleder, R., *Wiley Interdiscipl. Rev. Nanomed. Nanobiotechnol*. **2010**, *2*, 291-304.

89. Ahuja, R. T.; Kumar, D., *Sens. Actuators B.* **2009**, *136*, 275-86.

90. Lei, J.; Ju, H., *Chem. Soc. Rev*. **2012**, *41*, 2122-34.

91. Zhang, Y.; Guo, Y.; Xianyu, Y.; Chen, W.; Zhao, Y.; Jiang, X., *Adv. Mater*. **2013**, *25*, 3802-19.

92. Tokel, O.; Inci, F.; Demirci, U., *Chem Rev.* **2014**, *114*, 5728-52.

93. Daniel, M.-C.; Astruc, D., *Chem Rev.* **2004**, *104*, 293-346.

94. Parolo, C.; Merkoci, A., *Chem Soc Rev.* **2013**, *42*, 450-7.

95. Chan, W. C. W.; Nie, S., *Science.* **1998**, *281*, 2016-8.

96. Chen, D.; Feng, H.; Li J., *Chem Rev.* **2012**, *112*, 6027-53.

97. Li, Z.; Liu, Z.; Sun, H.; Gao, C., *Chem Rev.* **2015**, *115*, 7046-117.

98. Georgakilas, V.; Perman, J. A.; Tucek, J.; Zboril, R., *Chem Rev.* **2015**, *115*, 4744-822.

99. Morales-Narváez, E.; Merkoçi, A., *Adv Mater*. **2012,** *24*, 3298-308.

100. Pumera, M., *Mater Today.* **2011**, *14*, 308-15.

101. Bath, J.; Turberfield, A. J., *Nat. Nanotech*. **2007**, *2*, 275-84.

102. Simmel, F. C.; Dittmer, W. U., *Small*. **2005**, *1*, 284-99.

103. Idili, A.; Vallee-Belisle, A.; Ricci, F., *J. Am. Chem. Soc*. **2014**, *136*, 5836-9.

104. Modi, S.; Swetha, M. G.; Goswami, D.; Gupta, G. D.; Mayor, S.; Krishnan, Y., *Nature Nanotech*. **2009,** *4*, 325-30.

105. Chakraborty, S.; Sharma, S.; Maiti, P. K.; Krishnan, Y., *Nucl. Acids Res*. **2009**, *37*, 2810-7.

106. Burge, S.; Parkinson, G. N.; Hazel, P.; Todd, A. K.; Neidle, S., *Nucl. Acids Res*. **2006**, *34*, 5402-15.

107. Song, S.; Wang, L.; Li, J.; Fan, C.; Zhao, J., *Trends Anal. Chem*. **2008**, *27*, 108-17.

108. Tombelli, S.; Minunni, M.; Mascini, M., *Biosens. Bioelectron*. **2005**, *20*, 2424-34.

109. Yurke, B.; Turberfield, A. J.; Mills Jr, A. P.; Simmel, F. C.; Neumann, J. L., *Nature*. **2000**, *406*, 605-8.

110. Han, J.; Burgess, K., *Chem. Rev*. **2010,** *110*, 2709-28.

111. McGlynn, S. P., *J. Am. Chem. Soc.* **1966,** *88*, 5688.

112. Wang, H.; Wang, D.; Wang, Q.; Li, X.; Schalley, C. A., *Org. Biomol. Chem*. **2010,** *8*, 1017-26.

113. Cibele G., Prof. Pier Andrea Serra (Ed.), **2011**. ISBN: 978-953-307-443-6, InTech, Europe. DOI: 10.5772/928.

114. Cengiz, E.; Tamborlane, W. V., *Diabetes Tech. Therapeutics*. **2009,** *11*, S11-6.

115. Morris M. C., *J. Biosens. Bioelectron*. **2012**, *3*, e111.

Chapter 2

Catalytic Properties of APE1 Based on Substrate Diversity

2.1. Background

APE1 is a base excision repair enzyme, incising the DNA 5' phosphodiester backbone to AP site and generating a nick with 5'-deoxyribose phosphate and 3'-hydroxyl ends[1-8]. Many catalytic properties studies have been done to demonstrate that APE1 can successfully incise DNA with 3' modifications to AP site and remove nucleoside analogues from the 3' ends of DNA, which indicated that APE1 has a great tolerance with 3' changes[9-12]. Excluding DNA with 3' modifications to AP site, however, there is no report to systematically illustrate the catalytic properties of APE1 based on various DNA substrates.

Search for APE1 inhibitors from natural products and synthetic compounds has been conducted in the past to discover APE1-interacting anticancer drug candidates[13-15]. Even though there has been no FDA-approved APE1 inhibitors for clinical treatment of cancers thus far, two of the low molecular APE1 inhibitors, methoxyamine and lucanthone, have been in Phase 2 and Phase 1 clinical trials separately at the present time. These clinical trial studies exemplify the impacts of APE1 inhibitors on discovery of new anticancer chemotherapeutic agents. Many previously identified low molecular weight APE1 inhibitors, on the other hand, are known to interact with more than one biological targets in cells. Methoxyamine and lucanthone, for example, are capable of intercalating duplex DNA[16] and inhibiting human thrombin respectively[17] besides their function as APE1 inhibitors. It is believed that substrate-based inhibitors are generally specific because specified recognitions and interactions occur between substrate analogs and functional groups of active sites of enzymes[18]. However, development of substrate-based APE1 inhibitors have not yet been attempted thus far.

In this chapter, we are planning to design and synthesize a series of substrate-based oligonucleotides of APE1 and identify reactivity of APE1 in the presence of those designed substrates under physiological buffer conditions. Herein, we select three types of oligodeoxyribonucleotides as substrates to investigate substrate diversity of APE1:

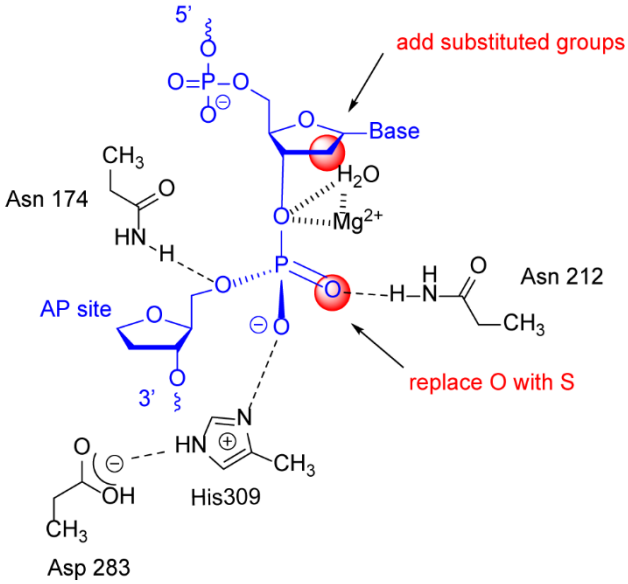

Figure 2.1 Illustration of two pathway of 5' modification basing on APE1 catalysis mode.

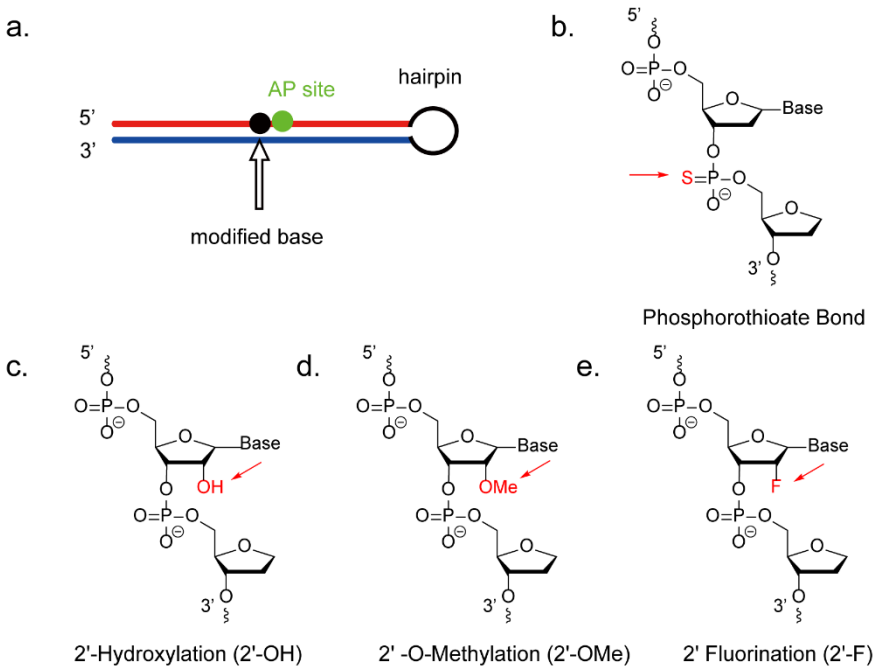

Figure 2.2 Illustration of the structures of DNA with modifications to 5' AP site as APE1 substrates. (a) Position of modified base. (b) Phosphorothioate bond modification. (c) 2'-Hydroxylation (2'-OH) modification. (d) 2' -O-Methylation (2'-OMe) modification. (e) 2' Fluorination (2'-F) modification.

(1) DNA with modifications to 5' AP site. In contrast to 3' modification to AP site, there are few studies on how different modifications to 5' AP site affect the reactivity of DNA to APE1. Meanwhile, the mode of action of APE1 on its substrates has been well characterized in the past[19]. Once APE1 recognizes and binds to DNA sequence around an AP site of duplex DNA, a water molecule as a nucleophile will attach the phosphate at the 5' end of AP site to form hexahedron structure[19]. Oxygen atom in 5' phosphate group on AP site coordinates with metal ions such Mg^{2+}, Ca^{2+} and Mn^{2+} or forms hydrogen bond with hydrogen from amino groups to lower the energy of transition state[20-22]. Since APE1 chiefly recognizes and binds the base pairs surrounding AP site, we think that the coordination effect and steric effect may have a significant influence on the reactivity between substrates and

APE1 (**Figure 2.1**). Herein, we design four oligodeoxyribonucleotides containing AP stie which have the same nucleotides sequence with various modification to 5' AP as APE1 substrates, meanwhile may be possible as APE1 inhibitors. One oligodeoxyribonucleotide has a phosphorothioate modification on the 5' AP site. Resulting from different ability of coordination and hydrogen bond formation between S and O, different transition state may change the catalytic reactivity. We believed that the weak electronegativity of sulfur atom would strengthen the chemical bond that will be broken down by APE1, thus delaying the reactant-product conversion process. The other three oligodeoxyribonucleotides are both modified on 2' position of the ribose linked to 5' AP site, which are 2'-Hydroxylation (2'-OH), 2' -O-Methylation (2'-OMe) and 2' Fluorination (2'-F), respectively. By inducing different groups on 2' position, the stabilization of O from phosphate group with metal ion can be affected. The structures of modified part are shown in **Figure 2.2**.

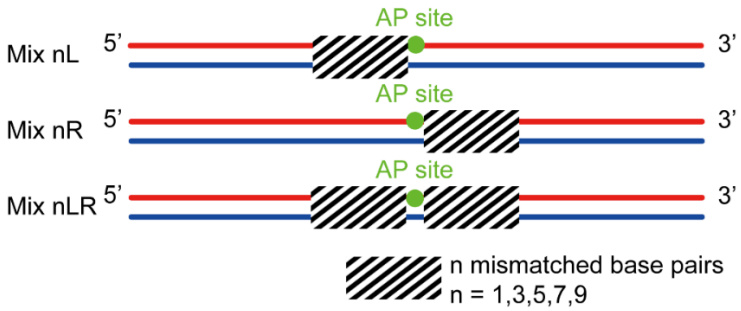

Figure 2.3 Illustration of the structures of mismatched DNA as APE1 substrates.

(2) Mismatched DNA. DNA mismatch is a type of DNA damage generated by nucleotide misincorporation during DNA complication and recombination[23]. These DNA base-base mismatches usually cause by DNA polymerase slippage, leading to mutations with high potential[24-27]. DNA mismatch pair attracts many researchers' attention to study on its mechanisms and functions[23, 28-33]. Therefore, we assume that mismatched DNA containing

AP site should be a substantial type of oligodeoxyribonucleotides as APE1 substrates. To find out how mismatched pairs affect the activity of DNA as APE1 substrates, we decide to discuss two aspects: one is the number of mismatched pairs, and the other is the location of the mismatched area towards AP site. Thus, we design 51-mer DNA whose AP site is positioned in the center, and 1,3,5,7 and 9 mismatched base pairs are respectively placed before AP site (adjacent to 5' of AP site, called 5' mismatched DNA), after AP site (adjacent to 3' of AP site, called 3' mismatched DNA) or on both sides of AP site relying on the 5' to 3' direction of the single strand containing AP site (**Figure 2.3**).

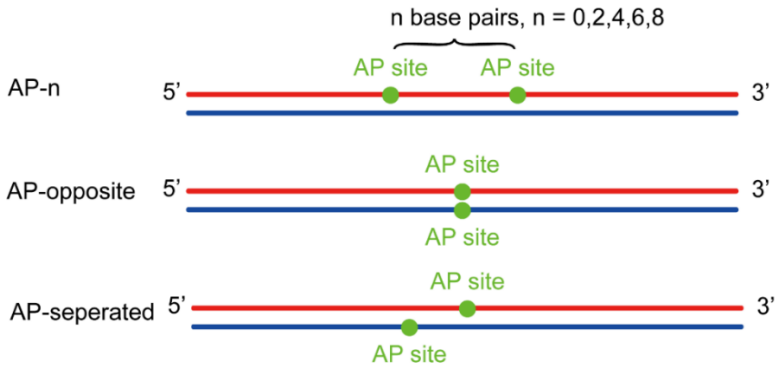

Figure 2.4 Illustration of the structures of DNA containing two AP sites as APE1 substrates.

(3) DNA containing two AP sites. DNA in cells with more than one AP site is possibly formed. Nobody has reported whether APE1 can cleave DNA containing multiple AP sites. We consequently study the effect of DNA containing two reaction sites on APE1 reactivity. First, we consider the situation that two AP sites are located in the same strands. Two AP sites are divided by 0, 2, 4, 6 and 8 nucleotides respectively and positioned in the same single strand (**Figure 2.4**). Followed by annealing with complementary single strand, we construct various DNA depended on the distance between two AP sites. In addition, the situation of two AP sties locate in different strands should be considered. Therefore, we design two kinds

of DNA containing two AP sites according to the position of two AP sites is in paired or not (**Figure 2.4**).

2.2 Study on DNA with modifications to 5' AP site as APE1 substrates

2.2.1 DNA sequences

Name of DNA	Nucleotides sequence (5' to 3')
Mod sd	ACTGGAGCGG/idSp/TCGACGACGCGAAGCGTCGTCGACC CGCTCCAGT
Mod P	ACTGGAGCGG*/idSp/TCGACGACGCGAAGCGTCGTCGACC CGCTCCAGT
Mod OH	ACTGGAGCG/rG//idSp/TCGACGACGCGAAGCGTCGTCGACC CGCTCCAGT
Mod OMe	ACTGGAGCG/i2OMeG//idSp/TCGACGACGCGAAGCGTCGTCG ACCCGCTCCAGT
Mod F	ACTGGAGCG/i2FG//idSp/TCGACGACGCGAAGCGTCGTCGAC CCGCTCCAGT

Table 2.1 Nucleotides sequences of APE1 substrates with 5' modifications. /idSp/ = dSpacer (AP site). * = Phosphorothioate. /rG/ = RNA G. /i2OMeG/ = 2`-O-Methyl G. /i2FG/ = 2F-RNA G.

2.2.2 Materials and Methods

Product(s)	Manufacturer
Oligodeoxyribonucleotides	Sangon Biotech (Shanghai, China)
APE1	New England Biolabs (Singapore)
Acrylamide	Invitrogen (Carlsbad, CA, USA)
N,*N'*-Methylenebisacrylamide	Sigma-Aldrich (USA)
Ammonium persulfate	Bio-Rad Laboratories (Singapore)
TEMED	Bio-Rad Laboratories (Singapore)
5bp DNA ladder	Thermo Fisher (Vilnius, Lithuania)
Ethidium bromide solution, 10mg/ml	Bio-Rad Laboratories (Singapore)
6 × DNA loading dye	Fermentas (Waltham, MA, USA)
1M Tris buffer, pH 8.0	1st Base (Singapore)
10 × Tris-borate-EDTA (TBE) buffer, pH 8.3	Vivantis (Malaysia)
Eppendorf tubes, Pipette tips	Greiner (Singapore)
Vortex mixer	Labnet international (Edison, NJ, USA)
Electrophoresis power supply	Consort (Turnhout, Belgium)
G:BOX Chemi gel doc system	Syngene (Cambridge, UK)

Table 2.2 Materials used study on DNA with modifications to 5' AP site as APE1 substrates. Other chemicals used in this study (such as salts and buffers) were supplied by Sigma-Aldrich with analytical grade or molecular biology grade.

Annealing for Oligodeoxyribonucleotides modified to 5' AP site

100 μM stock solutions were respectively prepared by adding deionized water to dissolve oligodeoxyribonucleotides with 5' modification (in **Table 2.1**). Diluting the stock solutions with deionized water, pH buffer and salt, new mixed solutions in total volume of

100 µl with 10 µM oligodeoxyribonucleotides, 10 mM Tris buffer (pH 8.0) and 50 mM NaCl were formed. These mixed solutions were incubated for 5 min at 95 °C, and subsequently slowly cooled down to room temperature (25 ^{o}C) for 2 h in air. The secondary structures of unimolecular DNA (Mod-sd, Mod-P, Mod-OH, Mod-OMe and Mod-F) were constructed after annealing process.

Catalytic reaction of 5' modifications DNA with APE1

10 pmol annealed 5' modification DNA (Mod-sd, Mod-P, Mod-OH, Mod-OMe and Mod-F) were respectively reacted with 5 nM APE1 in APE1 buffer (20 mM Tris-acetate (pH 8.0), 50 mM CH_3COOK, 10 mM $Mg(CH_3COO)_2$ and 1 mM DTT) for 2 h at 37 °C in a total volume of 20 µl. Different concentrations of APE1 and incubation times were used according to reaction conditions as mentioned in the results and discussion section.

Polyacrylamide Gel electrophoresis

15 % non-denaturing polyacrylamide gel was prepared with 142.5 g acrylamide, 7.5 g *N,N'*-methylenebisacrylamide and DI water forming 1 L solution. By adding 4 µl 6 × DNA loading dye to 20 µl samples after reaction, the mixtures were rapidly loaded on a 15 % non-denaturing polyacrylamide gel. Gel electrophoresis were conducted at 300 V in 1 × TBE buffer solution for 4 h. Then polyacrylamide gels were stained in 1 × TBE buffer of ethidium bromide for 30 min. Data was analyzed by using G:BOX iChemi gel documentation system (Syngene).

2.2.3 Results and Discussion

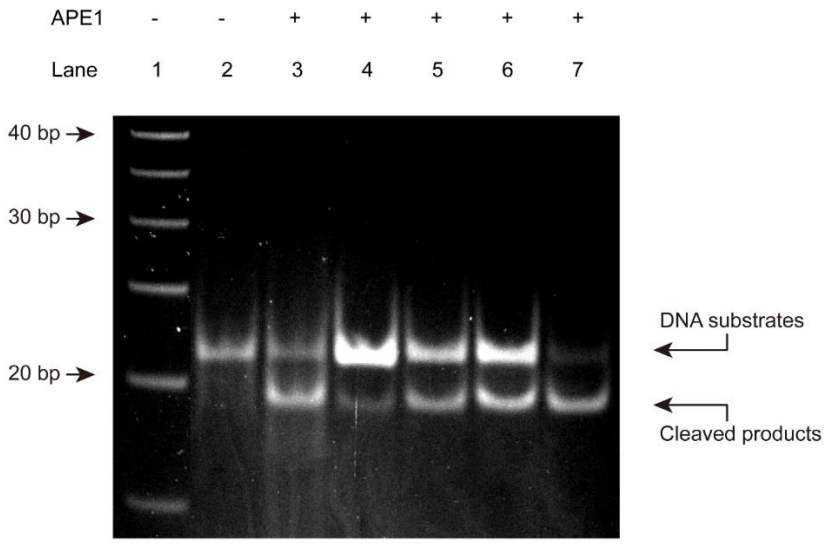

Figure 2.5 Gel electrophoretic analysis of DNA with modifications to 5' AP site as APE1 substrates. Lane 1: 5 bp DNA ladder; Lane 2: Mod-sd without APE1; Lane 3: Mod-sd in the presence of APE1; Lane 4: Mod-P in the presence of APE1; Lane 5: Mod-OH in the presence of APE1; Lane 6: Mod-OMe in the presence of APE1; Lane 7: Mod-F in the presence of APE1.

As shown in **Figure 2.5**, by comparing the results of Mod-sd in the absence of APE1 with in the presence of APE1 (Lane 2 and Lane 3), it indicated that the upper band was unreacted substrate, and the lower band was APE1 cleaved product. Meanwhile, comparison between Lane 1 and Lane 3, the length of the upper band in Lane 3 was ranged from 20 bp to 25 bp while the length of the upper band was ranged from 15 bp to 20 bp. Thus, the upper band was in accordance with the fact that substrate Mod-sd was annealed from a 45-mer oligonucleotide with a thermostable hairpin. Moreover, since AP site was positioned 10 bp away from the end, cleaved oligonucleotide part was easily dissociated from double-strand DNA, leading to the result that cleaved product migrated faster than substrate. Thus, we confirmed that the upper band presented substrate and the lower band presented product.

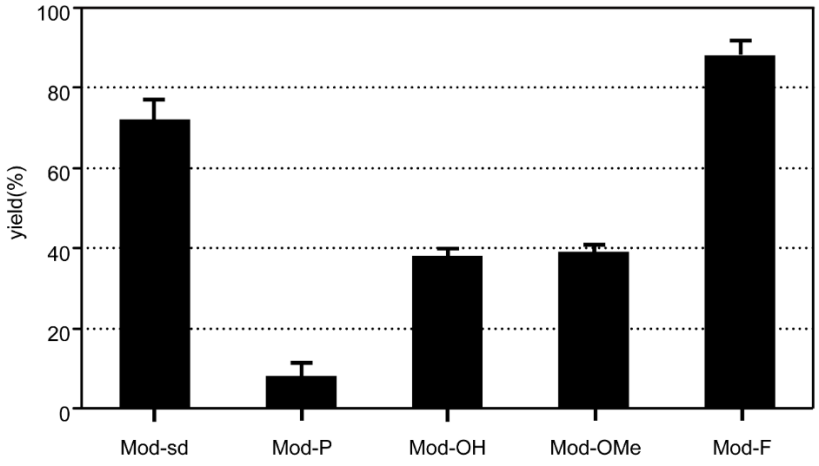

Figure 2.6 Quantitative analysis of activity of DNA with modifications to 5’ AP site as APE1 substrates. Yields were calculated according to relative fluorescence intensity by Gene Tools.

The ratios of bands were analyzed by Gene Tools. **Figure 2.6** presented the results of quantitative analysis. Normal DNA substrate without any modification (Mod-sd) showed 72 % of product, while substrate modified with phosphorothioate bond (Mod-P) demonstrated lowest activity and only generated 8 % of product. Substrates with modification of 2’-OH (Mod-OH) and 2’-OMe (Mod-OMe) showed moderate activity with 38 % and 39 % yield, respectively. With generating 88 % yield of product, 2’-F modified substrate (Mod-F) presented highest activity towards APE1 even higher than Mod-sd.

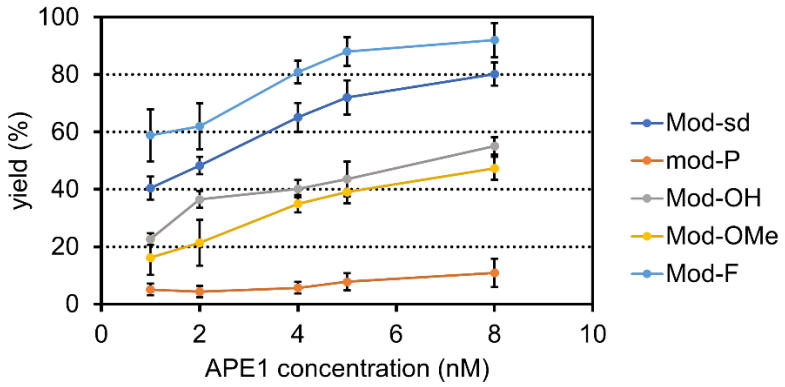

Figure 2.7 Correlation between APE1 concentration and yield of DNA with modifications to 5’ AP site as APE1 substrates. Yields were calculated according to relative fluorescence intensity by Gene Tools.

To investigate activity of DNA with different modifications to 5’ AP site towards APE1 comprehensively, we studied reaction yield of modified substrates depending on APE1 concentration. By changing the concentrations of APE1 from 1 nM to 8 nM and fixing the incubation time as 2 h, gel electrophoretic analyses were conducted, and specific data was calculated by Gene Tools. Correlation between APE1 concentration and percent of product was shown in **Figure 2.7**. From the curve trends, we found that when the concentrations of APE1 were below 5 nM, the overall reaction rate changed fast. The yields of products were in almost constant level when the concentrations of APE1 were over 5 nM. Therefore, 5 nM APE1 was used as a standard condition for further investigations in this chapter. Meanwhile, comparing with different curves, Mod-F gave higher yields than Mod-sd. Mod-OH and Mod-OMe showed moderate yields, while Mod-P remained very low level of yields which were below 10 %.

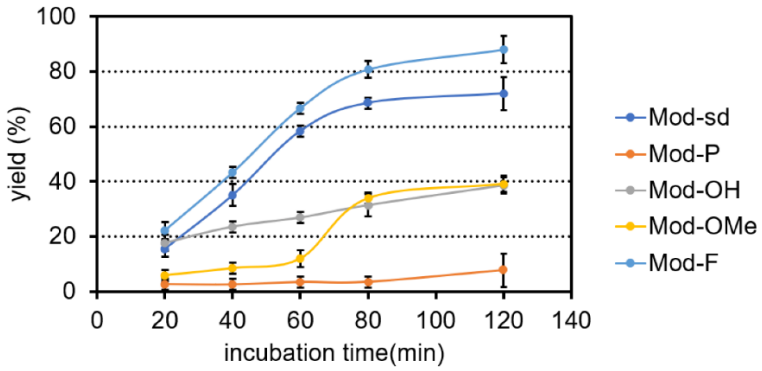

Figure 2.8 Correlation between incubation time and yield of DNA with different modifications to 5' AP site as APE1 substrates. Yields were calculated according to relative fluorescence intensity by Gene Tools.

In addition, control experiment towards incubation time was conducted. From **Figure 2.8**, it can be seen that yields of products were increased rapidly within 1 h at 37 °C according to correlation between reaction time and percent of product. Thus, we chose 2 h incubation time to make sure the substrates were sufficiently reacted. Incubation time-dependent experiment also indicated that activity order of substrates towards APE1 from high to low was Mod-F, Mod-sd, Mod-OH similar as Mod-OMe and Mod-P.

2.2.4 Conclusions

Modification on the 5' AP site can highly affect activity of DNA as APE1 substrates, which is consistent with our proposal. In detail, phosphorothioate modification on the 5' AP site of DNA shows poor compatibility as APE1 substrate, since the original oxygen atom substituted by sulfur atom gets involved in the process of strand cleavage. 2'-Hydroxylation and 2' -O-Methylation on the ribose linked to 5' AP site of DNA present lower activity than AP site containing DNA without any modification, may resulting from the steric effects of -

OH and -OMe group. Surprisingly, DNA which is modified by 2'-Fluorination on the ribose linked to 5' AP site can be incised more effectively and efficiently than normal APE1 substrate. To find out the effect of 2' fluorine, we need further exploration in the future.

In conclusion, activity order of DNA with different modifications to 5' AP site towards APE1 from high to low is: (1) DNA with 2'- Fluorination on the ribose linked to 5' AP site (2) DNA without any modification (3) DNA with 2'-Hydroxylation on the ribose linked to 5' AP site similar as DNA with 2' -O-Methylation on the ribose linked to 5' AP site (4) DNA with phosphorothioate modification on the 5' AP site. In addition, we believe that DNA with phosphorothioate modification on the 5' AP site will be suitable as APE1 inhibitor since it can be recognized but hardly cleaved by APE1.

2.3 Study on mismatched DNA as APE1 substrates

2.3.1 DNA sequences

Name of DNA	**Nucleotides sequence (5' to 3')**
Mix sdA	ATGGTACCGCCTGGACGAGCCTCGA/idSp/GCTGCACCCGTGC TACCGGACCACG
Mix sdB	CGTGGTCCGGTAGCACGGGTGCAGCATCGAGGCTCGTCCAG GCGGTACCAT
Mix 1L	CGTGGTCCGGTAGCACGGGTGCAGCAACGAGGCTCGTCCAG GCGGTACCAT
Mix 1R	CGTGGTCCGGTAGCACGGGTGCAGGATCGAGGCTCGTCCAG GCGGTACCAT

Mix 1LR	CGTGGTCCGGTAGCACGGGTGCAGGAACGAGGCTCGTCCAG GCGGTACCAT
Mix 3L	CGTGGTCCGGTAGCACGGGTGCAGCAAGCAGGCTCGTCCAG GCGGTACCAT
Mix 3R	CGTGGTCCGGTAGCACGGGTGCTCGATCGAGGCTCGTCCAG GCGGTACCAT
Mix 3LR	CGTGGTCCGGTAGCACGGGTGCTCGAAGCAGGCTCGTCCAG GCGGTACCAT
Mix 5L	CGTGGTCCGGTAGCACGGGTGCAGCAAGCTCGCTCGTCCAG GCGGTACCAT
Mix 5R	CGTGGTCCGGTAGCACGGGTCGTCGATCGAGGCTCGTCCAG GCGGTACCAT
Mix 5LR	CGTGGTCCGGTAGCACGGGTCGTCGAAGCTCGCTCGTCCAG GCGGTACCAT
Mix 7L	CGTGGTCCGGTAGCACGGGTGCAGCAAGCTCCGTCGTCCAG GCGGTACCAT
Mix 7R	CGTGGTCCGGTAGCACGGCACGTCGATCGAGGCTCGTCCAG GCGGTACCAT
Mix 7LR	CGTGGTCCGGTAGCACGGCACGTCGAAGCTCCGTCGTCCAG GCGGTACCAT
Mix 9L	CGTGGTCCGGTAGCACGGGTGCAGCAAGCTCCGAGGTCCAG GCGGTACCAT
Mix 9R	CGTGGTCCGGTAGCACCCCACGTCGATCGAGGCTCGTCCAG GCGGTACCAT

Mix 9LR	CGTGGTCCGGTAGCACCCCACGTCGAAGCTCCGAGGTCCAG GCGGTACCAT

Table 2.3 Nucleotides sequences of mismatched DNA. /idSp/ = dSpacer (AP site).

Mismatched pairs were highlighted in red color.

2.3.2 Materials and Methods

Product(s)	**Manufacturer**
Oligodeoxyribonucleotides	Sangon Biotech (Shanghai, China)
APE1	New England Biolabs (Singapore)
Acrylamide	Invitrogen (Carlsbad, CA, USA)
N,N'-Methylenebisacrylamide	Sigma-Aldrich (USA)
Ammonium persulfate	Bio-Rad Laboratories (Singapore)
TEMED	Bio-Rad Laboratories (Singapore)
5bp DNA ladder	Thermo Fisher (Vilnius, Lithuania)
Ethidium bromide solution, 10mg/ml	Bio-Rad Laboratories (Singapore)
6 × DNA loading dye	Fermentas (Waltham, MA, USA)
1M Tris buffer, pH 8.0	1st Base (Singapore)
10 × Tris-borate-EDTA (TBE) buffer, pH 8.3	Vivantis (Malaysia)
Eppendorf tubes, Pipette tips	Greiner (Singapore)
Vortex mixer	Labnet international (Edison, NJ, USA)
Electrophoresis power supply	Consort (Turnhout, Belgium)
G:BOX Chemi gel doc system	Syngene (Cambridge, UK)

Table 2.4 Materials used study on mismatched DNA as APE1 substrates. Other chemicals used in this study (such as salts and buffers) were supplied by Sigma-Aldrich with analytical grade or molecular biology grade.

Annealing for mismatched DNA

100 μM stock solutions were respectively prepared by adding deionized water to dissolve oligodeoxyribonucleotides (in **Table 2.3**). 1 nmol of single-strand DNA containing AP site (Mix sdA), 1 nmol of different partly complementary single-strand DNA (Mix sdB, Mix nL, Mix nR, Mix nLR) were incubated in 10 mM Tris-HCl (pH 8.0) and 50 mM NaCl in a total volume of 100 μl for 5 min at 95°C. Followed by slowly cooling down to room temperature (25 ^{o}C) in air for 2 h. 10 μM annealed mismatched DNA were formed, named by corresponding unique single-strand DNA' name respectively (Mix-sd, Mix-nL, Mix-nR, Mix-nLR).

Catalytic reaction of mismatched DNA with APE1

10 pmol annealed mismatched DNA (Mix-sd, Mix-1L, Mix-1R, Mix-1LR, Mix-3L, Mix-3R, Mix-3LR, Mix-5L, Mix-5R, Mix-5LR, Mix-7L, Mix-7R, Mix-7LR, Mix-9L, Mix-9R, Mix-9LR) were respectively incubated with 5 nM APE1 in APE1 buffer (20 mM Tris-acetate (pH 8.0), 50 mM CH_3COOK, 10 mM $Mg(CH_3COO)_2$ and 1 mM DTT) for 2 h at 37 °C in a total volume of 20 μl.

Polyacrylamide Gel electrophoresis of the results

15 % non-denaturing polyacrylamide gel was prepared with 142.5 g acrylamide, 7.5 g *N,N'*-methylenebisacrylamide and DI water forming 1 L solution. By adding 4 μl 6 × DNA loading dye to 20 μl samples after reaction, the mixtures were rapidly loaded on a 15 % non-denaturing polyacrylamide gel. Gel electrophoresis were conducted at 350 V in 1 × TBE

buffer solution for 10 h. Then polyacrylamide gels were stained in 1 × TBE buffer of ethidium bromide for 30 min. Data was analyzed by using G:BOX iChemi gel documentation system (Syngene).

2.3.3 Results and Discussion

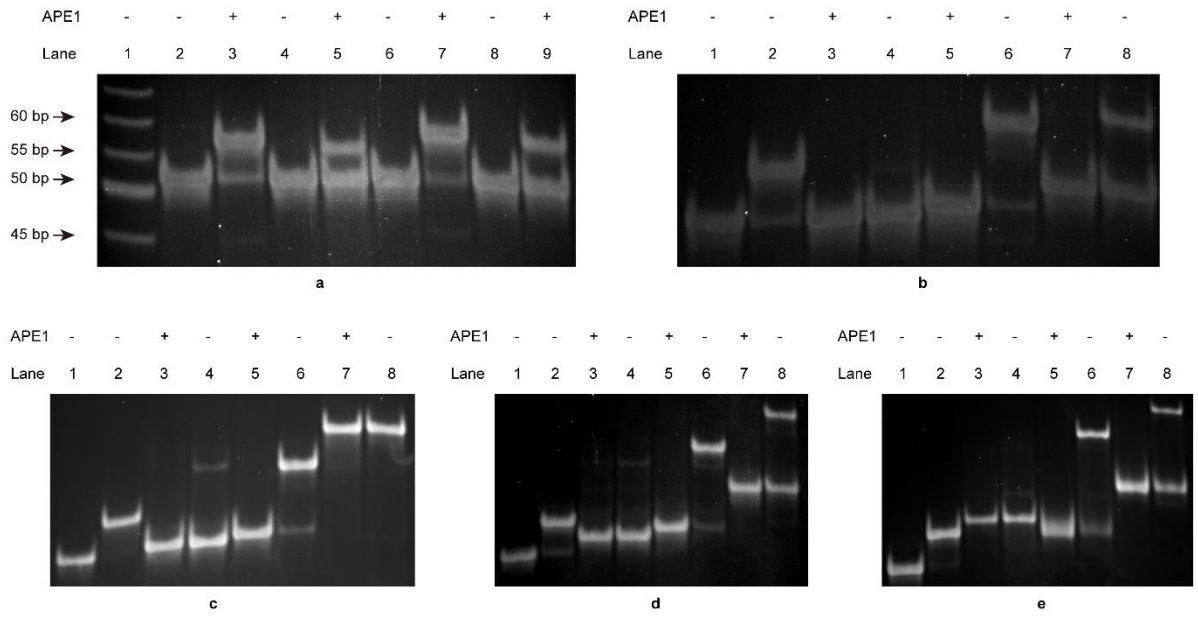

Figure 2.9 Gel electrophoretic analysis of mismatched DNA as APE1 substrates. (a) Lane 1: 5 bp DNA ladder (Bands: 65 bp, 60 bp, 55 bp, 50 bp and 45 bp); Lane 2: Mix-sd only; Lane 3: Mix-sd with APE1; Lane 4: Mix-1L only; Lane 5: Mix-1L with APE1; Lane 6: Mix-1R only; Lane 7: Mix-1R with APE1; Lane 8: Mix-1LR only; Lane 9: Mix-1LR with APE1. (b) Lane 1: Mix-sd only; Lane 2: Mix-sd with APE1; Lane 3: Mix-3L only; Lane 4: Mix-3L with APE1; Lane 5: Mix-3R only; Lane 6: Mix-3R with APE1; Lane 7: Mix-3LR only; Lane 8: Mix-3LR with APE1. (c) Lane 1: Mix-sd only; Lane 2: Mix-sd with APE1; Lane 3: Mix-5L only; Lane 4: Mix-5L with APE1; Lane 5: Mix-5R only; Lane 6: Mix-5R with APE1; Lane 7: Mix-5LR only; Lane 8: Mix-5LR with APE1. (d) Lane 1: Mix-sd only; Lane 2: Mix-sd with APE1; Lane 3: Mix-7L only; Lane 4: Mix-7L with APE1; Lane 5: Mix-7R only; Lane 6:

Mix-7R with APE1; Lane 7: Mix-7LR only; Lane 8: Mix-7LR with APE1. (e) Lane 1: Mix-sd only; Lane 2: Mix-sd with APE1; Lane 3: Mix-9L only; Lane 4: Mix-9L with APE1; Lane 5: Mix-9R only; Lane 6: Mix-9R with APE1; Lane 7: Mix-9LR only; Lane 8: Mix-9LR with APE1.

After annealing, corresponding mismatched DNA was formed. 5' mismatched DNA substrates included Mix-1L, Mix-3L, Mix-5L, Mix-7L and Mix-9L. 3' mismatched DNA substrates included Mix-1R, Mix-3R, Mix-5R, Mix-7R and Mix-9R. Substrates with both 5' and 3' mismatched included Mix-1LR, Mix-3LR, Mix-5LR, Mix-7LR and Mix-9LR. Comparing the results in the absence of APE1 with in the presence of APE1 showed in **Figure 2.9**, it was clear that the lower band was unreacted substrate, and the upper band was APE1 cleaved product. Comparison between Lane 1 and Lane 3 in **Figure 2.9**(a), the length of the lower band in Lane 3 was ranged from 50 bp to 55 bp while the length of the upper band was ranged from 55 bp to 60 bp. Thus, the lower band was in accordance with the fact that substrate Mix-sd was annealed from two separated 51-mer oligonucleotides. In addition, in this case AP site was positioned 25 bp away from the end, the cleaved oligonucleotide part was hardly dissociated from double-strand structure, forming a double-strand DNA with a nick. This kind of product was not compact form, and easily rotated or changed the configuration during electrophoresis owing to the presence of nick. Thus, we concluded that cleaved product migrated slower than substrate and the upper band presented product.

No matter what the numbers of mismatched base pairs were, the position of mismatched base pairs showed significantly influence on the activity of DNA as APE1 substrates. There was no difference on the activity between 3' mismatched DNA and no mismatched DNA, because all 3' mismatched DNA substrates were almost cleaved by APE1.

On the contrary, 5’ mismatched DNA substrates were hardly incised and only trace amounts of product were observed, indicating that 5’ mismatched DNA substrates were inert in the presence of APE1. And DNA substrates with both 5’ and 3’ mismatched showed lower activity than no mismatched DNA due to the partial incision.

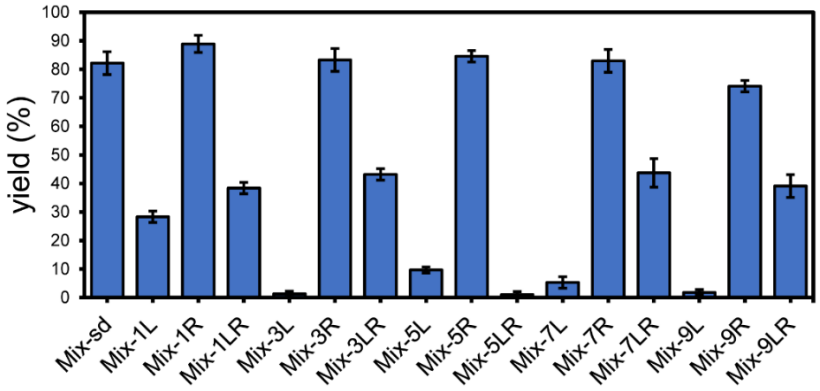

Figure 2.10 Quantitative analysis of activity of mismatched DNA as APE1 substrates. Yields were calculated according to relative fluorescence intensity by Gene Tools.

Quantitative analysis was shown in the column graph (**Figure 2.10**). From this specific data, it can be clearly seen that activity order of mismatched DNA towards APE1 from high to low was: (1) 3’ mismatched DNA same as DNA without mismatch (2) both 5’ and 3’ mismatched DNA (3) 5’ mismatched DNA. On the other hand, we investigated how the number of mismatched pairs influenced the activity of DNA as APE1 substrates. For 5’ mismatched DNA, with the numbers of mismatched base pairs increasing, activity was decreased a lot since the yield in Mix-1L was 28 % while Mix-3L, Mix-5L, Mix-7L and Mix-9L presented significantly low yields below 2 %. For 3’ mismatched DNA, there was no obvious difference in the activity as the mismatched base pairs extended. All the yields were higher than 74 %. For both 5’ and 3’ mismatched DNA, all the yields were around 40 % except Mix-5LR. Mix-5LR showed quite low yield which was only 1.1 %. Considering the

results from 5’ mismatched DNA and 3’ mismatched DNA, we think that catalytic pathways were different between Mix-1LR/Mix-3LR and Mix-7LR/Mix-9LR. As for Mix-1LR and Mix-3LR, the mismatched areas were short, so APE1 can recognize the substrates and cut them partly due to proofreading ability. With mismatched areas increasing, proofreading ability declined rapidly. When the mismatched area was longer than 14 bp, APE1 will recognize the mismatched DNA as single-strand DNA to cleave the AP site (To confirm single-strand DNA can be cleaved by APE1, see **Figure 2.12**(a) in **Chapter 2.4**). Thus, Mix-7LR and Mix-9LR also showed moderate yields in this experiment. Mix-5LR can neither be recognized by APE1 as double-strand substrate nor be recognized as single-strand substrate, leading to a quite low yield.

2.3.4 Conclusions

Through the investigation on mismatched DNA as APE1 substrates, we conclude that mismatched DNA adjacent to 5’ of AP site show very low activity resulting in significantly incompatibility as APE1 substrates. Meanwhile, as the mismatched area is longer than 3 base pairs, APE1 can hardly incise the 5’ mismatched DNA. But DNA containing mismatched base pairs at the 3’ end of AP site confers high specificity and sensitivity of APE1, whose activity is similar as normal DNA without mismatch. Besides, DNA with both 5’ and 3’ mismatched can be partly incised by APE1.

Our experiments substantiated that APE1 shows great tolerance to the flexibility at the 3’ end of AP site, revealing an important biological role for APE1 which is proofreading misinsertions of 3’ ends during BER to generate suitable substrates for further repairing[9-12]. Although 5’ mismatched DNA presents low activity toward APE1, it may not be a proper

type of inhibitors. Because mismatched base pairs are unfavourable for APE1 recognizing and binding to substrates.

2.4 Study on DNA containing two AP sites as APE1 substrates

2.4.1 DNA sequences

Name of DNA	Nucleotides sequence (5' to 3')
AP sdA	ATGGTACCGCCTGGACGAGC/idSp/TCGATGCTGCACCCGTGC TACCGGACCACG
AP sdB	CGTGGTCCGGTAGCACGGGTGCAGCATCGAGGCTCGTCCAG GCGGTACCAT
Ap 0	ATGGTACCGCCTGGACGAGC/idSp//idSp/CGATGCTGCACCCG TGCTACCGGACCACG
Ap 2	ATGGTACCGCCTGGACGAGC/idSp/TC/idSp/ATGCTGCACCCG TGCTACCGGACCACG
Ap 4	ATGGTACCGCCTGGACGAGC/idSp/TCGA/idSp/GCTGCACCCG TGCTACCGGACCACG
Ap 6	ATGGTACCGCCTGGACGAGC/idSp/TCGATG/idSp/TGCACCCG TGCTACCGGACCACG
Ap 8	ATGGTACCGCCTGGACGAGC/idSp/TCGATGCT/idSp/CACCCG TGCTACCGGACCACG
Ap o	CGTGGTCCGGTAGCACGGGTGCAGCATCGA/idSp/GCTCGTCC AGGCGGTACCAT

Ap d	ATGGTACCGCCTGGACGAGCCTCGA/idSp/GCTGCACCCGTGC TACCGGACCACG

Table 2.5 Nucleotides sequences of DNA containing two AP sites. /idSp/ = dSpacer (AP site).

2.4.2 Materials and Methods

Product(s)	**Manufacturer**
Oligodeoxyribonucleotides	Sangon Biotech (Shanghai, China)
APE1	New England Biolabs (Singapore)
Acrylamide	Invitrogen (Carlsbad, CA, USA)
N,N'-Methylenebisacrylamide	Sigma-Aldrich (USA)
Urea	Sigma-Aldrich (USA)
Ammonium persulfate	Bio-Rad Laboratories (Singapore)
TEMED	Bio-Rad Laboratories (Singapore)
5bp DNA ladder	Thermo Fisher (Vilnius, Lithuania)
Ethidium bromide solution, 10mg/ml	Bio-Rad Laboratories (Singapore)
ViSafe Red Gel Stain (10000 × in water)	Vivantis (Malaysia)
6 × DNA loading dye	Fermentas (Waltham, MA, USA)
Denaturing gel loading dye	Fermentas (Waltham, MA, USA)
1M Tris buffer, pH 8.0	1st Base (Singapore)
10 × Tris-borate-EDTA (TBE) buffer, pH 8.3	Vivantis (Malaysia)
Eppendorf tubes, Pipette tips	Greiner (Singapore)

Vortex mixer	Labnet international (Edison, NJ, USA)
Electrophoresis power supply	Consort (Turnhout, Belgium)
G:BOX Chemi gel doc system	Syngene (Cambridge, UK)

Table 2.6 Materials used study on DNA containing two AP sites as APE1 substrates. Other chemicals used in this study (such as salts and buffers) were supplied by Sigma-Aldrich with analytical grade or molecular biology grade.

Annealing for DNA containing two AP site

100 μM stock solutions were respectively prepared by adding deionized water to dissolve oligodeoxyribonucleotides (in **Table 2.5**). 1 nmol of single-strand DNA containing two AP sites with different distance (AP 0, AP 2, AP 4, AP 6, AP 8), 1 nmol of complementary single-strand DNA (sdB) were incubated in 10 mM Tris-HCl (pH 8.0) and 50 mM NaCl in a total volume of 100 μl for 5 min at 95°C. Followed by slowly cooling down to room temperature (25 ^{o}C) in air for 2 h. 10 μM annealed DNA substrates (named AP-0, AP-2, AP-4, AP-6, AP-8) containing two AP sites were formed.

Following same annealing procedure above, standard AP-sd was annealed by AP sdA and AP sdB. AP-O was annealed by AP o and AP sdA. AP-D was annealed by AP o and AP d.

Catalytic reaction of DNA containing two AP site with APE1

10 pmol annealed DNA containing two AP sites (AP-sd, AP-0, AP-2, AP-4, AP-6, AP-8, AP-O and AP-D) were respectively incubated with 5 nM APE1 in APE1 buffer (20 mM Tris-acetate (pH 8.0), 50 mM CH_3COOK, 10 mM $Mg(CH_3COO)_2$ and 1 mM DTT) for 2 h at 37 °C in a total volume of 20 μl.

Polyacrylamide Gel electrophoresis of the results

For non-denaturing gel electrophoretic analyses: 15 % non-denaturing polyacrylamide gel was prepared with 142.5 g acrylamide, 7.5 g *N,N'*-methylenebisacrylamide and DI water forming 1 L solution. By adding 4 µl 6 × DNA loading dye to 20 µl samples after reaction, the mixtures were rapidly loaded on a 15 % non-denaturing polyacrylamide gel. Gel electrophoresis were conducted at 350 V in 1 × TBE buffer solution for 10 h. Then polyacrylamide gels were stained in 1 × TBE buffer of ethidium bromide for 30 min. Data was analyzed by using G:BOX iChemi gel documentation system (Syngene).

For denaturing gel electrophoretic analyses: 15 % denaturing polyacrylamide gel was prepared with 142.5 g acrylamide, 7.5 g *N,N'*-methylenebisacrylamide, 420 g urea and DI water forming 1 L solution. Followed by adding denaturing gel loading dye, the mixtures were rapidly loaded on a 15 % denaturing polyacrylamide gel (containing urea). Electrophoretic analyses were conducted at 800 V in 1 × TBE buffer solution for 2 h. Then polyacrylamide gels were stained in 1 × TBE buffer of ViSafe Red for 30 min. Data analysis of gel electrophoresis images was used G:BOX iChemi gel documentation system (Syngene).

2.4.3 Results and discussion

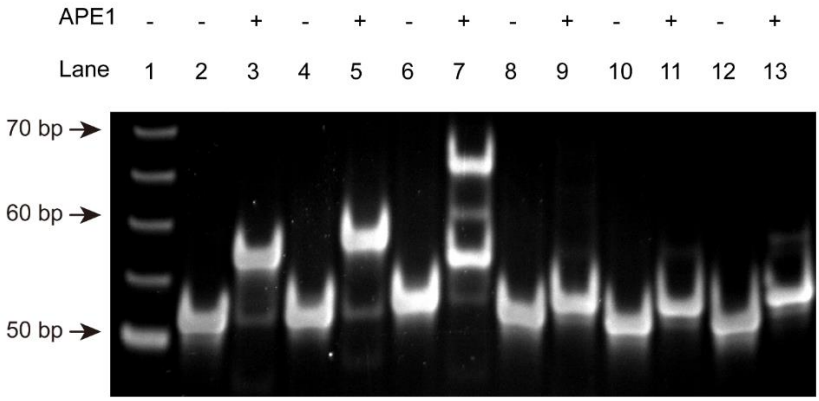

Figure 2.11 Non-denaturing gel electrophoretic analysis of DNA containing two AP sites in the same single strand as APE1 substrates. Lane 1: 5 bp DNA ladder (Bands: 70 bp, 65 bp, 60 bp, 55 bp and 50 bp); Lane 2: AP-sd only; Lane 3: AP-sd with APE1; Lane 4: AP-0 only; Lane 5: AP-0 with APE1; Lane 6: AP-2 only; Lane 7: AP-2 with APE1; Lane 8: AP-4 only; Lane 9: AP-4 with APE1; Lane 10: AP-6 only; Lane 11: AP-6 with APE1; Lane 12: AP-8 only; Lane 13: AP-8 with APE1.

At first, the results of DNA containing two AP sites in the same single strand as APE1 was analyzed by non-denaturing gel electrophoresis in **Figure 2.11**. Comparing the results in the absence of APE1 with in the presence of APE1, it made sense that the lower bands were unreacted substrates and the upper bands were different APE1 cleaved products. According to comparison between Lane 1 and Lane 3, the length of the lower band in Lane 3 was ranged from 50 bp to 55 bp while the length of the upper band was ranged from 55 bp to 60 bp. Therefore, the lower band was in accordance with the fact that substrate AP-sd was annealed from two separated 51-mer oligonucleotides. Meanwhile, in this case AP site was positioned at least 20 bp away from the end, the cleaved oligonucleotide residue longer than 20 bp was hardly dissociated from double-strand structure. Product with nicks was not compact form, and easily rotated or changed the configuration during electrophoresis. Thus, we confirmed that cleaved product migrated slower than substrate and the upper band presented product.

From the results in Lane 5 and Lane 7, we found that majority of substrates AP-0 and AP-2 were cleaved by APE1, remaining a few substrates. For the results in Lane 9, Lane 11 and Lane 13, the cleaved products were a little bit higher than the substrates and the lower band substrates almost disappeared, demonstrating that all the three substrates AP-4, AP-6 and AP-8 were totally cleaved. Therefore, these results substantiated that substrates with two AP sites in the same single strand can be successfully cleaved by APE1. Interestingly, Lane 7 showed more than one upper bands. In our opinion, multiple products indicated that two AP site can not be totally recognized and cleaved by APE1 at the same time in this case.

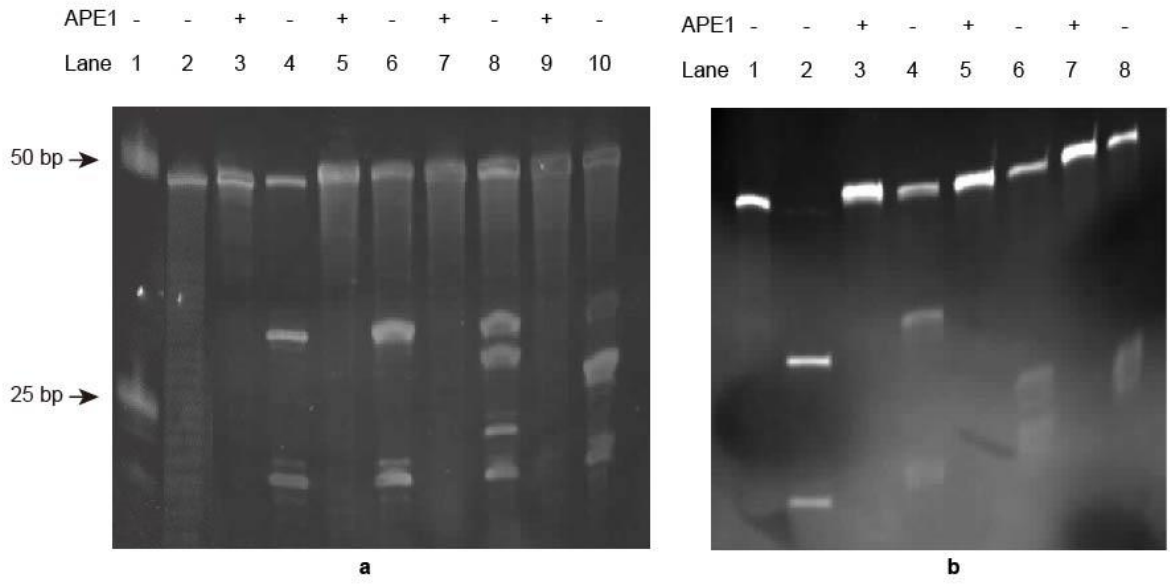

Figure 2.12 Denaturing gel electrophoretic analysis of DNA containing two AP sites in the same single strand as APE1 substrates. (a) Lane 1: 25 bp DNA ladder (Bands: 50 bp, 25 bp); Lane 2: Single strand AP sdB only; Lane 3: Single strand AP sdA only; Lane 4: Single strand AP-sdA with APE1; Lane 5: AP-sd only; Lane 6: AP-sd with APE1; Lane 7: AP-0 only; Lane 8: AP-0 with APE1; Lane 9: AP-2 only; Lane 10: AP-2 with APE1. (b) Lane 1: Single strand AP sdA only; Lane 2: Single strand AP-sdA with APE1; Lane 3: AP-4 only; Lane 4:

AP-4 with APE1; Lane 5: AP-6 only; Lane 6: AP-6 with APE1; Lane 7: AP-8 only; Lane 8: AP-8 with APE1.

Subsequently, denaturing gel experiments were carried out under the same reaction conditions. Firstly, we investigated whether single-strand DNA (ssDNA) with AP site can be cleaved by APE1. Comparing Lane 3 with Lane 4 in **Figure 2.12**(a), it can be seen than 51mer single-strand AP sdA was incised into to two different short fragments, certifying that APE1 can cleave ssDNA partly. As DNA ladder indicated, the upper band was 30 bp fragment and the lower band was 20 bp fragment. Meanwhile, Lane 6, the result of AP-sd in the presence of APE1 was similar as Lane 4. Thus, Lane 3 could work as a more accurate ladder and make a great contribution for us to analyse the remaining results. From Lane 8, Lane 10 in **Figure 2.12**(a) and Lane 4, Lane 6, Lane 8 in **Figure 2.12**(b), the single-strand fragments were clearly observed from the areas which were much lower than the position of 51-mer single-strand DNA and located between 20 bp band and 30 bp band. This outcome further illustrated sites were indeed cleaved by APE1. Particularly, Lane 8, Lane 10 in **Figure 2.12**(a) showed at least four fragment bands. Considering the fact shown in nondenatured gel, we further confirmed the conclusion that two AP site can not be totally recognized and cleaved by APE1 at the same time in AP-0 and AP-2.

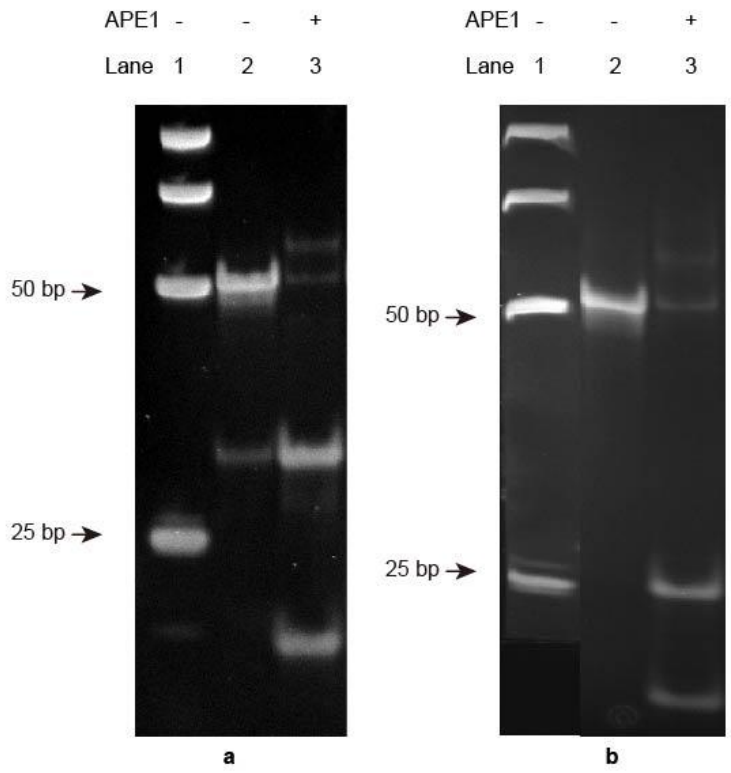

Figure 2.13 Non-denaturing gel electrophoretic analysis of DNA containing two AP sites in different single strand as APE1 substrates. (a) Lane 1: 25 bp DNA ladder (Bands: 100 bp, 75 bp, 50 bp, 25 bp); Lane 2: AP-O only; Lane 3: AP-O with APE1. (b) Lane 1: 25 bp DNA ladder (Bands: 100 bp, 75 bp, 50 bp, 25 bp); Lane 2: AP-D only; Lane 3: AP-D with APE1. Gel electrophoresis were conducted at 350 V in 1 × TBE buffer solution for 5 h.

Figure 2.13 showed the results about two AP sites locating in different strand. DNA containing two AP sites in pair position (AP-O) presented two bright lower bands indicated there were 20-mer and 30-mer cleavage products. It verified that AP-O was mainly cleaved into two separated double-strand DNA by APE1. Similarly, DNA with two AP sites in unpair position (AP-D) was almost turned into two lower bands. One band was located around 25 bp area, the other was located around 20 bp area. According to the sequence of AP-D, these products were formed by cleaving both two AP sites. These demonstrated that DNA containing two AP sites locating in different strand can be recognized by APE1.

2.4.4 Conclusions

When two AP sites are positioned in same single strand, no matter how many bases between two AP sites, all substrates show high efficiency towards APE1. And the reactions may generate multi-products due to more than one reactive site in the structure. Meanwhile, we confirm that single-strand DNA can also be recognized and cleaved by APE1. On the other hand, when two AP sites are in different single strand, both AP-AP paired DNA substrate and AP-AP unpaired DNA substrate can be fully cleaved into fragments. Overall, adding extra AP site makes little difference to the activity of APE1 substrates, which means that APE1 is a powerful enzyme with great ability to proofread multiple errors at the same time. APE1 can favourably repair DNA with damages.

References

1. Thakur, S.; Dhiman, M.; Tell, G.; Mantha, A. K., *Cell biochemistry and function.* **2015,** *33*, 101-12.
2. Li, M.; Wilson III, D. M., *Antioxidants & redox signaling.* **2014,** *20*, 678-707.
3. Antoniali, G.; Lirussi, L.; Poletto, M.; Tell, G., *Antioxidants & redox signaling.* **2014,** *20*, 621-39.
4. Esqueda, A.; Mohammed, M. Z.; Madhusudan, S.; Neamati, N., *Methods in molecular biology.* **2012,** *928*, 161-74.
5. Kelley, M. R.; Georgiadis, M. M.; Fishel, M. L., *Current molecular pharmacology.* **2012,** *5*, 36-53.

6. Luo, M.; Delaplane, S.; Jiang, A.; Reed, A.; He, Y.; Fishel, M.; Nyland II, R. L.; Borch, R. F.; Qiao, X.; Georgiadis, M. M.; Kelley, M. R., *Antioxidants & Redox Signaling.* **2008,** *10*, 1853-67.
7. McNeill, D. R.; Wilson III, D. M., *Mol. Cancer Res.* **2007,** *5*, 61-70.
8. Myles, G. M.; Sancar, A., *Chemical Research in Toxicology*. **1989,** *2*, 197-226.
9. Whitaker, A. M.; Freudenthal, B. D., *DNA repair*. **2018**, *71*, 93-100.
10. Whitaker, A. M.; Flynn, T. S.; Freudenthal, B. D., *Nat Commun.* **2018,** *9*, 399.
11. Parsons, J. L.; Dianova, I. I.; Dianov, G. L., *Nucleic acids research*. **2004,** *32*, 3531-6.
12. Izumi, T.; Hazra, T. K.; Boldogh, I.; Tomkinson, A. E.; Park, M. S.; Ikeda, S.; Mitra, S., *Carcinogenesis*. **2000,** *21*, 1329-34.
13. Thakur, S.; Sarkar, B.; Cholia, R. P.; Gautam, N.; Dhiman, M.; Mantha, A. K., *Experimental & molecular medicine.* **2014,** *46*, e106.
14. Al-Safi, R. I.; Odde, S.; Shabaik, Y.; Neamati, N., *Current molecular pharmacology.* **2012,** *5*, 14-35.
15. Al-Safi, R. I.; Odde, S.; Shabaik, Y.; Neamati, N., *Current molecular pharmacology.* **2012,** *5*, 14-35.
16. Bailly, C.; Waring, M. J., *Biochemistry.* **1993,** *32*, 5985-93.
17. Longas, M. O.; Finlay, T. H., *Int J Biochem.* **1980,** *11*, 565-7.
18. Tal-Gan, Y.; Freeman, N. S.; Klein, S.; Levitzki, A.; Gilon, C., *Bioorganic & medicinal chemistry.* **2010,** *18*, 2976-85.
19. Mol, C. D.; Izumi, T.; Mitra, S.; Tainer, J. A., *Nature.* **2000,** *403*, 451-6.
20. Lipton, A. S.; Heck, R. W.; Primak, S.; McNeill, D. R.; Wilson III, D. M.; Ellis, P. D., *J. Am. Chem. Soc*. **2008,** *130*, 9332-41.
21. Schermerhorn, K. M.; Delaney, S., *Biochemistry*. 2013, *52*, 7669-77.

22. Beernink, P. T.; Segelke, B. W.; Hadi, M. Z.; Erzberger, J. P.; Wilson III, D. M.; Rupp, B., *J.Mol. Biol.* **2001,** *307*, 1023-34.
23. Li, G.-M., *Cell Research*. **2008,** *18*, 85-98.
24. Kunkel, T. A., *J. Biol. Chem.* **2004,** *279*, 16895-8.
25. Fijalkowska, I. J.; Schaaper, R. M.; Jonczyk, P., *FEMS microbiology reviews*. **2012,** *36*, 1105-21.
26. Makiela-Dzbenska, K.; Maslowska, K. H.; Kuban, W.; Gawel, D.; Jonczyk, P.; Schaaper, R. M.; Fijalkowska, I. J., *DNA Repair*. **2019,** *83*, 102643.
27. Tiraby, J. G.; Fox, M. S., *Proc Natl Acad Sci USA.* **1973,** *70*, 3541-5.
28. Kolodner, R. D.; Marsischky, G. T., *Curr Opin Genet Dev.* **1999,** *9*, 89-96.
29. Kunkel, T. A.; Erie, D. A., *Annu Rev Biochem*. **2005,** *74*, 681-710.
30. Modrich, P.; Lahue, R., *Annu Rev Biochem.* **1996,** *65*, 101-33.
31. Buermeyer, A. B.; Deschenes, S. M.; Baker, S. M.; Liskay, R. M., *Annu Rev Genet*. **1999,** *33*, 533-64.
32. Jiricny, J., *Nat Rev Mol Cell Biol*. **2006,** *7*, 335-46.
33. Yang, W., *Mutat Res*. **2000,** *460*, 245-56.

Chapter 3

Study on Graphene Quantum Dot-Based Biosensor for APE1 in Cell-Free Systems

3.1 Background

Nowadays, as DNA-based nanobiosensors develop rapidly, various cellular enzymes have been successfully examined in cell-free systems[1-8]. For the detection of APE1, a label-free method was developed based on the concept of isothermal amplification in 2017[1]. During the sensing, designed DNA fragments were generated after reacting with APE1, subsequently constructing G-quadruplexes under certain conditions. The structures of G-quadruplexes can interact with fluorescence dyes by binding effect, leading to the appearance of fluorescence signals as indicator. However, there are still some limitations remaining such as the high cost of this biosensor, complicated operations and impossibility of applying in living cell systems due to the utilization of polymerase-based amplification.

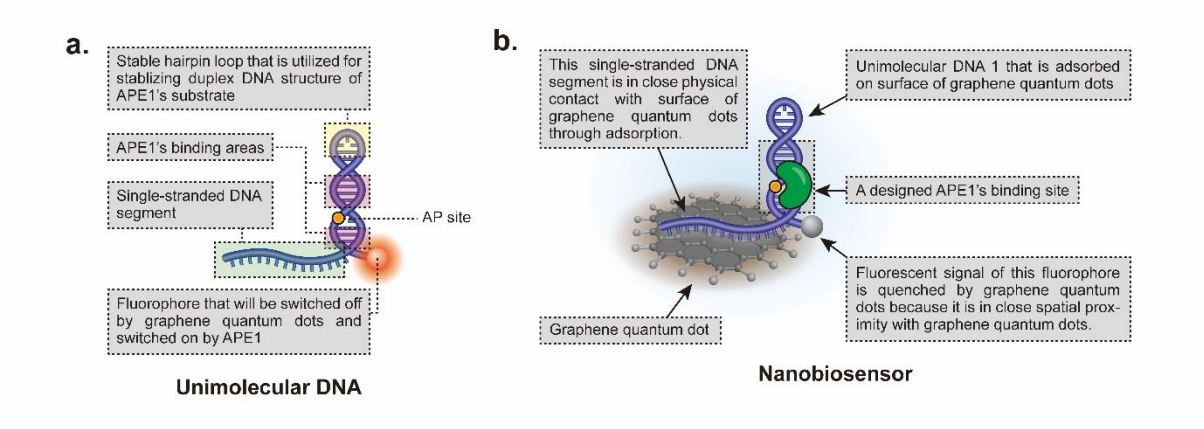

Figure 3.1 Illustration on the structure of newly designed graphene quantum dot-based biosensor. (a) Unimolecular DNA portion. (b) The whole structure of graphene quantum dot-based biosensor.

To solve these problems, a series of graphene quantum dot-based biosensors (**Figure 3.1**(b)) are constructed in our studies by two types of components, which one is meticulously designed unimolecular DNA structures (**Figure 3.1**(a)), the other is fine-sized graphene

quantum dots. The unimolecular DNA structures we designed are supposed to achieved following four functions: (i) act as APE1's substrates, by containing an AP site in double-strand unit; (ii) make sure the entire DNA structure tightly stick onto the surface of graphene quantum dots, by designing a single-strand DNA segment with suitable length; (iii) modify the APE1's substrate by covalently linking a fluorophore (Here, we chose Cy3), so that the signal of fluorophore can be quenched by graphene quantum dots prior to the treatment with APE1 and will reappear after the catalytic reaction of APE1 and (iv) stabilize the duplex unit of the unimolecular structure by inserting a short single-strand extraordinarily thermostable hairpin loop. For graphene quantum dots part of our new nanobiosensor, we choose them due to two advantages: (i) can quench the fluorescence signals of Cy3 in APE1 substrates prior to the reaction with APE1 and (ii) can assist the designed nanobiosensor into living cell system thought endocytosis as the abilities of biocompatible[9-13] and nontoxic[14-18].

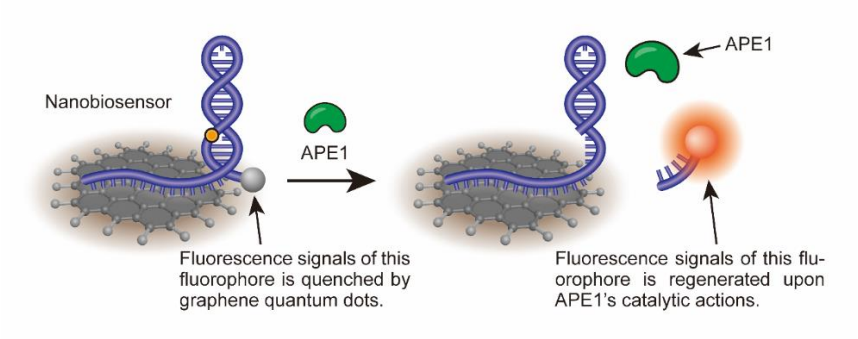

Figure 3.2 Illustration on fluorescent response from graphene quantum dot-based biosensor to APE1's enzymatic activity in cell-free systems.

Considering all factors above, it is feasible for us to construct graphene quantum dot-based biosensors to diagnose cancer biomarker APE1 with high sensitivity and selectivity in cell free systems. These graphene quantum dot-based biosensors are low-cost and convenient

to use due to the clear principle of detection APE1 (**Figure 3.2**). In addition, the utilization of graphene quantum dots makes it possible for APE1 diagnosis in living cells.

3.2 DNA sequences

Name of DNA	Nucleotide sequence (5’ to 3’)	Modification
Oligo 1	ATGTACTTCGGCTAATCTTCTAGAGGGTACCG GTCGCGAAGCGACCGGTACC /idSp/TCTAGA	5’ Cy3
Oligo 2	ATGTACTTCGGCTAATCTTCTAGAGGGTACCG GTCGCGAAGCGACCGGTACCCTCT /idSp/GA	5’ Cy3
Oligo 3	ATGTACTTCGGCTAATCTTCTAGAGGGTACCG GTCGCGAAGCGACCGGTACCCT /idSp/TAGA	5’ Cy3
Oligo 4	ATGTACTTCGGCTAATCTTCTAGAGGGTACCG GTCGCGAAGCGACCGGTA /idSp/CCTCTAGA	5’ Cy3
Oligo 5	ATGTACTTCGGCTAATCTTCTAGAGGGTACCG GTCGCGAAGCGACCGG /idSp/ACCCTCTAGA	5’ Cy3
Oligo 1A	ATGTACTTCGGCTAATCTTCTAGAGGGTACCG GTCGCGAAGCGACCGGTACCCTCTAGA	5’ Cy3

Table 3.1 Nucleotide sequences of oligonucleotides used in study on graphene quantum dot-based biosensors for APE1 diagnosis in cell-free system. /idSp/ = dSpacer (AP site). Cy3 = Cyanine 3.

3.3 Materials and Methods

Product(s)	**Manufacturer**
Oligodeoxyribonucleotides	Sangon Biotech (Shanghai, China)
APE1	New England Biolabs (Singapore)
DNA polymerase beta (POLB)	Abcam
DNA ligase 1 (LIG1)	New England Biolabs
flap endonuclease 1 (FEN1)	New England Biolabs
exonuclease 1 (EXO1)	New England Biolabs
poly(A)-specific ribonuclease (PARN)	Novus Biologicals
human topoisomerase I (Topo I)	TopoGEN
human topoisomerase IIα (Topo II)	TopoGEN
AR03	Axon Medchem LLC
APE1 Inhibitor III	Axon Medchem LLC
CRT0044876	Sigma-Aldrich
Acrylamide	Invitrogen (Carlsbad, CA, USA)
N,N'-Methylenebisacrylamide	Sigma-Aldrich (USA)
Ammonium persulfate	Bio-Rad Laboratories (Singapore)
TEMED	Bio-Rad Laboratories (Singapore)
5bp DNA ladder	Thermo Fisher (Vilnius, Lithuania)
Ethidium bromide solution, 10mg/ml	Bio-Rad Laboratories (Singapore)
6 × DNA loading dye	Fermentas (Waltham, MA, USA)
1M Tris-HCl, pH 8.0	1st Base (Singapore)
10 × Tris-borate-EDTA (TBE) buffer, pH 8.3	Vivantis (Malaysia)
Eppendorf tubes, Pipette tips	Greiner (Singapore)
Vortex mixer	Labnet international (Edison, NJ, USA)

Electrophoresis power supply	Consort (Turnhout, Belgium)
G:BOX Chemi gel doc system	Syngene (Cambridge, UK)

Table 3.2 Materials used in study on graphene quantum dot-based biosensors for APE1 diagnosis in cell-free system. Other chemicals used in this study (such as salts and buffers) were supplied by Sigma-Aldrich with analytical grade or molecular biology grade.

Synthesis of graphene quantum dots

To synthesize the fine-sized graphene quantum dots, a modified acidic oxidation method was used. Graphene oxide sheets purchased from Sigma-Aldrich were used as starting materials. Graphene oxide sheets were dried using lyophilizer then cool down in ice-water bath. By adding a concentrated H_2SO_4 solution and 50 wt% $KMnO_4$, the suspension was formed and stirred at room temperature for 1 h. Followed by heating to 60 °C, the reaction mixture was further stirred at the same temperature for another 2 h. Next the new solution was quenched by pouring over a mixture of ice and water. After cooling down to room temperature, the obtained yellow mixture was sonicated using an ultrasonic bath sonicator (Elma Transsonic 660/H) for 30 min. The suspension was centrifuged at 14,000 rpm for 10 min. Supernatant was collected followed by rotary evaporating to remove remaining solvents, desired graphene quantum dots formed and can be directly used without further purification.

Atomic force microscopy for characterization of graphene quantum dots

Atomic force microscopy (AFM) was used for characterizing the size of graphene quantum dots by modified spin-coating technique. Respective amount of deionized water was added to graphene quantum dots to prepare an aqueous dispersion of 1 mg/mL. Freshly

cleaved micas were performed by cleaving micas substrate with sharp razor blade. 30 μL of aqueous dispersion was deposited onto the surface of freshly cleaved micas followed by spin coating at 1,000 rpm for 90 seconds. The micas loaded with graphene quantum dots were dried under vacuum condition for 15 min. A Multimode-8 atomic force microscopy (Veeco) machine linked with a NanoScope V controller was processing AFM imaging. Under ScanAsyst imaging mode with SCANASYST-AIR probes (Bruker), these samples of graphene quantum dots were scanned in air and the frequency of scan speed was 2.0 Hz per line. NanoScope Analysis Version 1.50 program was used for conducting morphological analysis of the imaging data.

Transmission electron microscopy for characterization of graphene quantum dots

For the characterization through transmission electron microscopy (TEM), respective amount of deionized water was added to graphene quantum dots to prepare an aqueous dispersion of 1 mg/mL. 5 μL of aqueous dispersion was deposited onto 300 mesh Cu grid with lacey carbon support film (Ted Pella) then dried in air. Under 100 kV operating voltage, a JEOL JEM-1400 transmission electron microscopy machine was processing TEM imaging.

Infrared Spectroscopy for characterization of graphene quantum dots

Prepared graphene quantum dots were grinded with a drop of mineral oil Nujol. The mixture was transferred to the plate for sample holder. The spectrum of infrared (IR) absorption data was collected with Fourier transform infrared spectrophotometry with IRPrestige-21 (SHIMADZU). The frequency range of IR measurement was 4000-600 cm^{-1}.

Preparation of graphene quantum dot-based biosensors

100 μM stock solutions were respectively prepared by adding deionized water to dissolve fluorophore-modified single-strand oligodeoxyribonucleotides (Oligos 1-5 and Oligo 1A shown in **Table 3.1**). Diluting the stock solutions with deionized water, pH buffer and salt, new mixed solutions were formed containing 10 μM oligodeoxyribonucleotides, 10 mM Tris-HCl (pH 8.0) and 50 mM NaCl in a total volume of 100 μL. These mixed solutions were subsequently incubated for 5 min at 95 °C. Followed by slowly cooling down to room temperature (25°C) in air for 2 h. The secondary structures of unimolecular DNA (Unimolecular DNAs 1-5 and Unimolecular DNA 1A) were constructed after annealing process. 1 μM unimolecular DNA and 10 mg/mL aqueous solutions of prepared graphene quantum dots (other nanomaterials such as graphene oxide and reduced graphene oxide were also used according to the experimental conditions as mentioned in the results and discussion section) were incubated for 4 h at room temperature (25 °C), forming respective graphene quantum dot-based biosensors (Nanobiosensors 1-5 and Nanobiosensor 1A). The final solutions of the nanosensors were stored in fridge at 4 °C for further use. Absorptions of fluorescence-labelled unimolecular DNA on carbon nanomaterials were verified through fluorescence spectroscopic examinations at 37 °C using Cary Eclipse Fluorescence Spectrometer (Varian).

Dynamic light scattering and zeta potential measurements of nanobiosensors

Nanobiosensor 1 with DNA concentration of 100 nM and aqueous dispersion of graphene quantum dots that contained about 1 mg/mL of graphene quantum dots were loaded into folded capillary cells (DTS1070) respectively. Size and zeta potential measurements were subsequently carried out at room temperature using a Zetasizer NANO system (Malvern).

Fluorescence spectroscopic analysis on nanobiosensors in cell-free systems

Constructed nanobiosensors with DNA concentration of 100 nM were incubated with 1 nM of APE1 in the presence of 20 mM Tris-acetate (pH 7.9), 50 mM CH_3COOK, 10 mM $Mg(CH_3COO)_2$ and 1 mM DTT at 37 °C for 2 h (Different concentrations of APE1 and incubation times were used according to reaction conditions as mentioned in the results and discussion section). Fluorescence spectroscopic analysis on reaction mixtures of the nanobiosensors were carried out at 37 °C in a quartz cuvette (1 cm light path) using Cary Eclipse Fluorescence Spectrometer (Varian). Fluorescence emission spectra were measured at an angle of 90 ° to the 515 nm excitation laser and emission signals were recorded for every nanometer from 535 nm to 655 nm. Both excitation and emission slits were set at 10 nm. The experimental procedures for conducting examinations shown in Figure 3.10(b), Figure 3.10(c) and Figure 3.11 were the same as those in Figure 3.10(a) except that different concentrations of APE1 were used (Figure 3.10(b)), different intervals of reaction time were selected (Figure 3.10(c)), 10 μM of AR03, CRT0044876 and APE1 Inhibitor III were included in the reaction mixtures (Figure 3.11) separately. For specificity tests shown in Figure 3.12, the experiments were carried out in the same ways as those shown in Figure 3.10(a) except that APE1 was replaced with DNA polymerase beta, DNA ligase 1, human topoisomerase I, human topoisomerase IIα, histones separately.

Fluorescence imaging of nanobiosensors under ultraviolet illumination

Nanobiosensor 1 with DNA concentration of 100 nM was incubated with/without 1 nM APE1 in the presence of 20 mM Tris-acetate (pH 7.9), 50 mM CH_3COOK, 10 mM $Mg(CH_3COO)_2$ and 1 mM DTT at 37 °C for 2 h. The mixture was next condensed under vacuum and then transferred into a quartz cuvette (Hellma Absorption cell 100-OS). Colorimetric photographs of color variations were acquired through using a Sony A7II digital camera under ultraviolet radiation (302 nm) in a dark room.

Gel electrophoresis of the results

1 nM annealed Unimolecular DNA 1 were incubated with 1 nM APE1 in APE1 buffer (20 mM Tris-acetate (pH 7.9), 50 mM CH_3COOK, 10 mM $Mg(CH_3COO)_2$ and 1 mM DTT) for 2 h at 37 °C in a total volume of 20 µl. 15 % non-denaturing polyacrylamide gel was prepared with 142.5 g acrylamide, 7.5 g *N,N'*-methylenebisacrylamide and DI water forming 1 L solution. By adding 4 µl 6 × DNA loading dye to 20 µl samples after reaction, the mixtures were rapidly loaded on a 15 % non-denaturing polyacrylamide gel. Gel electrophoresis were conducted at 10 V/cm in 1 × TBE buffer solution for 10 h. Then polyacrylamide gels were stained in 1 × TBE buffer of ethidium bromide for 30 min. Data was analyzed by using G:BOX iChemi gel documentation system (Syngene).

3.4 Results and Discussion

3.4.1 Characterization of the structure of graphene quantum dot-based biosensors

The fine-sized graphene quantum dots were synthesized from graphene oxide as starting material by a modified acidic oxidation method[19-20]. The formation of graphene quantum dots was confirmed by characterizing their shapes, dimensions, and surface morphology using transmission electron microscopy, atomic force microscopy and IR examination following standard characterization procedures[21-24].

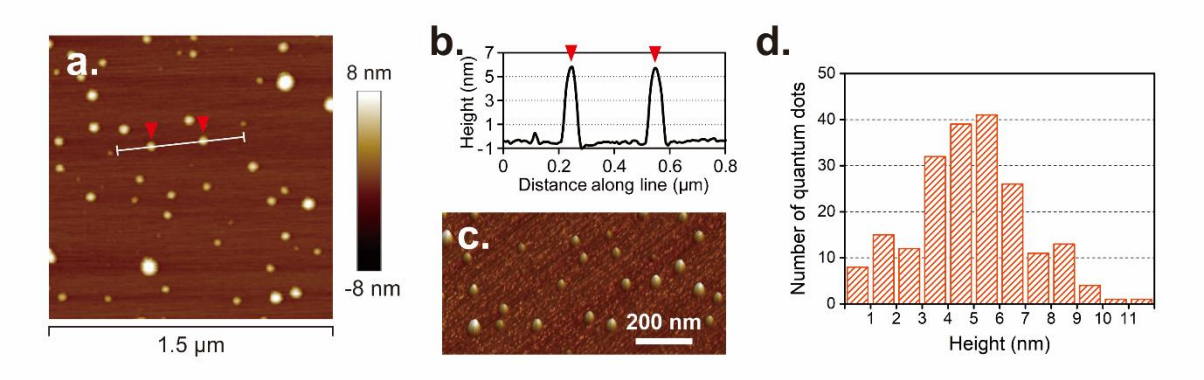

Figure 3.3 Characterization of our synthesized graphene quantum dots by atomic force microscopy (AFM). (a) Height image of graphene quantum dots captured by AFM. (b) Surface cross-sectional analysis along the line shown in the AFM image in (a). (c) Three-dimensional surface morphology of graphene quantum dots that were determined using AFM. (d) Height distribution of graphene quantum dots determined by AFM.

Atomic force microscopy (AFM) was used for characterizing the surface morphology and height of graphene quantum dots. **Figure 3.3**(a) was the height image of graphene quantum dots processing by AFM. And **Figure 3.3**(b) presented the sectional analysis of the surface along the line shown in **Figure 3.3**(a), indicating that graphene quantum dots whose height was around 5nm are predominant in **Figure 3.3**(a). **Figure 3.3**(c) showed the three-dimensional structure of graphene quantum dots. We concluded that the heights of graphene quantum dots were almost distributed within 3-7nm from **Figure 3.3**(d).

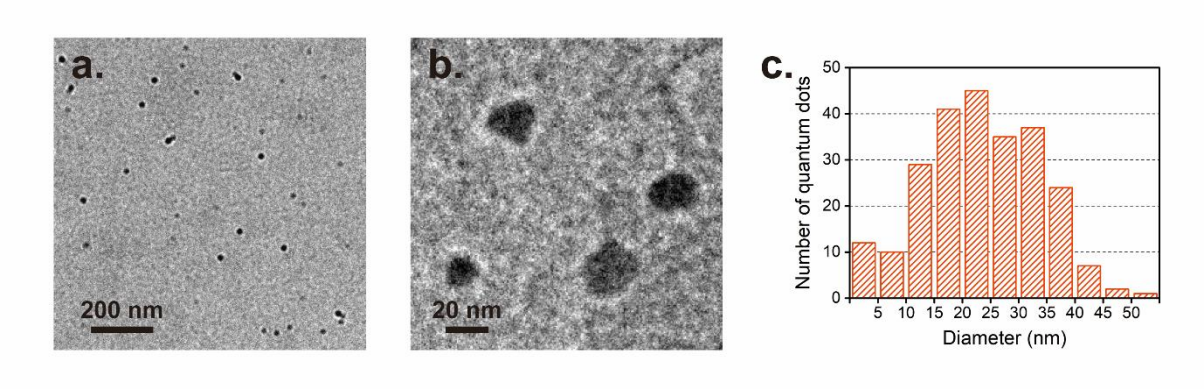

Figure 3.4 Characterization of our synthesized graphene quantum dots by transmission electron microscopy (TEM). (a, b) TEM images of graphene quantum dots prepared using graphene oxide as starting materials. (c) Lateral size distribution of graphene quantum dots determined by TEM imaging.

Transmission electron microscopy (TEM) was carried out for charactering the shapes and dimensions of graphene quantum dots. In **Figure 3.4**(a), it was clear that most of graphene quantum dots were rounded-like shapes. **Figure 3.4**(b) showed the TEM image when the scale bar was zoomed in to 20nm. From **Figure 3.4**(c), we can confirm that majority of graphene quantum dots ranged from 10-40 nm in diameter (lateral size).

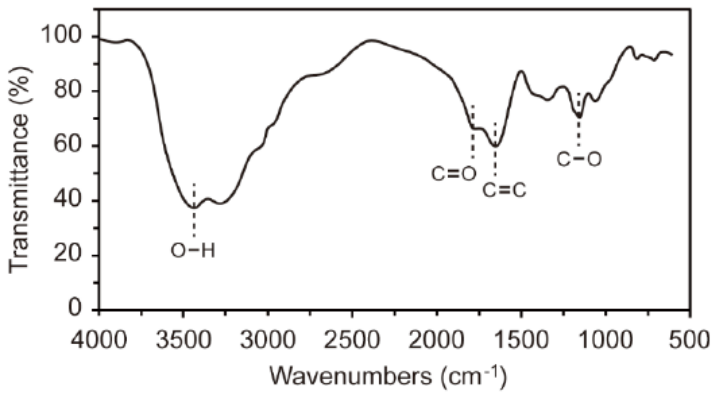

Figure 3.5 FTIR spectrum of our synthesized graphene quantum dots.

Infrared (IR) spectroscopy was conducted for confirming the correct chemical structure of graphene quantum dots. From **Figure 3.5**, the O-H stretch appeared as a strong, broad peak at 3500 cm^{-1} and the C=O stretch appeared as a peak at 1657 cm^{-1}. In addition, C=C and C-O stretch were shown in IR spectrum.

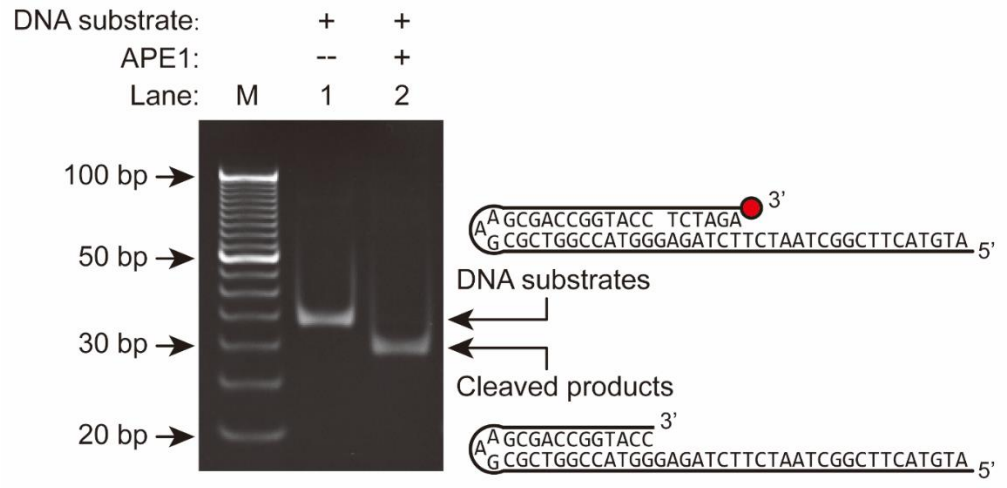

Figure 3.6 Gel electrophoretic confirmation of effectiveness of Unimolecular DNA 1 as APE1's substrate. M: 5 bp DNA ladder; Lane 1: 100 nM of Unimolecular DNA 1 alone; Lane 2: a mixture of 100 nM Unimolecular DNA 1 and 1 nM APE1 that was incubated at 37 °C for 2 h. Electrophoresis was performed using a 15 % non-denaturing gel in Tris-boric-EDTA buffer (pH = 8.0) at 10 V/cm for 2 h.

To prove that unimolecular DNA can be recognized by APE1, gel electrophoresis was utilized to distinguish the product from substrate. After staining with ethidium bromide, the result was shown in **Figure 3.6**. Comparing lane 1 with lane 2, lane 1 presented a bright band which was higher than the band in lane 2. Thus, the DNA molecules in lane 2 (product) migrated faster, which indicated that the DNA molecules in lane 2 were shorter than those in lane1 (substrate). We concluded that Unimolecular DNA 1 was cleaved by adding APE1 at 5' termini of AP sites, releasing shorter 52-mer DNA products. This gel electrophoresis experiment demonstrated that unimolecular DNA were effective as APE1's substrate.

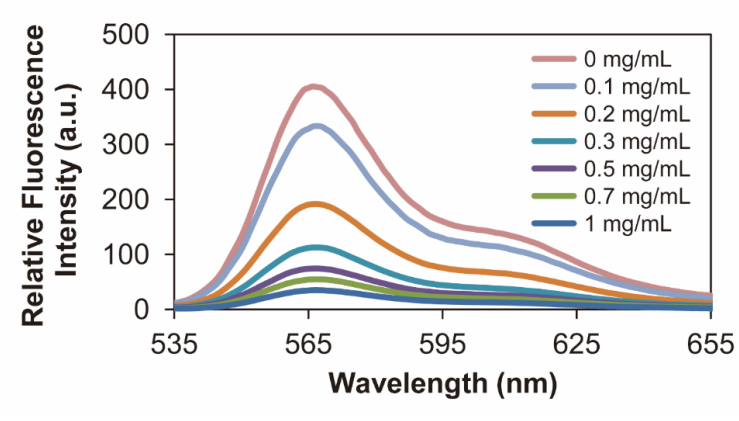

Figure 3.7 Decrease of fluorescence intensities in association with adsorption of fluorophore-labelled unimolecular DNA onto surfaces of graphene quantum dots. 100 nM of Unimolecular DNA 1 was incubated with various concentrations of graphene quantum dots at 37 °C for 2 h followed by fluorescent spectroscopic examination with excitation at 515 nm. Observed low fluorescence intensities are indications that fluorescence signals of fluorophore-labelled unimolecular DNA are quenched owing to their adsorption onto surfaces of graphene quantum dots.

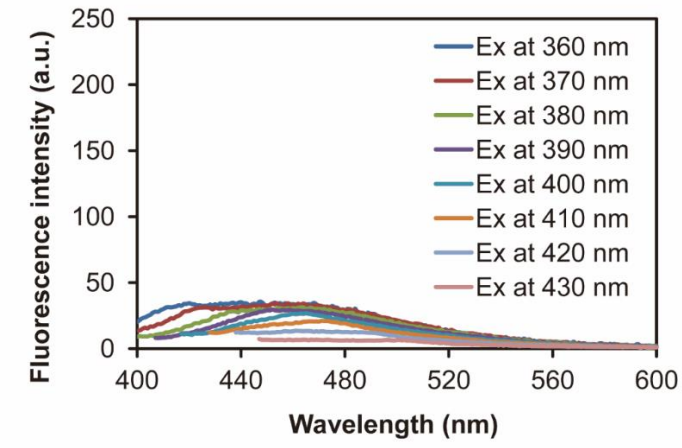

Figure 3.8 Fluorescence intensities of graphene quantum dots alone. Graphene quantum dots were prepared into aqueous solution in a concentration of 1 mg/ml, whose fluorescence intensities were then measured at various excitation wavelengths.

The key structure of the construction of graphene quantum dot-based biosensor was a single-strand DNA segment, which served as a link between the entire unimolecular DNA structure and the surface of graphene quantum dots. Meanwhile, the fluorophore modified at the 3’ end of the unimolecular DNA was closed to the surface of graphene quantum dots, resulting in the fluorescent can be easily quenched by graphene quantum dots. Herein, we designed fluorescence spectroscopic studies to illustrate the interaction between the unimolecular DNA and graphene quantum dots. As shown in **Figure 3.7**, 100 nM of Unimolecular DNA 1 was incubated with various concentrations of graphene quantum dots at 37 °C for 2 h followed by fluorescent spectroscopic examination with excitation at 515 nm. With the concentrations of graphene quantum dots increasing, fluorescence intensities gradually decreased. In **Figure 3.8**, graphene quantum dots were prepared into aqueous solution in a concentration of 1 mg/ml, whose fluorescence intensities were then measured at various excitation wavelengths. It proved that graphene quantum dots alone can not influence fluorescence intensities. Combining **Figure 3.7** and **Figure 3.8**, we can confirm that fluorescence signals of fluorophore-labelled unimolecular DNA were quenched owing to their adsorption onto surfaces of graphene quantum dots.

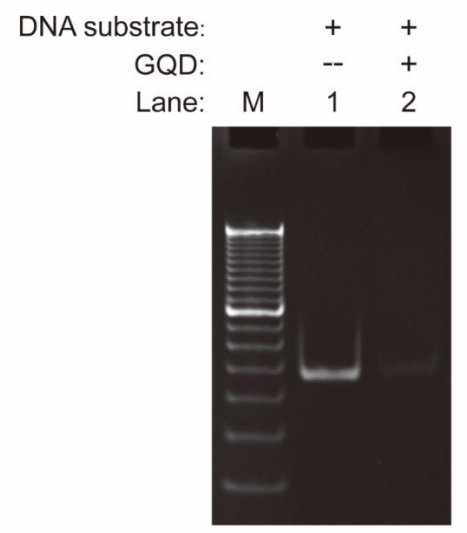

Figure 3.9 Gel electrophoretic analysis of graphene quantum dot-based biosensor in comparison with the unimolecular DNA substrates. M: O'RangeRuler 5 bp DNA Ladder; Lane 1: 100 nM of Unimolecular DNA 1 alone (DNA substrate); Lane 2: 100 nM (DNA concentration) of Nanobiosensor 1 (DNA substrate + graphene quantum dots/GQD). Electrophoresis was performed using a 15 % non-denaturing gel in Tris-boric-EDTA buffer at 10 V/cm for 2 h, followed by ethidium bromide staining.

Electrophoretic analysis can also confirm the integral structure of graphene quantum dot-based biosensor. **Figure 3.9** showed the image of gel electrophoresis. Comparing Lane 1 with Lane 2, the intensity of Lane 2 was much lower than the intensity of Lane 1. The significant difference of intensities indicated that most of unimolecular DNA 1 in Nanobiosensor 1 was not free while formed integrated structure through the interaction with graphene quantum dots. These integrated nanocomposites were too big to be loaded into polyacrylamide gel resulting in the low intensity.

Sample name	Particle size (d.nm) [a)]	Zeta potential (mV)
GQDs	32.87±6.85	-9.46±0.32
Nanobiosensor 1	50.32±17.36	-11.03±0.69

Table 3.3 Particle size measurements and zeta potential determination of graphene quantum dots (GQDs) and Nanobiosensor 1. [a)] Particle sizes (in diameter) were measured by Dynamic Light Scattering (DLS) system.

Structural construction of these nanobiosensors was further verified by DLS measurements. DLS results were shown in **Table 3.3**. It was obvious that particle sizes of Nanobiosensor 1 were larger than those of graphene quantum dots alone. Moreover, Nanobiosensor 1 with lower zeta potential validated that Unimolecular DNA 1 had been adsorbed on the surface of graphene quantum dots because of DNA with negative charge. DLS experiment illustrated the interaction between the unimolecular DNA and graphene quantum dots.

3.4.2 Investigation on graphene quantum dot-based biosensors for detecting APE1 in cell-free systems

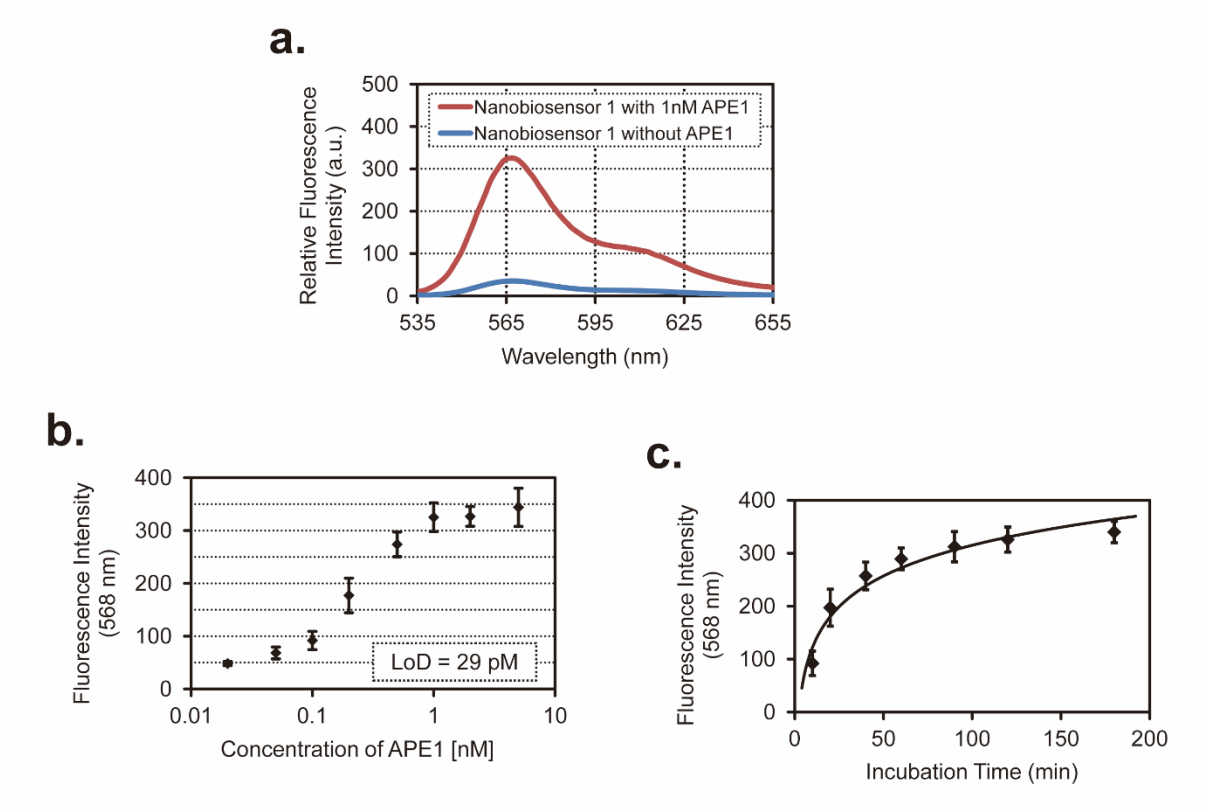

Figure 3.10 Fluorescent spectroscopic studies on Nanobiosensor 1 detecting APE1 in cell-free systems. (a) Fluorescence spectra of Nanobiosensor 1 in the absence (blue line) and presence (red line) of 1 nM APE1. (b) Correlation between APE1 concentration and fluorescence intensity generated from Nanobiosensor 1. (c) Correlation between incubation time and fluorescence intensity generated from Nanobiosensor 1.

At first, we designed fluorescence spectroscopic studies to detect the effectiveness and sensitivity of graphene quantum dot-based biosensors towards APE1 in cell-free system. Control experiments of Nanobiosensor 1 towards APE1 were conducted in **Figure 3.10**(a). Blue line presented the fluorescence intensities spectra of Nanobiosensor 1 in the absence APE1, meanwhile red line presented the fluorescence intensities spectra of Nanobiosensor 1 in the presence of 1 nM APE1. It can be clearly seen that red line was totally above blue line, which demonstrated that the fluorescence intensity of Nanobiosensor 1 in cell-free system was significantly increased after the reaction with APE1. From these experiments, we

concluded that Nanobiosensor 1 we designed can successfully serve as APE1's substrates and following by the backbone cleavage, the segments with fluorophores were free in the reaction system, regenerating the fluorescence signals of Cy3.

To investigate sensitivity of Nanobiosensor 1 towards APE1, we studied the fluorescence intensities of reaction mixture depending on APE1 concentration. Wavelength was set at 568nm which was the maximum fluorescence emission wavelength. By changing the concentration of APE1, correlation between APE1 concentration and fluorescence intensity generated from Nanobiosensor 1 was shown in **Figure 3.10**(b). Based on the general method for determination of limit of detection (LoD) reported[25], the detection limit of 1nM Nanobiosensor 1 was calculated to be 29 pM which proved that Nanobiosensor 1 was quite sensitive for APE1 detection.

Control experiment towards reaction time was conducted to detect the efficiency of Nanobiosensor 1 acting as APE1 substrates. From **Figure 3.10**(c), it can be seen that the fluorescence intensity was increased rapidly within 1 h at 37 °C according to correlation between reaction time and fluorescence intensity generated from Nanobiosensor 1. This time-dependent experiment indicated that AP site could be effectively cut by APE1 within 1 h.

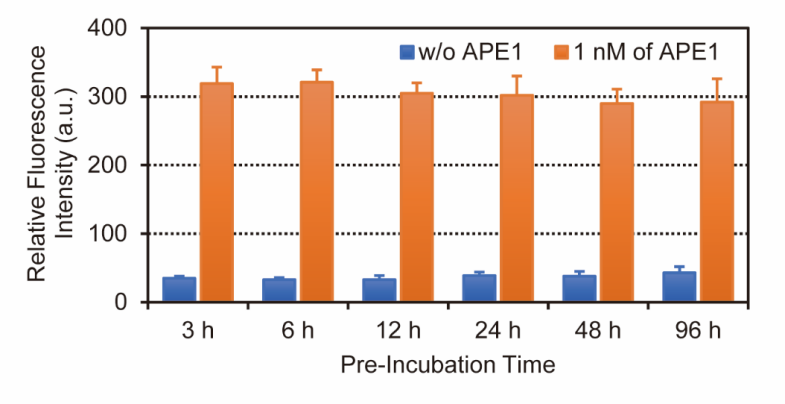

Figure 3.11 Examination of Nanobiosensor 1's structural stability and sensing activity after pre-incubation at 37 °C for various times. Nanobiosensor 1 suspensions (DNA concentration of 100 nM) were pre-incubated in aluminum-foil-protected microcentrifuge tubes in the presence of 20 mM Tris-acetate (pH 7.9), 50 mM potassium acetate, 10 mM magnesium acetate and 1 mM DTT at 37 °C for certain periods of time (blue bars) prior to the introduction of APE1 (1 nM) and further incubation of 2 hours (orange bars).

In addition, we tested the stability of graphene quantum dot-based biosensensors. The reaction time between Nanobiosensor 1 and APE1 was extended to 3 h, 6 h, 12 h, 24 h, 48 h and 96 h. From **Figure 3.11**, blue bars presented the results without APE1 while orange bars presented the results with 1nM of APE1. Comparing with fluorescence intensity, the outstanding stability of these nanobiosensors was substantiated by the high fluorescent signals remaining after 96 h of preincubation in physiological buffers in the presence of APE1.

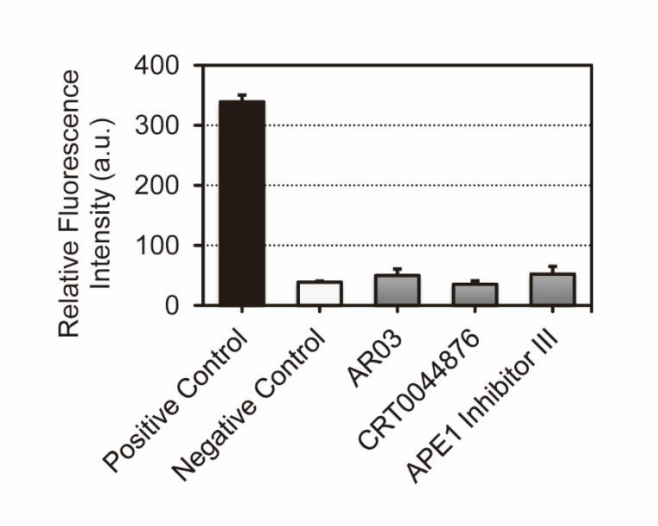

Figure 3.12 Influence of different APE1's inhibitors on Nanobiosensor 1 diagnosis in cell-free systems.

In **Figure 3.12**, we detected the influence of APE1 organic inhibitors (AR03, CRT0044876, APE1 Inhibitor III) to APE1 in our Nanobiosensor 1 reaction condition. From the results, all these APE1 organic inhibitors were showing excellent effect to decrease the activity of APE1. In the other word, this kind of nanobiosensor constructed from unimolecular DNA and graphene quantum dots has a great potential to be worked as effective biosensors for detection new APE1 inhibitors.

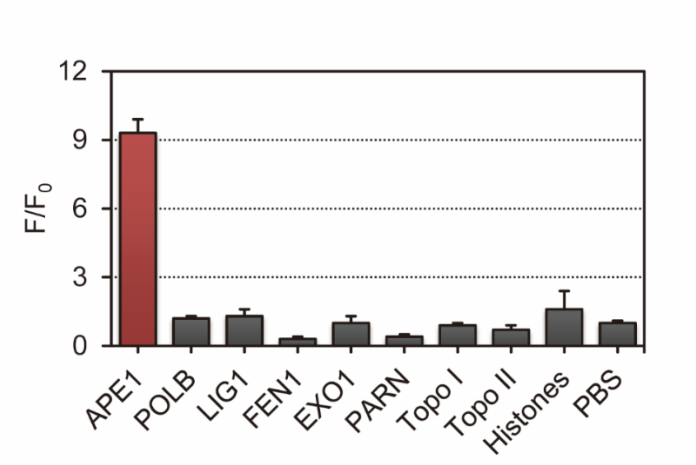

Figure 3.13 Influence of different types of enzymes/proteins on Nanobiosensor 1 diagnosis in cell-free systems.

To validate the selectivity of Nanobiosensor 1, further investigation was conducted. Different types of enzymes/proteins such as POLB, LIG1, FEN1, EXO1, PARN, Topo I, Topo II, Histones and PBS were chosen to detect the reactivity of Nanobiosensor 1. As the results shown in **Figure 3.13**, the reactivity of APE1 was much higher that the reactivity of other enzymes/proteins towards Nanobiosensor 1. The superior selectivity of Nanobiosensor 1 also gave us great confidence for the further investigation in living cells systems.

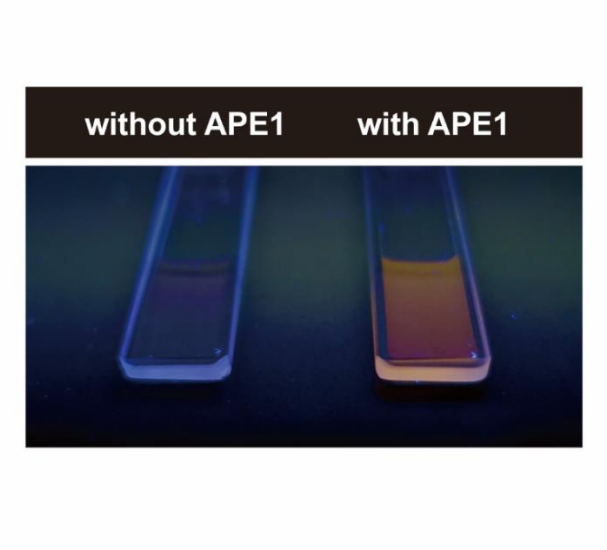

Figure 3.14 Colorimetric visualization of Nanobiosensor 1 in the absence and presence of APE1 under ultraviolet irradiation. Reactions were carried out at a substrate concentration of 1 nM (DNA concentration) in aluminum-foil-protected microcentrifuge tubes in the presence of 20 mM Tris−acetate (pH 7.9), 50 mM potassium acetate, 10 mM magnesium acetate, and 1 mM DTT at 37 °C for 2 h (unless otherwise stated).

Colorimetric visualization experiments further validated that reaction had happened between Nanobiosensor 1and APE1. Under ultraviolet irradiation, **Figure 3.14** showed that the reaction mixture of Nanobiosensor 1 and APE1 presented orange color, while nothing special appeared with Nanobiosensor 1 alone. Through these experiments, we can discover the regeneration of fluorescence signals of Cy3 visually.

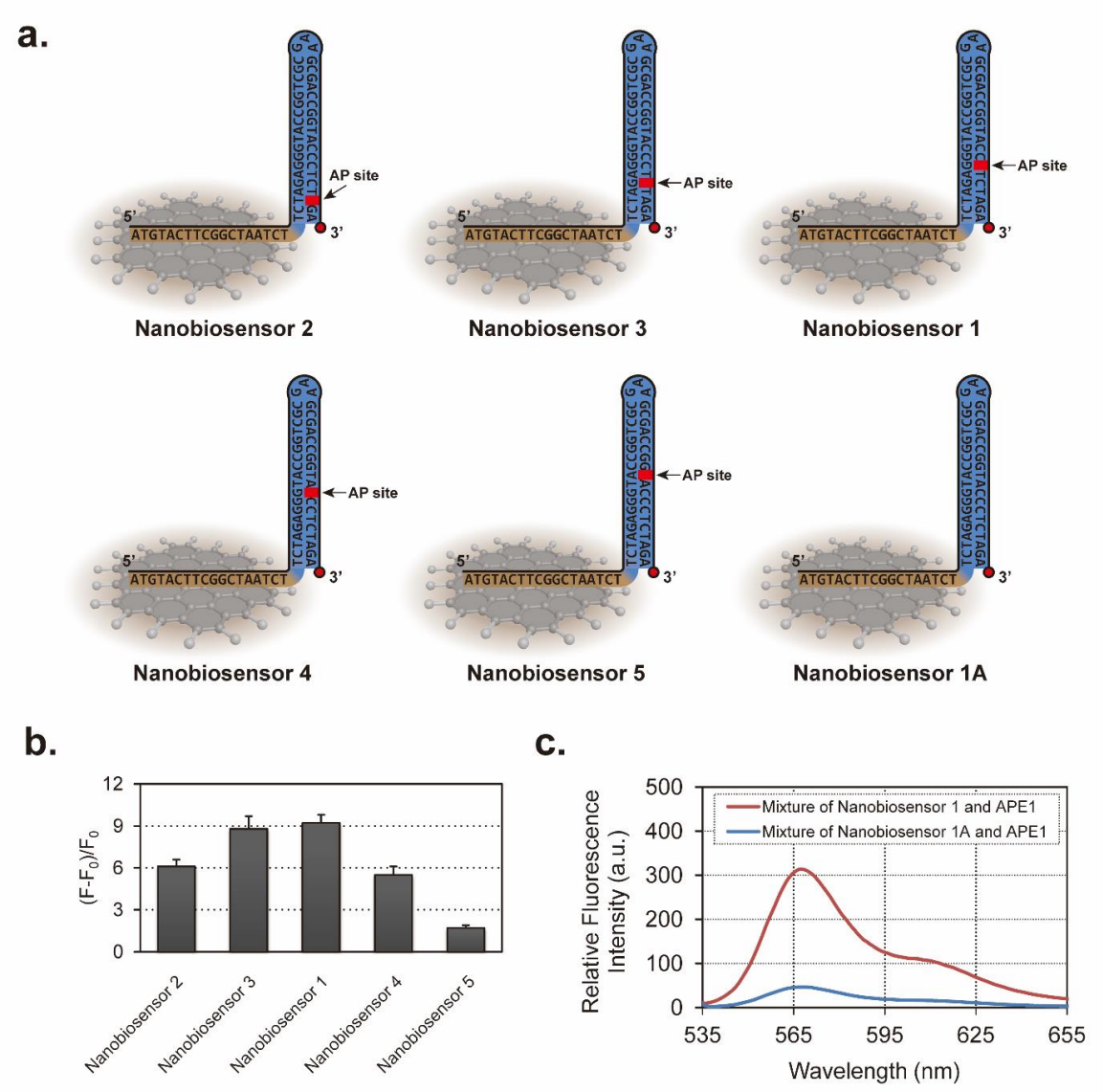

Figure 3.15 Investigation on the relation between different distance between AP sites and 3' ends of DNA and fluorescence intensity. (a) Illustration of structures of Nanobiosensors 1 to 5, in which AP sites appear at different locations in their unimolecular DNA components; and Nanobiosensor 1A which contains no AP site in their unimolecular DNA components. (b) Relative fluorescence intensities of Nanobiosensor 1 to 5 at an emission wavelength of 568 nm in their reactions with APE1. Data in this figure are representative of three independent experiments and values are expressed in mean ± SD. (c) Fluorescence spectra of reaction mixtures of Nanobiosensor 1A (blue) and reaction mixtures of Nanobiosensor 1 (red) with excitation at 515 nm. Samples for measurements of fluorescence intensities were carried out

by incubating graphene quantum dot-based biosensors (DNA concentration of 100 nM) with 1 nM of APE1 at 37 °C for 2 h.

In previous studies, we used Nanobiosensor 1 as model substrate to carry out various experiments. Focusing on the unimolecular DNA unit of Nanobiosensor 1, AP site was positioned six base pairs away from 3' end. To investigation how different distance between AP sites and 3' ends of DNA influence effectiveness of fluorescence, we chose a series of similar graphene quantum dot-based biosensors, in which AP sites were located 2 base pairs (Nanobiosensor 2), 4 base pairs (Nanobiosensor 3), 8 base pairs (Nanobiosensor 4) and 10 base pairs (Nanobiosensor 5) respectively away from 3' ends of DNA. **Figure 3.15**(a) illustrated structures of Nanobiosensors 1 to 5, demonstrating that distance between AP site and 3' ends of DNA was the same as distance between AP site and the surfaces of graphene quantum dots. **Figure 3.15**(b) showed relative fluorescence intensities (divide the difference between fluorescence intensities of in the presence of APE1 and prior to APE1 by the fluorescence intensities prior to APE1) of Nanobiosensors 1 to 5 at an emission wavelength of 568 nm in their reactions with APE1. We found that Nanobiosensor 1 and 3 in which AP site was positioned six and four base pairs away from 3' end of DNA presented highest effectiveness as biosensors for detecting APE1. This result validated the rationality of selecting Nanobiosensor 1 as suitable probe in both cell-free system and subsequently living cell system. In addition, Nanobiosensor 1A which contained no AP site comparing with Nanobiosensor 1, only replacing AP sites with regular nucleobases (cytosines) in its DNA unit, was constructed to conduct parallel experimentation. From **Figure 3.15**(c), it can be seen that little fluorescence signal was observed from the reaction mixtures of Nanobiosensor 1A and APE1. This parallel experimentation certified that the catalytic reaction between APE1 and AP site in Nanobiosensor 1 cause the increase of fluorescence intensity.

3.5 Conclusions

We have developed a novel type of biosensor which is constructed from well-designed unimolecular DNA and fine-sized graphene quantum dots. Atomic force microscopy (AFM), transmission electron microscopy (TEM) and infrared (IR) spectroscopy are utilized to identify the size and functional groups of graphene quantum dots. The structure of graphene quantum dot-based biosensor is characterized by gel electrophoresis, dynamic light scattering (DLS) and fluorescence spectroscopy.

Besides, a series of experiments depending on APE1 concentration, reaction time, APE1 inhibitors, different types of enzymes or proteins and different distance between AP sites and 3' ends of DNAs are conducted to substantiate the excellent sensitivity and specificity of quantum dot-based biosensor for APE1 diagnosis in cell-free systems. Good stability of sensing and colorimetric visualization experiment demonstrate that Nanobiosensor 1 is an efficient and convenient probe for detecting caner biomarker APE1.

References

1. Huang, Y.; Ma, Y.; Li, Y.; Xiong, M.; Li, X.; Zhang, L.; Zhao, S., *New J. Chem.* **2017,** *41*,1893-6.
2. Zhai, J.; Liu, Y.; Huang, S.; Fang, S.; Zhao, M. A., *Nucleic Acids Res.* **2017,** *45*, e45.
3. Li, X.; Xiong, M.; Huang, Y.; Zhang, L.; Zhao, S., *Anal. Methods*. **2019,** *11*, 739-43.
4. Zhang, Y.; Deng, Y.; Wang, C.; Li, L.; Xu, L.; Yu, Y.; Su, X., *Chem. Sci.* **2019,** *10*, 5959-66.

5. Ma, F.; Zhang, Q.; Zhang, C.-Y., *Nano Lett.* **2019,** *19*, 6370-6.
6. Hu, J.; Liu, M.-H.; Li, Y.; Tang, B.; Zhang, C.-Y., *Chem. Sci.* **2018,** *9*, 712-20.
7. Wang, L.-J.; Ren, M.; Zhang, Q.; Tang, B.; Zhang, C.-Y., *Anal. Chem.* **2017,** *89*, 4488-94.
8. Wang, L.-J.; Wang, Z.-Y.; Zhang, Q.; Tang, B.; Zhang, C.-Y., *Chem. Commun.* **2017,** *53*, 3878-81.
9. Sun, H.; Wu, L.; Wei, W.; Qu, X., *Mater. Today.* **2013,** *16*, 433042.
10. Zheng, P.; Wu, N., *Chem. Asian J.* **2017,** *12*, 2343-53.
11. Yin, S.; Wu, Y.-L.; Hu, B.; Wang, Y.; Cai, P.; Tan, C. K.; Qi, D.; Zheng, L.; Leow, W. R.; Tan, N. S.; Wang, S.; Chen, X., *Adv. Mater. Interfaces.* **2014,** *1*, 1300043.
12. Hong, G.; Diao, S.; Antaris, A. L.; Dai, H., *Chem. Rev.* **2015,** *115*, 10816-906.
13. Nurunnabi, M.; Parvez, K.; Nafiujjaman, M.; Revuri, V.; Khan, H. A.; Feng, X.; Lee, Y.-K., *RSC Adv.* **2015,** *5*, 42141-61.
14. Yan, Y.; Gong, J.; Chen, J.; Zeng, Z.; Huang, W.; Pu, K.; Liu, J.; Chen, P., *Adv. Mater.* **2019,** *31*, 1808283.
15. Zheng, X. T.; Ananthanarayanan, A.; Luo, K. Q.; Chen, P., *Small.* **2015,** *11*, 1620-36.
16. Wang, G.; Li, Z.; Ma, N., *ACS Chem. Biol.* **2018,** *13*, 1705-13.
17. Jiang, D.; Chen, Y.; Li, N.; Li, W.; Wang, Z.; Zhu, J.; Zhang, H.; Liu, B.; Xu, S., *PLoS One*. **2016,** *10*, e0144906.
18. Ma, C. B.; Zhu, Z. T.; Wang, H. X.; Huang, X.; Zhang, X.; Qi, X.; Zhang, H. L.; Zhu, Y.; Deng, X.; Peng, Y.; Han, Y.; Zhang, H. A., *Nanoscale* **2015,** *7*, 10162-9.
19. Fan, T.; Zeng, W.; Tang, W.; Yuan, C.; Tong, S.; Cai, K.; Liu, Y.; Huang, W.; Min, Y.; Epstein, A. J., *Nanoscale Res. Lett.* **2015,** *10*, 55.
20. Pan, D.; Zhang, J.; Li, Z.; Wu, M., *Adv. Mater.* **2010,** *22*, 734-8.
21. Zhang, H.; Ba, S.; Mahajan, D.; Lee, J. Y.; Ye, R.; Shao, F.; Lu, L.; Li, T., *Nano Lett.* **2018,** *18*, 7383-8.

22. Sun, Y.; Zheng, Y.; Pan, H.; Chen, J.; Zhang, W.; Fu, L.; Zhang, K.; Tang, N.; Du, Y., *npj Quantum Mater.* **2017,** *2*, 5.
23. Kim, J.; Cote, L. J.; Kim, F.; Huang, J., *J. Am. Chem. Soc.* **2010,** *132*, 260-7.
24. Guo, Z.; Tang, G.; Zhou, Y.; Shuwu, L.; Hou, H.; Chen, Z.; Chen, J.; Hu, C.; Wang, F.; De Smedt, S. C.; Xiong, R.; Huang, C., *Carbohydr. Polym.* **2017,** *69*, 198-205.
25. Armbruster, D. A.; Pry, T., *The Clinical Biochemist Reviews.* **2008,** *29*, S49-S52.

Chapter 4

Study on Graphene Quantum Dot-Based Biosensors for APE1 Diagnosis in Living Cells

4.1 Background

In 2017, a specific DNA nanoprobe was fabricated by magnetic nanoparticles coated with avidin-connected abasic site-containing DNA strands for detecting APE1 in living cells [1]. But this nanoprobe still contains limitations on applying for clinical cancer diagnosis resulting from poor biocompatibility of magnetic nanoparticles, instability of AP sites of DNA as APE1 substrates in their designed studies, and complicated procedures. More importantly, there is no nanobiosensor reported which is successfully utilized for determining different cellular levels of APE1 in same types of living cells whereas accurate diagnosis of variations in cancer biomarker abundance and activity is known to be vitally important for predicting how well a patient will respond to therapeutic treatments (predictions of cancer treatments) and forecasting how aggressive a given cancer is (cancer prognosis)[2-4].

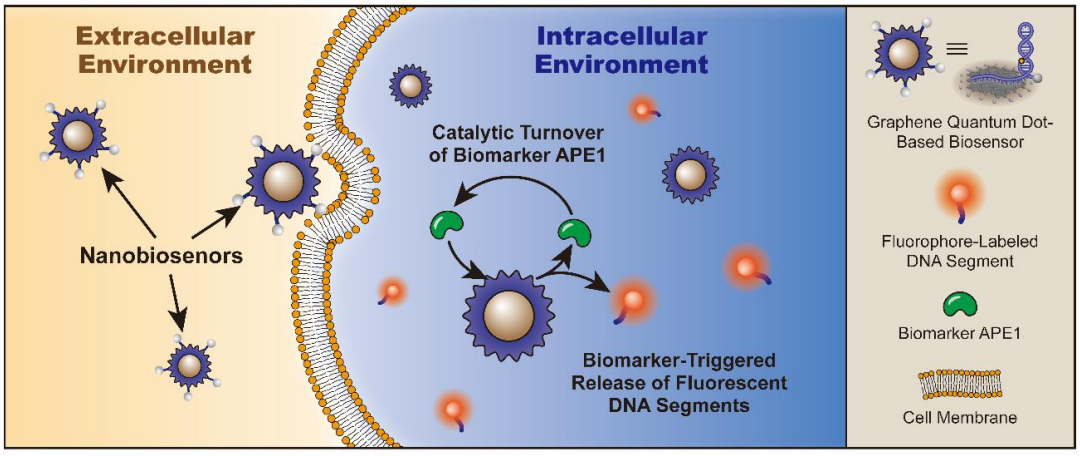

Figure 4.1 Illustration on fluorescent response from graphene quantum dot-based biosensor to APE1's enzymatic activity in living cells.

With the achievement of our graphene quantum dot-based biosensor applying in diagnosing APE1 in cell-free systems and the intention of diagnosing cellular levels of cancer

biomarker APE1 in living cells, we continue to verify the function of our newly designed graphene quantum dot-based biosensors for diagnose different cellular levels of cancer biomarker APE1 in certain types of living cells. **Figure 4.1** illustrates the general work mechanism of sensing cellular APE1.

Owing to the extremely high expression levels of APE1 in most cancerous cells[5-21], these newly designed nanobiosensors can therefore serve as powerful medical tools for cancer risk assessment, diagnosis, prognosis, and monitoring treatment response and recurrence.

4.2 DNA sequences

Name of DNA	Nucleotide sequence (5’ to 3’)	Modification
Oligo 1	ATGTACTTCGGCTAATCTTCTAGAGGGTACCG GTCGCGAAGCGACCGGTACC /idSp/TCTAGA	5’ Cy3
Oligo 1A	ATGTACTTCGGCTAATCTTCTAGAGGGTACCG GTCGCGAAGCGACCGGTACCCTCTAGA	5’ Cy3

Table 4.1 Nucleotide sequences of oligonucleotides used in study on graphene quantum dot-based biosensors for APE1 diagnosis in living cells. /idSp/ = dSpacer (AP site). Cy3 = Cyanine 3.

4.3 Materials and Methods

Product(s)	**Manufacturer**
Oligodeoxyribonucleotides	Sangon Biotech (Shanghai, China)
APE1	New England Biolabs (Singapore)
MCF-7 cell lines	American Type Culture Collection (ATCC)
PANC-1 cell lines	American Type Culture Collection (ATCC)
MCF-10A cell lines	American Type Culture Collection (ATCC)
Dulbecco's Modified Eagle Medium (DMEM)	Thermo Fisher Scientific
Fetal bovine serum	Thermo Fisher Scientific
Penicillin-streptomycin solution	Thermo Fisher Scientific
Trypsin (0.25 %)	Thermo Fisher Scientific
PBS buffer solution	Thermo Fisher Scientific
CellMask Deep Red Plasma membrane Stain	Thermo Fisher Scientific
NucBlue Live ReadyProbes Reagent	Thermo Fisher Scientific
Lipofectamine RNAiMAX Transfection Reagent	Thermo Fisher Scientific
Vybrant MTT Cell Proliferation Assay Kit	Thermo Fisher Scientific
Mammary Epithelial Basal Medium (MEBM)	Lonza
MEGM SingleQuots Supplements	Lonza
35 mm dishes (μ-Dish with an ibidi polymer coverslip bottom)	ibidi GmbH

APE1 siRNA (SMARTpool: ON-TARGETplus APEX1 siRNA)	Dharmacon
1M Tris buffer, pH 8.0	1st Base (Singapore)
Eppendorf tubes, Pipette tips	Greiner (Singapore)
Vortex mixer	Labnet international (Edison, NJ, USA)

Table 4.2 Materials used in study on graphene quantum dot-based biosensors for APE1 diagnosis in living cell. Other chemicals used in this study (such as salts and buffers) were supplied by Sigma-Aldrich with analytical grade or molecular biology grade.

Preparation of graphene quantum dot-based biosensors

Nanobiosensor 1, Nanobiosensor 1A, Nanobiosensor GO (Unimolecular DNA 1 with graphene oxide), and Nanobiosensor rGO (Unimolecular DNA 1 with reduced graphene oxide) were prepared following the same methods mentioned in **Chapter 3**.

Cell culture

Dulbecco's Modified Eagle Medium (DMEM, high glucose, GlutaMAX Supplement, pyruvate), 10 % (v/v) Fetal Bovine Serum (FBS) and 1 % (v/v) Penicillin-Streptomycin (P/S) were mixed as culture media for human breast cancer cell line MCF-7 and human pancreas cell line PANC-1. Under a humidified atmosphere of 5 % CO, different cell lines were separately cultivated with mixed culture media at 37 °C in a carbon dioxide incubator (Thermo Fisher Scientific). During of the culture, culture media were replaced every two days. During subculturing, 0.25 % trypsin was added into cells after reaching 80 % to 90 % confluency.

Transfection of siRNA

Cells were seeded and transfected with APE1 siRNA (SMARTpool: ON-TARGETplus APEX1 siRNA from Dharmacon) using Lipofectamine RNAiMAX Transfection Reagent following the manufacturer's instructions. SiRNA-lipid solution was made by two solutions which were 3 μL of Lipofectamine RNAiMAX Transfection Reagent and 1 μL of APEX1 siRNA (10 μM) diluted in serum-free DMEM respectively as volume ratio of 1 : 1. Followed by incubating for 5 min at room temperature, the obtained solution mixed with cells and further incubated for two days before using for experiments.

Confocal microscopy for live cell imaging

Seeding cells was conducted at a density of ~ 2×10^5 cells/cm^2 in 35 mm imaging dishes with ibidi polymer coverslip bottom. The conditions for cells growing are at 37 °C with 5 % CO_2. Until 70 % to 80 % confluency, the cells are ready for use. 100 nM Nanobiosensor 1 and 0.5 ml serum-free DMEM were preincubated at 37 °C for 10 mins. Followed by washing with phosphate buffered saline (PBS), freshly prepared mixtures were incubated with MCF-7 cells at 37 °C in a carbon dioxide incubator for 8 h. Then after washing again with PBS and replacing culture media with fresh DMEM without serum, 0.5 μL of membrane dye CellMask Deep Red Plasma Membrane Stains or 1 μL of NucBlue Live ReadyProbes reagent were added to the cells. Followed by incubated for additional 10 min, confocal examinations were conducted. A LSM 800 Laser Scanning Confocal Microscope (Carl Zeiss, Germany) coupled with 63 × or 40 × oil immersion objectives and 488 nm/640 nm multiline argon laser used for live cell imaging. ImageJ software (National Institutes of Health) conducted the average relative fluorescence intensities of cells, calculated by the

“mean grey value” function with background subtracted towards the areas manually selected and measured.

4.4 Results and Discussion

4.4.1 Sensitivity and selectivity of graphene quantum dot-based biosensor for APE1 diagnosis in living cells

After successfully serving as biosensor towards the cancer biomarker APE1 in cell-free systems, we further explored the potential of Nanobiosensor 1 working in live cell systems. At first, we used MCF-7 which was a breast cancer cell line and well known in biochemistry and biomedicine area[22] to construct living cells system for investigating sensitivity and effectiveness of these designed graphene quantum dot-based biosensors for diagnosing cellular APE1. Meanwhile, graphene quantum dots have attracted more attention serving as a novel nanocarrier in recent years. By well controlling the size, graphene quantum dots play a significant role in drug delivery and transmission due to the good biocompatibility[23-24]. We tried to figure out whether Nanobiosensor 1 can transport into the cell with the help of graphene quantum dots and diagnose APE1 inside the cell.

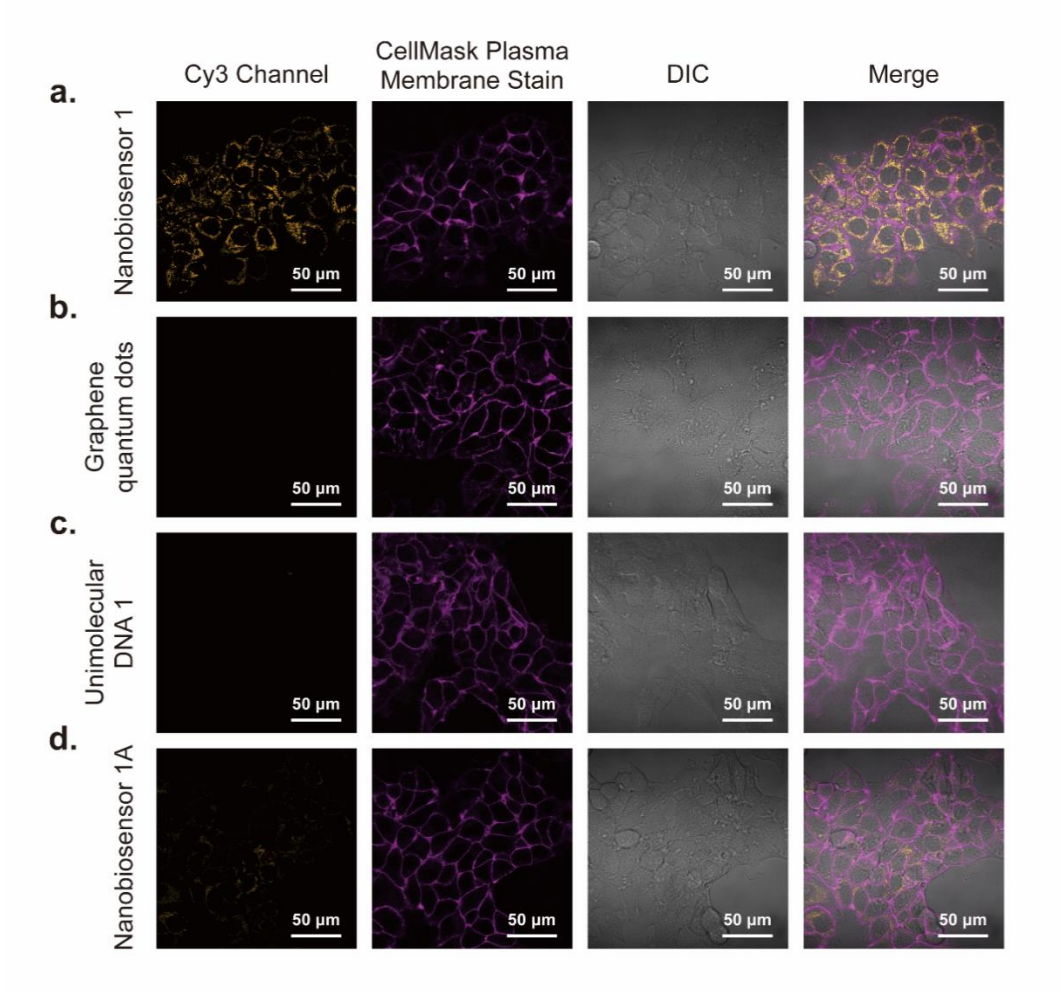

Figure 4.2 Confocal fluorescence microscopy images of different biosensor components treated with MCF-7 cells. MCF-7 cells were preincubated with 100 nM (DNA concentration) Nanobiosensor 1 (a), graphene quantum dots (b), Unimolecular DNA 1 (c), and Nanobiosensor 1 1A (d) at 37 °C for 8 h followed by plasma membrane labeling using CellMask Plasma Membrane Stain.

Confocal microscopy experiments were conducted in **Figure 4.2**. From **Figure 4.2**(a), it can be seen that fluorescence signals of Cy3 were occurred inside the living MCF-7 cells, which obviously validated that generation of fluorescence signals was controlled by cellular APE1 in living MCF-7. To further confirm these results, the graphene quantum dots and Unimolecular DNA 1 were separately used in parallel experiments. These studies from

confocal microscopy demonstrated that it was hard to recognize the fluorescence signals of Cy3 in MCF-7 cells alone with graphene quantum dots (**Figure 4.2**(b)) or Unimolecular DNA 1 (**Figure 4.2**(c)). Considering above observations (**Figure 4**(a)-(c)), we can verify that cellular of APE1 in MCF-7 led to significantly response of fluorescence signals to Nanobiosensor 1, and the integrated structure of Nanobiosensor 1 constructed from graphene quantum dots and unimolecular DNA was crucial for achieving its designated function as cellular APE1's probe.

In order to exclude the interference of other cellular enzymes/proteins and certify that APE1 is the only enzyme that results in fluorescence signals appearing in the reaction system with Nanobiosensor 1 and MCF-7 cells, we designed confocal microscopy examinations with Nanobiosensor 1A containing no AP site in MCF-7 living cells. Confocal fluorescence microscopy in **Figure 4.2**(d) clearly verified that very low fluorescence intensities were regenerated from the reaction system with Nanobiosensor 1A and MCF-7 cells. Comparing fluorescence intensities between Nanobiosensor 1 in MCF-7 cells and Nanobiosensor 1A in MCF-7 cells, the difference was obviously huge and the fluorescence signals of Nanobiosensor 1A and MCF-7 cells were negligible. Considering AP site was the only molecular structural difference between Nanobiosensor 1A and Nanobiosensor 1, which can only catalytically react with cellular APE1 in MCG-7 cells, it substantiated that cellular biomarker APE1 was the sole enzyme causing the generation of significant fluorescence signals from Nanobiosensor 1.

4.4.2 Graphene quantum dot-based biosensor for diagnosis of different expression levels of APE1 in living cells

APE1 has been recognized as a critical biomarker for diagnosing cancer. Due to its repair and redox activities, overexpression of APE1 is observed in many cancer cells, resulting in different expression levels between patients with cancer and without cancer[25]. As our previous proposal, the graphene quantum dot-base biosensors we designed are supposed to use as effective and sensitive probes to distinguish APE1-overexperssed cells (such as cancer cells) and APE1-deificient cells (such as normal cells and APE1 gene knockdown cells). To verify this function of our biosensors, we selected a human pancreatic cancer cell line PANC-1 in our experiments, since APE1 is overexpressed inPANC-1[26-27]. Over the last decades, people have developed many methods to knockdown gene in mammalian cells, and small interfering RNA (siRNA)-induced gene silencing is one of highly effective way[22]. As mentioned in the procedure, we achieved the transfection of APE1-specific siRNA into PANC-1 cells assisted by the Lipofectamine RNAiMAX reagent to knockdown APE1 gene.

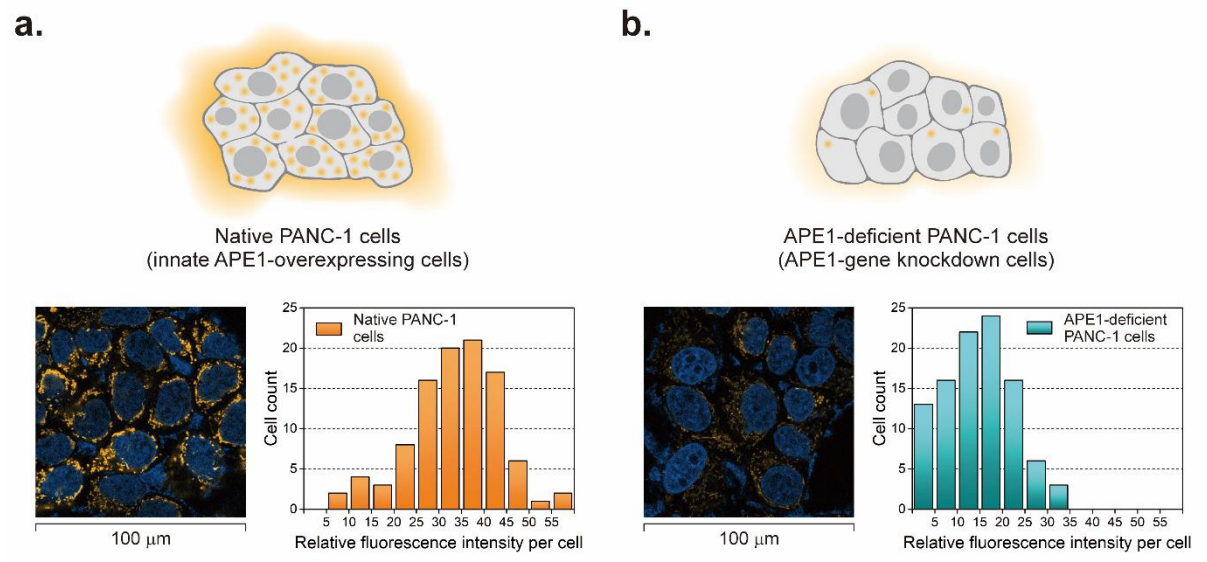

Figure 4.3 Confocal fluorescence microscopy images of native PANC-1 cells (a) and APE1 gene knockdown PANC-1 cells (b) using Nanobiosensor 1 as probes. These two types of cells were incubated with 100 nM (DNA concentration) Nanobiosensor 1 at 37 °C for 8 h prior to confocal examinations. Nuclei were stained with Hoechst 33342 (blue). Average

fluorescence intensity per cell (Cy3, yellow) was quantified from fluorescence microscopy images (n = 100 cells) using ImageJ.

After that, native PANC-1 cells (APE1-upregulated cells) and PANC-1 cells with APE1 gene knockdown (APE1-downregulated cells) separately treated with graphene quantum dot-based biosensor as parallel experiments. Followed by staining nuclei with Hoechst 33342 (blue), confocal fluorescence microscopic images were shown in **Figure 4.3**. Fluorescence intensities were obviously different between the two types of cells. To illustrate the difference in detail, we selected 100 cells randomly, average fluorescence intensity per cell (Cy3, yellow) was quantified from fluorescence microscopy images using ImageJ. From **Figure 4.3**(a), the relative fluorescence intensities of majority of native PANC-1 cells ranged from 25 to 45. Contrary to these native PANC-1 cells, it was clear that the relative fluorescence intensities of majority of APE1-gene knockdown PANC-1 cells were below 25. It demonstrated that Nanobiosensor 1 as a probe for diagnosing APE1 can apparently distinguish APE1-overexpression PANC-1 cells from APE1 gene-knockdown PANC-1 cells.

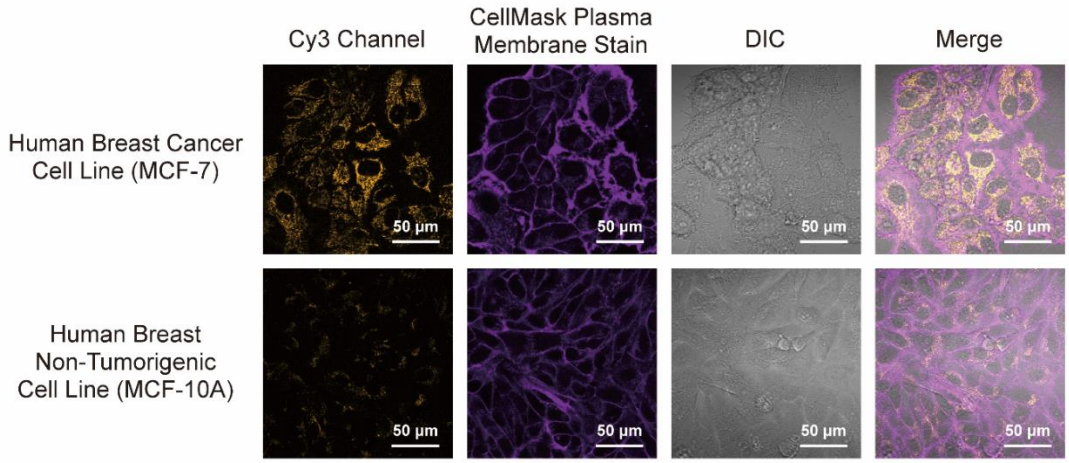

Figure 4.4 Confocal fluorescence microscopy images of human breast cancer cell line (MCF-7) and non-tumorigenic cell line (MCF-10A). These two types of cells were pre-incubated

with 100 nM (DNA concentration) of Nanobiosensor 1 at 37 °C for 8 h. Plasma membrane labelling using CellMask Plasma Membrane Stain was followed.

Besides, human breast cancer cells and human breast non-tumorigenic cells with normal expression levels of APE1 were subsequently detected. From confocal fluorescence microscopic images with different channels in **Figure 4.4**, fluorescence signal was significantly appeared in human cancer cell line (MCF-7) while no fluorescence signal was shown in non-tumorigenic cell line (MCF-10A). It certified that the expression level of APE1 in MCF-7 was much higher than the expression level in the normal cell line, which was in accordance with the previous reported results through cell extraction analysis[28].

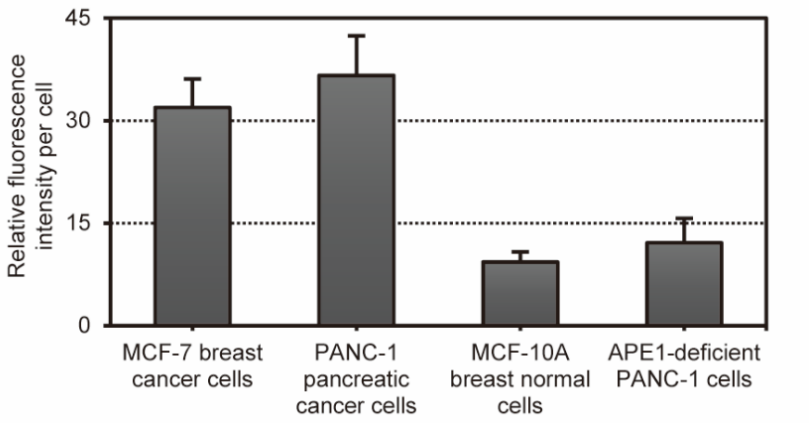

Figure 4.5 Quantitative analysis of APE1 expression levels in various types of human cell lines. Cells were incubated with 100 nM (DNA concentration) of Nanobiosensor 1 at 37 °C for 8 h followed by confocal microscopic analysis. Relative fluorescence intensity per cell were quantified from fluorescence microscopy images (n = 100 cells) using ImageJ.

By counting cells with similar relative fluorescence intensities in certain area, we can further figure out the APE1 expression levels in a quantitative method. According to the

results in **Figure 4.5**, the amount of MCF-7 breast cancer cells and PANC-1 pancreatic cancer cells were over 30. On the contrary, the amount of MCF-10A breast normal cells and APE1-deficient PANC-1 cells were below 15. The quantitative analysis proved that Nanobiosensor 1 can be used for diagnosis of different expression levels of APE1 in living cells.

In general, based on the examination towards four different living cells, it validated our earlier assumption that our designed graphene quantum dot-based biosensors can achieve effective distinction between same type of living cells with different expression levels of cellular APE1. Furthermore, our biosensors can work as effective and sensitive diagnostic probes and easily differentiate cancer cells from normal cells.

4.4.3 Cytotoxicity and cellular uptake efficiency of graphene quantum dot-based biosensors

As more and more biosensors are designed for diagnosing various targeted biomarkers in living cells, minimal toxicity towards living cells is considered as one of the most essential factors to achieve accurate and effective detection[29-30]. Therefore, we did cytotoxicity assays to investigate compatibility of our designed graphene quantum dot-based biosensors. In these experiments, we used PANC-1 as standard living cells to measure cell viability of graphene quantum dot-based Nanobiosensor 1, graphene oxide-based Nanobiosensor GO, and reduced graphene oxide-based Nanobiosensor rGO. These three nanobiosensors were constructed from the same substrates and conditions expect nanocarrier part, which was graphene quantum dot, graphene oxide and reduced graphene oxide, respectively.

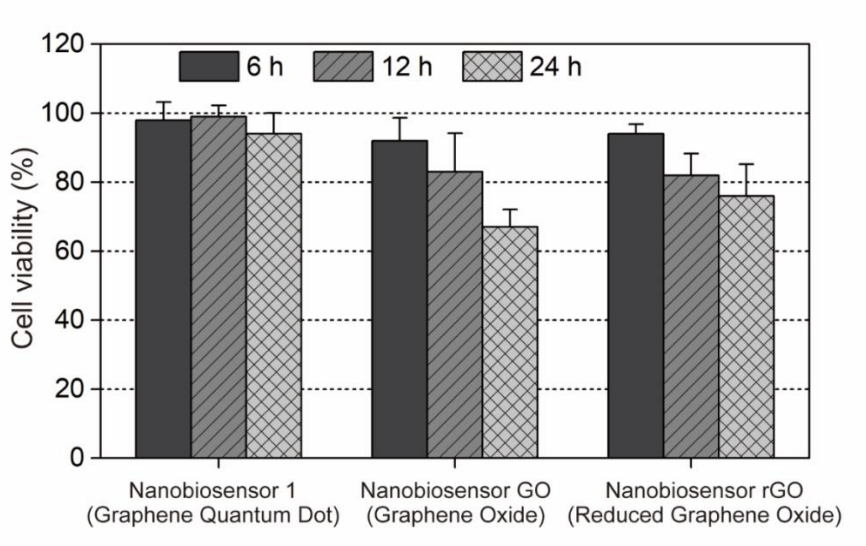

Figure 4.6 Cytotoxicity assays of graphene quantum dot-based Nanobiosensor 1, graphene oxide-based Nanobiosensor GO, and reduced graphene oxide-based Nanobiosensor rGO towards PANC-1 cell lines. Data in the chart are representative of three independent experiments, and values are expressed in mean ± SD.

Our results shown in **Figure 4.6** explicitly proved that Nanocomposite 1 displayed minimal cytotoxicity, as corroborated by our observations that the survival rate of PANC-1 cells in the presence of Nanocomposite 1 was 99 and 94% after 12 and 24 h of incubation, respectively (**Figure 4.6**). Contrary to Nanocomposite 1, cell survival rates at 12 and 24 h of incubations were 83 and 67% for Nanocomposite GO and 82 and 76% for Nanocomposite rGO, respectively. Thus, different nanocarriers resulted in different toxicity towards living cells. And graphene quantum dot-based biosensor showed better compatibility that the other two nanobiosensors. Further conclusion was made that cytotoxicity of nanobiosensor was determined by the intrinsic properties of the nanocarrier component.

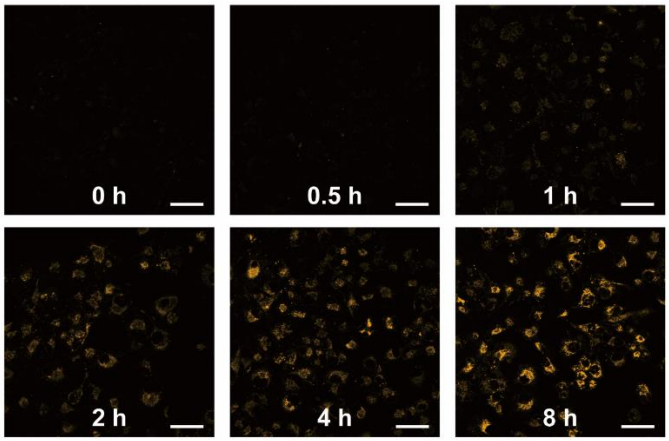

Figure 4.7 Confocal microscopic examinations of the cellular uptake of Nanobiosensor 1 by PANC-1 cells at varying time intervals. Confocal images were obtained from the Cy3 channel at 488 nm excitation. Scale bars indicate 50 μm.

Based on the high cell viability and minimal cytotoxicity of Nanobiosensor 1, it was feasible for Nanobiosensor 1 to serve as cytopathological probe for diagnosing cancer in living cells. Furthermore, to test the efficiency of graphene quantum dot-based biosensors, cellular uptake rates of Nanobiosensor 1 by PANC-1 cells were described through confocal microscopic examinations depending on time. From confocal fluorescence microscopic images shown in **Figure 4.7**, we can know that as the incubation time of PANC-1 cells and Nanobiosensor 1 increased, the fluorescence intensities increased correspondingly. In the first hour of incubation, low fluorescent signal was observed. During the time from 1 h to 4 h of incubation, a magnificent quantity of free fluorophores (Cy3) accumulated inside PANC-1 cells, which confirmed that Nanocomposite 1 could be uptaken by living cells in a rapid manner. Nowadays, the extraction of samples of human living cells from patients can be fast achieved by fine needle aspiration biopsy method[31]. Considering the high cellular uptake efficiencies, our newly designed graphene quantum dot-based biosensors can be suitable probes for quick cancer diagnosis combining with fine needle aspiration biopsy method.

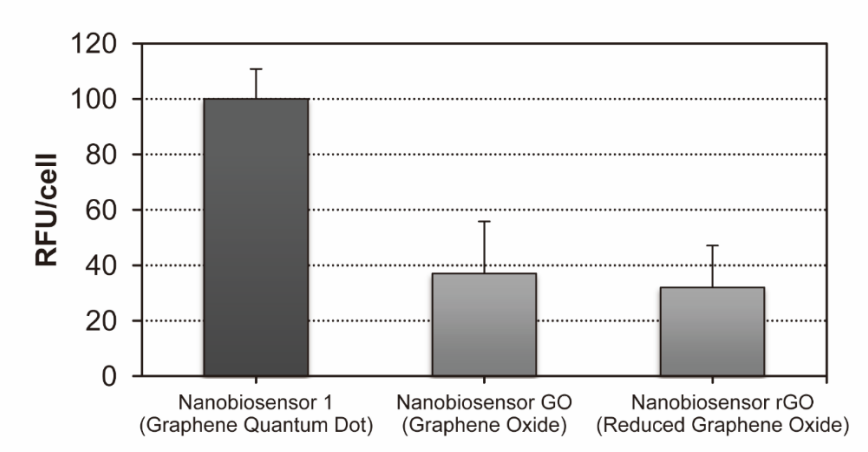

Figure 4.8 Comparison of cellular uptake efficiency of nanobiosensors with the use of different nanomaterials as their carriers. Relative fluorescence units (RFUs) among PANC-1 cells were determined after incubation with graphene quantum dot-based nanobiosensors (Nanobiosensor 1), graphene oxide-based nanobiosensors (Nanobiosensor GO) and reduced graphene oxide-based nanobiosensors (Nanobiosensor rGO) for 8 h, respectively. Average intensities of fluorescence were quantified from confocal microscopy images (n = 100 cells) using ImageJ.

Finally, we tested the uptake rates of Nanobiosensor 1, Nanobiosensor GO and Nanobiosensor rGO by PANC-1 cells. In **Figure 4.8**, relative fluorescence units (RFUs) among PANC-1 cells were used to determine cellular uptake efficiency of nanobiosensors. Comparing RFU was around 100 of Nanobiosensor 1, the RFU of Nanobiosensor GO and Nanobiosensor rGO were both below 40. The results proved that cellular uptake efficiency of Nanobiosensor 1 was significantly higher than the efficiency of Nanobiosensor GO and Nanobiosensor rGO. In addition, this experiment data as an evidence substantiated that graphene quantum dot was superior to graphene oxide and reduced graphene oxide in terms of building probes for cytopathological tests.

4.5 Conclusions

Graphene quantum dot-based biosensors integrated by unimolecular DNA and graphene quantum dots have been developed in our studies. These new nanobiosensors have been proved to be utilized for diagnosing cellular cancer biomarker APE1 in a highly sensitivity, exclusively selectivity, and quick manner. Meanwhile, graphene quantum dot-based biosensors are available for the diagnosis of different expression levels of APE1 in living cells with huge biocompatibility and high cellular uptake efficiency.

Since the abundance and activity of biomarker APE1 in living cells are commonly associated with the health status of human cells[25], it is our expectation that our newly developed nanocomposites could be widely applicable (i) as cytopathological probes for diagnosis of cancers as well as other APE1-dysregulated diseases and (ii) as cell-based high-content screening probes for identifying anticancer drugs from chemical compound libraries[32-33]. We also anticipate that our newly established concepts and rules in the current studies could serve as a foundation for designing DNA and quantum dot-based functional nanostructures for diagnosing many other cancer-affiliated endogenous biomarkers in living cells as well.

References

1. Zhai, J.; Liu, Y.; Huang, S.; Fang, S.; Zhao, M. A., *Nucleic Acids Res.* **2017,** *45*, e45.
2. Wu, L.; Qu, X., *Chem. Soc. Rev.* **2015,** *44*, 2963-97.
3. Nimse, S. B.; Sonawane, M. D.; Song, K. S.; Kim, T., *Analyst*. **2016,** *141*, 740-55.

4. Henry, N. L.; Hayes, D. F., *Mol. Oncol.* **2012,** *6*, 140-6.
5. Coskun, E.; Jaruga, P.; Reddy, P. T.; Dizdaroglu, M., *Biochemistry.* **2015,** *54*, 5787-90.
6. Woo, J.; Park, H.; Sung, S. H.; Moon, B. I.; Suh, H.; Lim, W., *PloS one.* **2014,** *9*, e99528.
7. Cesaratto, L.; Codarin, E.; Vascotto, C.; Leonardi, A.; Kelley, M. R.; Tiribelli, C.; Tell, G., *PloS one.* **2013,** *8*, e70909.
8. Di Maso, V.; Mediavilla, M. G.; Vascotto, C.; Lupo, F.; Baccarani, U.; Avellini, C.; Tell, G.; Tiribelli, C.; Croce, L. S., *PloS one.* **2015,** *10*, e0143289.
9. Wang, B.; Qiu, H., *Gouji Jianyan Yixue Zazhi.* **2013,** *34*, 3384-6.
10. Lou, D.; Zhu, L.; Ding, H.; Dai, H. Y.; Zou, G. M., *Oncology letters.* **2014,** *7*, 1078-82.
11. Canbay, E.; Cakmakoglu, B.; Zeybek, U.; Sozen, S.; Cacina, C.; Gulluoglu, M.; Balik, E.; Bulut, T.; Yamaner, S.; Bugra, D., *Current medical research and opinion.* **2011,** *27*, 1295-302.
12. Fishel, M. L.; He, Y.; Reed, A. M.; Chin-Sinex, H.; Hutchins, G. D.; Mendonca, M. S.; Kelley, M. R., *DNA repair.* **2008,** *7*, 177-86.
13. Al-Attar, A.; Gossage, L.; Fareed, K. R.; Shehata, M.; Mohammed, M.; Zaitoun, A. M.; Soomro, I.; Lobo, D. N.; Abbotts, R.; Chan, S.; Madhusudan, S., *British journal of cancer.* **2010,** *102*, 704-9.
14. Kelley, M. R.; Cheng, L.; Foster, R.; Tritt, R.; Jiang, J.; Broshears, J.; Koch, M., *Clinical cancer research : an official journal of the American Association for Cancer Research.* **2001,** *7*, 824-30.
15. Evans, A. R.; Limp-Foster, M.; Kelley, M. R., *Mutation research.* **2000,** *461*, 83-108.
16. Jiang, S.; Zhu, L.; Tang, H.; Zhang, M.; Chen, Z.; Fei, J.; Han, B.; Zou, G. M., *International journal of oncology.* **2015,** *47*, 610-20.
17. Thakur, S.; Sarkar, B.; Cholia, R. P.; Gautam, N.; Dhiman, M.; Mantha, A. K., *Experimental & molecular medicine.* **2014,** *46*, e106.

18. Qing, Y.; Yang, X. Q.; Zhong, Z. Y.; Lei, X.; Xie, J. Y.; Li, M. X.; Xiang, D. B.; Li, Z. P.; Yang, Z. Z.; Wang, G.; Wang, D., *BMC cancer.* **2010,** *10*, 71.

19. Sak, S. C.; Harnden, P.; Johnston, C. F.; Paul, A. B.; Kiltie, A. E., *Clinical cancer research : an official journal of the American Association for Cancer Research.* **2005,** *11*, 6205-11.

20. Zhang, Y.; Fan, S.; Wang, Dong.; Yang, Z.; Xiang, D.; Li, Z.; Chen, J.; Jiang, Y., *J Third Mil Med Univ.* **2007,** *29*, 776-778.

21. Shin, J. H.; Choi, S.; Lee, Y. R.; Park, M. S.; Na, Y. G.; Irani, K.; Lee, S. D.; Park, J. B.; Kim, J. M.; Lim, J. S.; Jeon, B. H., *Cancer research and treatment : official journal of Korean Cancer Association.* **2015,** *47*, 823-33.

22. Holliday, D. L.; Speirs, V., *Breast Cancer Res.* **2011,** *13*, 215.

23. Su, Y.-L.; Yu, T.-W.; Chiang, W.-H.; Chiu, H.-C.; Chang, C.-H.; Chiang, C.-S.; Hu, S.-H., *Adv. Funct. Mater.* **2017,** *27*, 1700056.

24. Xue, Z.; Sun, Q.; Zhang, L.; Kang, Z.; Liang, L.; Wang, Q.; Shen, J.-W., *Nanoscale*. **2019,** *11*, 4503-14.

25. Shah, F.; Logsdon, D.; Messmann, R. A.; Fehrenbacher, J. C.; Fishel, M. L.; Kelley, M. R., *npj Precis. Oncol.* **2017,** *1*, 19.

26. Zou, G. M.; Maitra, A., *Mol. Cancer Ther.* **2008,** *7*, 2012-21.

27. Kim, M.-H.; Kim, H.-B.; Acharya, S.; Sohn, H.-M.; Jun, J. Y.; Chang, I.-Y.; You, H. J., *Mol. Cell. Biol.* **2009,** *29*, 2264-77.

28. Kirkali, G.; Jaruga, P.; Reddy, P. T.; Tona, A.; Nelson, B. C.; Li, M.; Wilson, D. M., III; Dizdaroglu, M., *PLoS One.* **2013,** *8*, e69894.

29. Turner, A. P., *Chem. Soc. Rev.* **2013,** *42*, 3184-96.

30. Chen, F.; Gao, W.; Qiu, X.; Zhang, H.; Liu, L.; Liao, P.; Fu, W.; Luo, Y., *Front. Lab. Med.* **2017,** *1*, 192-9.

31. Willen, H.; Akerman, M.; Carlen, B., *Cytopathology.* **1995,** *6*, 236-47.

32. Usaj, M. M.; Styles, E. B.; Verster, A. J.; Friesen, H.; Boone, C.; Andrews, B. J., *Trends Cell Biol.* **2016,** *26*, 598-611.

33. Nierode, G.; Kwon, P. S.; Dordick, J. S.; Kwon, S. J., *J. Microbiol. Biotechnol.* **2016,** *26*, 213-225.

Chapter 5

Summary and Future Outlook

As an essential enzyme involved in the DNA base excision repair pathway, Apurinic/apyrimidinic endonuclease 1 (APE1) is overexpressed in various types of cancer cells, proving that APE1 is a valid biomarker for cancer diagnosis and prognosis, and a potent biomolecular target of both monotherapy and combination therapy for fighting cancers. With the development of DNA-based bionanosensors in recent years, several cellular biomarkers have been successfully detected under physiological conditions. However, various aspects of translational research about APE1 have not yet been carried out thus far. Most critically, few methods as well as other currently available techniques are applicable for determining different cellular levels of APE1 in same types of living cells.

In **Chapter 2**, we describe the catalytic properties of APE1 by investigating substrate diversity using gel electrophoresis, which makes a great contribution to understand the catalytic properties of APE1 and further explore sequence-specific DNA as APE1 inhibitors. In **Chapter 3** and **Chapter 4**, we report our biocompatible functional graphene quantum dot-based biosensor constructed from well-designed unimolecular DNA and prepared graphene quantum dots. Upon utilization of these nanobiosensors, different cellular levels of the cancer biomarker APE1 in living cells can be diagnosed in a highly sensitive, exclusively selective, and quick manner.

For the next stage, according to the results about APE1 substrate diversity from **Chapter 2**, we aim to design and synthesize a variety of substrate-based APE1 inhibitors that will be subsequently tested for their inhibitory effects against APE1 under physiological buffer conditions. It is believed that substrate-based inhibitors are generally specific because specified recognitions and interactions occur between substrate analogs and functional groups of active sites of enzymes.

Furthermore, all the synthesized APE1 inhibitors will be examined for their potencies toward selected cancer tissue, cultured cancer cells and mouse models. We hope that this thesis could have certain implications for diagnosis and therapy of cancer-affiliated endogenous biomarkers in living cells.